3-2020

Assessing Challenges Associated with Sampling Hexavalent Chromium under New Consensus Guidelilnes

Megan L. Steele

ASSESSING CHALLENGES ASSOCIATED WITH SAMPLING HEXAVALENT CHROMIUM UNDER NEW EXPOSURE GUIDELINES

THESIS

Megan L. Steele, contractor

AFIT-ENV-MS-20-M-242/243

DEPARTMENT OF THE AIR FORCE
AIR UNIVERSITY

AIR FORCE INSTITUTE OF TECHNOLOGY

Wright-Patterson Air Force Base, Ohio

AFIT-ENV-MS-20-M-242/243

ASSESSING CHALLENGES ASSOCIATED WITH SAMPLING HEXAVALENT CHROMIUM UNDER NEW GUIDELINES

THESIS

Presented to the Faculty

Department of Systems Engineering and Management

Graduate School of Engineering and Management

Air Force Institute of Technology

Air University

Air Education and Training Command

In Partial Fulfillment of the Requirements for the

Degree of Master of Science in Industrial Hygiene

Degree of Master of Science in Environmental Engineering

Megan L. Steele, BS

Contractor

March 2020

AFIT-ENV-MS-20-M-242/243

ASSESSING CHALLENGES ASSOCIATED WITH SAMPLING HEXAVALENT CHROMIUM UNDER NEW CONSENSUS GUIDELINES

Megan L. Steele, BS

Contractor

Committee Membership:

Dr. Jeremy Slagley
Chair

Col Robert Eninger, PhD
Member

Lt Col Casey Cooper, PhD
Member

Dr. Dirk Yamamoto
Member

Abstract

Hexavalent chromium is a corrosion inhibitor found in the primer of most aircraft platforms across the Department of Defense (DoD), from fighter jets to transports. It is also known to cause cancer in humans. Currently, the Occupational Safety and Health Administration (OSHA) legal exposure limit is 5 $\mu g/m^3$ for workers exposed to hexavalent chromium. A non-regulatory scientific body has recently recommended lowering this exposure level over a factor of ten and sampling with a different sampler that collects particles with the same efficiency as the nose during inhalation. This inhalable sampler collects more particles than the one currently used to comply with OSHA law. An early estimate of the cost of adopting this non-regulatory exposure standard is $900M over five years across the DoD, due in no small part to the likelihood that workers would need new, more restrictive personal protective equipment. Before adopting this new standard, two open points exist: based on DoD processes, is the inhalable sampler necessary and what impact to the sampler efficiency occurs if the flow rate is increased. To answer the first question, real world abrasive blasting processes were sampled and analyzed for particle size distribution. For the second aim, the mass concentrations of samplers operating at their design 2 L/min flow rate were compared to the mass concentrations reported by samplers operating at 6 L/min. From the abrasive blasting processes sample analysis, it was determined use of the inhalable sampler is justified. A 30% positive bias was found when comparing the higher flow rate to the lower flow rate mass concentrations. If the DoD adopts the new recommendation, it is likely over-reporting of hexavalent chromium concentrations in the workplace will occur.

Acknowledgments

I would first like to thank Dr. Slagley for his tireless optimism, willingness to talk through problems during impromptu visits, and gentle reminders that not every rabbit hole needs to be explored. I would like to thank Colonel Eninger for his early engagement in the key decision points for this thesis. Without his support, I wouldn't have been able to turn a vague sketch on a whiteboard into an aerosol chamber. Lieutenant Colonel Cooper's guidance with data analysis has allowed me to interrogate my results with statistical rigor. I am grateful to Dr. Yamamoto for the funding for this project and the leeway given in fulfilling its aims. I would like to acknowledge the Bioenvironmental Flight at Hill AFB for their willingness to support multiple data gathering endeavors. Their support was invaluable and greatly enriched our understanding abrasive blasting aerosol characteristics. Finally, I would like to thank my husband for his support.

Megan L. Steele

Table of Contents

Page

List of Figures

Page

List of Tables

Page

List of Equations

Page

ASSESSING CHALLENGES ASSOCIATED WITH SAMPLING HEXAVALENT CHROMIUM UNDER NEW CONSENSUS GUIDELINES

I. Introduction

1.1 General Issue

1.1.1 Exposure Standard for Hexavalent Chromium

Hexavalent chromium (Cr(VI)) is a known carcinogen with an Occupational Safety and Health Administration (OSHA) permissible exposure limit (PEL) of 5 $\mu g/m^3$ for workers. This standard is based on epidemiological data which suggests 10 – 45 workers per 1000 will develop cancer if exposed to levels at or above the PEL (OSHA, 2006). The American Conference of Governmental Industrial Hygienists (ACGIH) has gone a step further and suggested a threshold limit value (TLV) of 0.2 $\mu g/m^3$, a level they consider low enough to prevent nasal irritation and the development of sores (ACGIH, 2018).

In addition to lowering the limit, ACGIH recommends using a sampler that adheres to the inhalable particulate matter (IPM) convention. IPM is part of a practice known as particle size selective (PSS) sampling. With PSS, sampling focuses on particles sizes based on penetration in the respiratory system. If the primary health effect is associated with irritation in the alveoli, it is recommended an industrial hygienist sample with a respirable sampler. For effects on the bronchi, a thoracic sampler should be used. In the case of hexavalent chromium, where effects are prominent in the head, an inhalable sampler, capable of collecting particles from 1 – 100 μm is appropriate. One of the most

commonly used inhalable sampler is the Institute of Occupational Medicine sampler (IOMs).

1.1.2 Ubiquity in Industry

Chromium (Cr) exposure occurs frequently in a variety of industries, including electroplating, stainless steel manufacture and welding, textile manufacturing and leather tanning, paint and pigment manufacturing, printing ink manufacturing, catalyst producing, and wood preservation. (National Toxicology Program, 2019; NIOSH, 2013). It was estimated in 2006 that over half a million workers in the United States were exposed to Cr(VI) as part of their job duties (NIOSH, 2013).

1.1.3 Cr(VI) Exposure Assessments in Relevant Occupations

Bennett et al. (2016) conducted an exposure assessment of seven workers engaged in painting a Navy fighter jet after it had been sand-blasted. The three primary processes observed were wiping the aircraft down with solvent, applications of the primer via spray guns, then application of one of two topcoats in the correct color. Velocity measurements of the air within the hangar were made before work began, after priming, and after the conclusion of all work. Four workers directly engaged in priming had air samples taken from outside their personal protective equipment (PPE) for volatile organic compound (VOC) and Cr(VI) exposure. Within this group of workers, two were engaged in spraying and two were engaged in managing the hoses. Those engaged in spraying had elevated exposures compared to those who managed the hoses.

An evaluation of 21 sites representing a variety of industrial processes was performed by the National Institute of Occupational Safety and Health (NIOSH) using personal air samples and ventilation equipment (Blade, 2007). One of the key goals of the

study was to determine the effectiveness of controls so all personal breathing zone (PBZ) samples were taken external to workers' PPE (Blade, 2007). Of those exposures relevant to the Air Force, welding had the lowest exposure followed by sanding, then abrasive blasting, with priming having the greatest exposures.

Depainting and scuff sanding are distinct tasks with potential for hexavalent chromium exposure. Depainting is the removal of paint via mechanical or chemical means while scuff sanding is the roughing up of a primed surface in preparation for applying the top coat (Carlton, 2003a). Of the three processes monitored in this study, the highest potential exposure occurred during painting, followed by sanding, with the lowest exposure attributed to hand-applying chromic acid in a process call "chromating" (Carlton, 2003a). These results are consistent with prior studies conducted by the same industrial hygiene team.

A summary of the exposure assessments discussed above is shown in Table 1.

Table 1. Occupational Exposures in Industry and the Military

Industry	Task Name	Ventilation Velocity (m/s)	Mean Hexavalent Chromium Concentration ($\mu g/m^3$) [8-hr time weighted average]				Number of Samples Taken (personal)	Number of Samples Taken (area)	Study	Aircraft	Sample Type
			Blasting	Sanding	Priming	Welding					
Navy	Hose man	0.94			120 [8.3]		6	12	Bennett, 2016	F/A-18	CFC*
Navy	Sprayer	0.94			500 [38]		6	12	Bennett, 2016	F/A-18	CFC
Construction	Painter	N/A	0.43				8	0	Blade, 2007	N/A	CFC
Manufacturing	Painter	N/A			[16]		5	0	Blade, 2007	N/A	CFC
Manufacturing	Painter	N/A			[0.23]		13	0	Blade, 2007	N/A	CFC
Manufacturing	Sander	N/A		[0.27 - 2.1]			4	0	Blade, 2007	N/A	CFC
Manufacturing	MIG*** Welder	N/A				[2.8 - 5.2]	2	0	Blade, 2007	N/A	CFC
Manufacturing	MIG/TIG*** Welder	N/A				[2.0 - 3.7]	2	0	Blade, 2007	N/A	CFC
Manufacturing	MIG Welder	N/A				[0.84]	4	0	Blade, 2007	N/A	CFC
Manufacturing	MIG/TIG/ SMAW***/Cutting	0				[6.6]	4	0	Blade, 2007	N/A	CFC
Manufacturing	TIG Welder	N/A				[0.65]	1	0	Blade, 2007	N/A	CFC

Table 1. Occupational Exposures in Industry and the Military Continued

Industry	Task Name	Ventilation Velocity (m/s)	Mean Hexavalent Chromium Concentration ($\mu g/m^3$) [8-hr time weighted average]				Number of Samples Taken (personal)	Number of Samples Taken (area)	Study	Aircraft	Sample Type
			Blasting	Sanding	Priming	Welding					
Navy	Welder	N/A				[0.36]	3	0	Blade, 2008	N/A	CFC
Air Force	Sanding	N/A		16.4 [5.33]**			42	0	Carlton, 2003a	Various	Modified CFC
Air Force	Priming	N/A			831.9 [83.8]**		15	0	Carlton, 2003a	Various	Modified CFC
Air Force	Chromating	N/A			9.66 [0.48]**		9	0	Carlton, 2003a	Various	Modified CFC
Air Force	Abrasive Blasting	N/A	130				77	0	Carlton, 2000	Various	Button Sampler
Air Force	Surface prep	unmitigated		18.1 [8.7]			Unknown	Unknown	England, 1998	F-16	Modified CFC
Air Force	Dust removal	unmitigated	245 [12.3]				Unknown	Unknown	England, 1998	F-16	Modified CFC
Air Force	Priming	0.13 - 0.58			625 [75.5]		Unknown	Unknown	England, 1998	F-16	Modified CFC
Air Force	Surface prep	9.9		3.85 [0.99]			Unknown	Unknown	England, 1998	F-16	Modified CFC

* closed-face cassette (CFC)

** as Cr

*** metal inert gas (MIG); tungsten inert gas (TIG); shielded metal arc welding (SMAW)

1.1.4 Air Force Specific Exposures to Hexavalent Chromium

Cr exposure is a concern for the Air Force in corrosion control, as the primer that is used to bond bare metal to paint contains Cr(VI) (Aizenberg, 2000). Any operation where primer is applied or disturbed, such as sand blasting in preparation for a repainting operation, has the potential to expose workers to Cr(VI) particulate. Since 2008, over 9,100 air samples for Cr(VI) have been loaded into the Defense Occupational and Environmental Health Readiness System (DOEHRS) (DOEHRS, 2018).

Metallic structures external to the aircraft are prone to corrosion from reactions with oxygen in the ambient environment. To prevent degradation, aircraft are initially coated with corrosion inhibitors then painted with a top coat. Throughout its life, an aircraft undergoes periodic reapplication of paint through a series of established processes.

The following stages are described in DTIC Report IERA-RS-BR-TR-2000-0001, called "Assessing Worker Exposures During Abrasive Blasting: Industrial Hygiene Field Guidance for Bioenvironmental Engineers". The first stage requires the aircraft be cleaned to remove fluids and grease. The potential for exposure is low, though samples have been taken by base-level shops. The second stage requires the removal of the top layer of paint. For minor cosmetic repair, areas may be abraded with an orbital sander (sanded). For major servicing, the entire aircraft may be blasted with an abrasive to expose bare metal (blasting). A conversion coat containing chromic acid is applied to bare metal (also called brightening or Alodine application). The reaction with chromic acid is quenched at a prespecified time either by wiping excess material off small areas or rinsing the aircraft with water. Post-conversion, chromated primer is applied with a spray

nozzle to the aircraft. The type of nozzle and carrier fluid vary. At the time of the 2000 report, most base-level shops used compressed air as the carrier fluid and high volume low pressure (HVLP) nozzles to minimize overspray. Larger depots sometimes had pressurized water as the carrier fluid (Aqua Miser). Finally, a chromium-free topcoat is applied. Depainting, conversion coat application, and priming represent the major exposure points. A diagram of the process flows is shown in Figure 1, where green has the least exposure, yellow has moderate exposure, and red has the highest exposure.

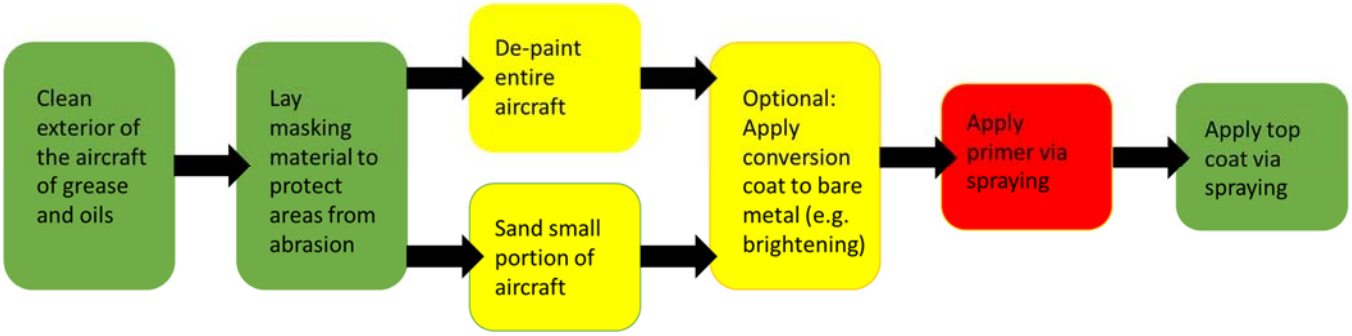

Figure 1. Corrosion Control Process Flow with Relative Cr(VI) Exposure Potential

The Air Force has moved away from using sand for blasting and instead opts for other media such as walnut husks, plastic beads, glass beads, and aluminum oxide (Carlton, 2000). Presumably media type impacts the aerosol properties of removed coatings during depainting operations, though Carlton (2000) concludes there is no easy way to characterize these properties. Instead, he suggests relying on inhalable sampling devices to best describe worker exposures. Of the surveys conducted, the top six average exposures to Cr(VI) occurred with plastic blast media.

1.2 Problem Statement

Moving from total dust sampling using a closed face cassette (CFC) to a sampler that follows the inhalable particulate matter (IPM) convention presents practical challenges as the change requires additional training for field technicians and an altered sample handling protocol. Additional complications are introduced by simultaneously lowering the exposure threshold by over a factor of 10.

In practice, the limit of detection (LOD) for a specific method and analytical instrument is three times the signal-to-noise ratio and the limit of quantitation (LOQ) is ten times. The LOD represents the ability to determine the presence or absence of a contaminant while the LOQ represents the lower limit of a contaminant concentration that can be assigned a numeric value. The current LOD for the USAF School of Aerospace Medicine (USAFSAM) Occupational and Environmental Health Department (OE) laboratory for hexavalent chromium is 30 ng and the LOQ is 100 ng.

In Industrial Hygiene (IH), the best practice LOQ would be one tenth of the exposure limit or lower. Given the recommended eight-hour time weighted average (8hr-TWA) for hexavalent chromium is 0.2 $\mu g/m^3$ and the prescribed sample flow rate is 2 L/min, an environment at the 8h-TWA concentration when sampled all day (8 hours) would only yield 192 ng of chromium in a sample. In order to follow IH best practice, the laboratory would need to be able to quantify 19 ng per sample, below even their limit of detection.

Therefore, either the analytical LOD and LOQ need to be lowered or more mass needs to be deposited per sample. As hexavalent chromium samples make up approximately 40% of the workload for the USAFSAM OE lab, their scientists and

technicians have already expended great effort to achieve the lowest possible LOD and LOQ given real world constraints (Mattingly, 2019). This suggests that depositing more mass on the filter may be necessary.

The mass deposited on a sample filter is a direct function of the concentration of contaminant in the air and the flow rate at which air is moved through it. As contaminant concentration is not controlled directly by the IH during surveillance, the only variable is the sampling pump flow rate. Simple calculations were undertaken to determine that 6 L/min is the minimum flow rate necessary to achieve enough mass on the filter while meeting an LOQ of 50% of the exposure limit (

Appendix B). Fifty percent was chosen since the best practice 10% of the exposure limit yielded results outside the range of personal sampling pump capability. In IH a common rule of thumb is 50% signifies the action level, a level generally accepted as indicating that the process is poorly controlled and should be evaluated more closely to prevent overexposures. While a rule of thumb, this percentage is based in statistics, where if a single sample is taken from a process with a narrow geometric standard deviation and that sample is below the action level, decision makers can be reasonably assured that the workplace exposure is below the permissible exposure limit (Rock, 1982).

While it is to calibrate a pump to operate at a higher flow rate, there is a byproduct, namely the capture efficiency of the sampler attached to the pump is affected. PSS sampling was introduced as a way to collect particulate matter size fractions relevant to human health (Phalen, 1999). The IPM convention mimics the size of particles that penetrate the nose and mouth during normal inspiration. This convention has the largest particle distribution (1 – 100 μm) and one of the samplers most commonly selected to meet the convention is the IOMs.

If the DoD decides to continue with the OSHA PEL and use a CFC for total dust sampling, the LOQ problem remains. The flow rate for the CFC would need to be increased to collect enough mass. Considering the opening to a CFC is not a sharp edge and is only 4 mm wide, it is likely the performance will suffer significantly, changing the upper cut point from 20 μm to even smaller.

The IOMs was designed to follow the IPM when operated at 2 L/min. Sampler efficiency is affected by both the freestream velocity of the air in the environment and the sampling flow rate (Appendix C). There is the possibility that by altering the flow rate,

the IOM's efficiency will deviate from the IPM convention substantially, thus negating the reason for using it.

Published literature suggests that the IOM's performance is not significantly altered when operated at 10 L/min for efficiency by particle count (Anthony, 2016), by mass (Stewart, 2017), or by fluorescent concentration (Zhou, 2009). Much of the research focused on particles ≤ 60 µm. It is anticipated that any affect to the IOM's adherence to the IPM convention will occur nearer to 100 µm (Appendix C).

1.3 Research Objectives

The first research objective is to determine if use of an inhalable sampler is justified during abrasive blasting procedures. The assumption underlying the use of the sampler is that hexavalent chromium is found in all particle sizes. If the particles containing chromium are less than 20 µm, the CFC is still appropriate for use and avoids the complications introduced by using the IOM.

The second research objective is to better characterize the aerosols generated during abrasive blasting. At present, no particle size distributions or particle shape characteristics are documented in literature. Carlton (2002) asserted that particles could range from 1 – 1000 µm in size, but no data were presented that indicated what the distribution of particles by size was. In order to make use of thousands of historical chromium exposure samples collected with CFCs, an appropriate conversion between IOM particle capture compared to the CFC is needed. The conversion factor cannot be derived without an understanding of the particle composition and distribution above 20 µm.

The third and final research objective is to determine if a 25% difference in the mean mass concentration measured by an IOM operating at 2 L/min and 6 L/min exists. In NIOSH method development, a 25% deviation from an established sampling method means the new method is not comparable to the first. In this case, the 6 L/min sampling flow rate is treated as a new method. A 25% increase or decrease in sample collection represents a significant enough under- or overestimate of risk to warrant consideration.

1.4 Thesis Outline

This thesis is composed of five chapters. Chapter I covers the general issues, problem statement, research questions, and scope. Chapters II – IV answer the research questions and are intended to be independent papers to be submitted to peer-reviewed journals. The chapters are more detailed than what is anticipated to be published to allow for transparency in methods and analysis. Chapter II covers the design and characterization of an aerosol chamber used for the experiments presented in Chapter IV. Chapter III presents a characterization of the aerosols produced by abrasive sand blasting in a corrosion control operation at Hill AFB. Chapter IV contains the experiments with IOMs operating at 2 L/min and 6 L/min in the aerosol chamber. The final chapter presents the conclusions and impact of the body of the research conducted.

II. Aerosol Test Chamber Characterization

Chapter Overview

This chapter encompasses the work surrounding designing and characterizing the aerosol chamber used in Chapter IV. While this chapter does not directly answer any research objectives, it was a critical step in getting to the point where it was possible to

evaluate objective three. The work presented in this chapter was conducted in collaboration with Ms. Emily Titus, Mr. George Lemmer, and Mr. Jacob Denney.

This paper will target publication in Aerosol Science and Technology.

2.1 Introduction

Test chambers are used when conducting aerosol research in order to protect the health of researchers, prevent cross contamination of the lab and test environment, and maintain the aerosol in a well-defined space (Lidén *et al.*, 1998; Lundgren, 2006; Hagerman *et al.*, 2014). Based on the ultimate aims of the research, chamber design must consider materials of construction, the point of introduction of study aerosols, and location of any sampling ports (Lidén *et al.*, 1998; Lundgren, 2006). Temperature, pressure, and relative humidity can all have substantial effects on aerosol characteristics so researchers must decide from the outset if the chamber should be designed to control these parameters or if it is sufficient to simply monitor them (Rønborg *et al.*, 1996; Lidén *et al.*, 1998; Lundgren, 2006; Isaxon *et al.*, 2013; Hagerman *et al.*, 2014). Even after construction, work cannot begin without a thorough understanding of the chamber characteristics, to include the achievable air velocities, airflow patterns, and spatial and temporal variability of particle movement (Lidén *et al.*, 1998; Lundgren, 2006; Lundgren *et al.*, 2006; Pieretti and Hammad, 2018). Since the air speed within the chamber as well as air exchange rates have considerable effects on aerosol behavior, it is crucial to understand what operating parameters impact their values (Lidén *et al.*, 1998; Lundgren *et al.*, 2006; Isaxon *et al.*, 2013; Pieretti and Hammad, 2018). In addition, the mixing

behavior of the chamber has significant effects on aerosol behavior as it impacts evenness of exposures (Lidén *et al.*, 1998; Lundgren, 2006; Isaxon *et al.*, 2013).

2.1.1 Chamber Design Considerations

This work aims to describe the design, construction, and characterization of an aerosol exposure chamber for wide-ranging experiments with a variety of test aerosols. The design was based on accomplishing two near-term research projects: testing the operational parameters of the Institute of Occupational Medicine (IOM) inhalable samplers and the decontamination of a litter-bound patient. As these projects had quite different requirements, the design of the chamber was meant to maximize flexibility. Due to the size of a standard NATO litter (23” x 90” x 6.5”) and space available at the research facility it was decided that 2.5 feet by 2.5 feet would be the minimum cross section considered (NATO, 2013). Air velocities inside the chamber needed to be similar to those encountered in common indoor workplaces, from office spaces which approach calm environments (<0.3 m/s) to those spaces which require robust ventilation to protect against particulate hazards (≥ 0.5 m/s) (Baldwin and Maynard, 1998; Bennett, 2018). Considering the desire to mimic workplace environments, it was determined that ambient air condition would be suitable and no effort was made to control temperature and humidity. In order to accommodate yet unknown future research needs, modularity was desirable.

Early designs aimed for laminar flow inside the chamber and basic fluid dynamics calculations were undertaken to determine if this would be possible within the space constraints. First, the effect of temperature was considered, and the Reynolds number

(Re) was determined for a range of temperatures from 55-85°F, as this represented what could reasonably be expected in indoor workplaces. For each temperature, the appropriate density and dynamic viscosity were used (Engineers' Edge, 2019). The square cross-section of 2.5 feet was converted to equivalent pipe diameter and air velocities from 0.1-1 m/s were considered. The Re was calculated using Equation 1.

Equation 1. Reynolds Number

$$\mathrm{Re} = \frac{Du\rho}{\mu}$$

where,

$\mathrm{Re} = Reynolds\ number$
$D = the\ pipe's\ diameter\ (m)$
$u = fluid\ velocity\ \left(\frac{m}{s}\right)$
$\mu = the\ fluid's\ \ viscosity\ (\frac{N * s}{m^2})$
$\rho = the\ fluid's\ \ density\ (\frac{kg}{m^3})$

This resulted in Reynolds number ranging from 4,265 to 59,468 (conditions of T = 85°F, u = 0.1 m/s and T = 55°F, u = 1 m/s respectively). No conditions considered resulted in laminar flow, thus turbulent flow equations were used for subsequent design iterations.

While lacking the consistent uniformity of laminar flow, it has been documented that turbulent flow can fully develop to approximate predictable behavior. For the purpose of this design, flow was considered fully developed if the boundary layers converged (de Nevers, 2005). In order to determine if this condition could be met, boundary layer calculations for smooth surface with 2.5-foot cross-section were carried

out. A simplified equation for boundary layer thickness on a flat plate was used, due to the difficulties involved in determining numerical solutions for turbulent airflow (Equation 2) (de Nevers, 2005). Air temperature was assumed to be 21°C (the midpoint of the range tested for the Re), giving air a kinematic viscosity of 1.156 x 10^{-5} m^2/s. The same air velocities were used as for the Re calculations and the distance from the chamber entrance (z in Equation 2) was varied from 0.5 to 12 feet.

Equation 2. Boundary Layer Thickness

$$\delta = 0.37z\left(\frac{v}{u_{infinity}z}\right)^{\frac{1}{5}}$$

where,

$\delta = boundary\ layer\ thickness\ (m)$
$z = distance\ along\ z-axis\ (m)$
$v = kinematic\ viscosity\ of\ the\ fluid\ (\frac{m^2}{s})$
$u_{infinity} = final\ velocity\ (\frac{m}{s})$

These conditions resulted in boundary layer thicknesses ranging from 0.35 to 7.08 inches (corresponding to u = 1 m/s, z = 0.5 feet and u = 0.1 m/s, z = 12 feet respectively). These calculations show that fully developed flow does not occur by the midpoint of a 2.5 ft square chamber, which adds an additional degree of difficulty, due to the need to carefully characterize all locations within the chamber in order to conduct reproducible experiments.

As calculations indicated that achieving laminar and fully developed turbulent flow would be impossible within the real-world space constraints, the final design was a rectangular chamber with dimensions of 3 x 3 x 21 feet. Polycarbonate was chosen as the

material for the walls, in order to allow researchers to monitor experiments. As the chamber would not be subjected to either vacuum or pressure, 0.3” wall thickness was deemed adequate. The frame was constructed out of aluminum (80/20 Inc, Columbia City, IN). The final chamber design and fabrication was conducted by the AFIT Model shop in three seven-foot sections which could be joined at the seams to form a single continuous chamber (Figure 2). The middle section included a door which opened for access to the interior of the chamber. Air enters and is exhausted through banks of HEPA filters. Air is moved through the chamber by a centrifugal fan equipped with a variable frequency drive located downstream (Model HDBI-120, Cincinnati Fans, Cincinnati, OH).

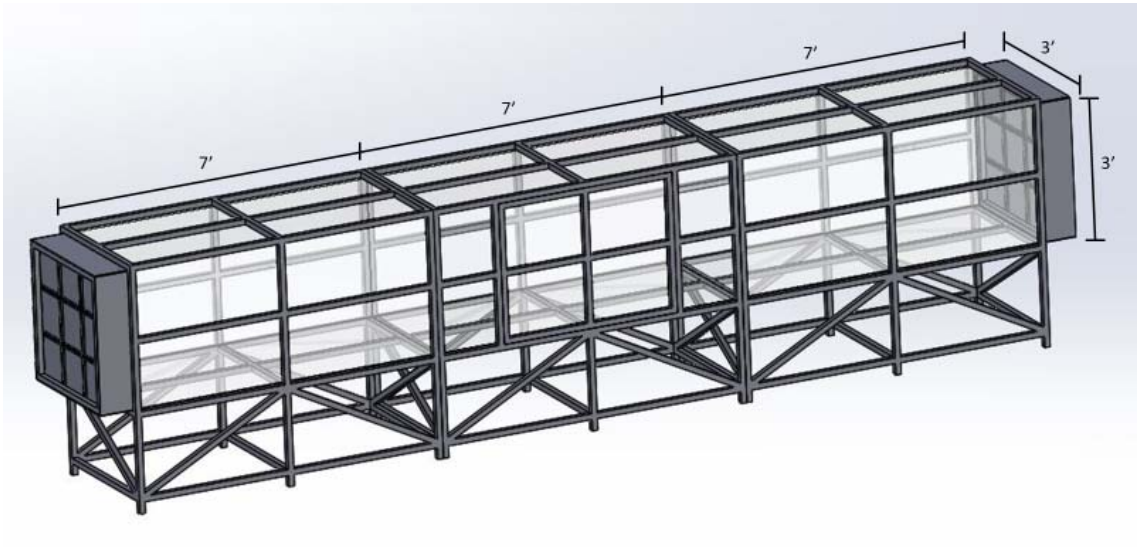

Figure 2. Final Chamber Design

After construction and delivery of the final chamber, all inside seams were caulked to seal them and the seams between chamber sections were sealed with Gorilla

Tape® to facilitate removal if the chamber sections needed to be detached for cleaning or relocation. Once these activities were completed, characterization of the chamber began.

As turbulence was expected, tests were conducted with and without a flow straightener (Model: AS100, Ruskin, Kansas City, MO) in place. As the door was placed in the center section to allow access to equipment, all tests with the flow straightener took place with the straightener located on the seam between the inlet chamber and the center chamber. All tests without the flow straightener included measurements from all three chambers while those with the flow straightener excluded the first chamber.

2.2 Chamber Characterization Methodology

2.2.1 Velocity Mapping

Velocity mapping was done to understand the air speed characteristics along the face of each plane and longitudinally along the length of the chamber. Mapping was done using a VelGrid attached to an AirData Multimeter (ADM-880c) data logger (Shortridge Instruments, Inc, Scottsdale, AZ).

The VelGrid is designed for measuring the face velocity profile. It consists of two crossed pieces, each with a smaller crossed piece near the end of each arm. There are 16 holes to capture air, four on each arm of the device. The VelGrid covers a 14” x 14” square area and records the average velocity from all 16 points within this square. In this experiment, three VelGrids were used simultaneously to cover a vertical slice of a face of the chamber (Figure 3).

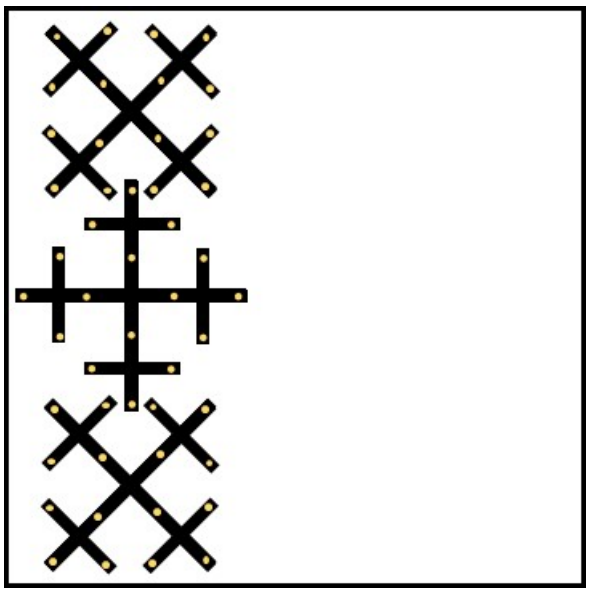

Figure 3. VelGrid Configuration in Chamber Cross-Section

Data were recorded using the ADM-880c logger in automatic mode. In this mode, data points were recorded as quickly as the machine could process them, no more than 10 seconds apart. The logger stored all data points which were downloaded from the device at regular intervals. The ADM-880c has the capability to automatically correct velocity for atmospheric temperature and pressure variations, as shown in Equation 3.

Equation 3. Temperature Correction for Velocity

$$Local\ Density\ Velocity = Velocity\ in\ local\ density\ mode * \sqrt{\frac{460 + °F}{530}}$$

While the ADM-880c has the ability to automatically correct velocity for temperature and pressure, it cannot account for relative humidity. This was done manually (shown in Appendix D) by using the air temperature and relative humidity collected by a Kestrel 4000 Pocket Weather Tracker (KestrelMeters.com, Boothwyn,

PA). The instrument was set to record all data, every 20 minutes. The relative humidity data from the Kestrel 4000 was used to correct the velocity measurements for humidity.

To measure the velocity in the aerosol chamber, the chamber was divided into imaginary block 1 foot x 1 foot x 1 foot. Starting in chamber one, located at the opposite end from the fan (the air inlet), the chamber was labelled in one-foot increments along the z-axis. The chamber was lettered along the x-axis, with the imaginary cube on the side of the chamber furthest from the door being labelled 'A', the one in the middle 'B', and the one nearest the door labelled 'C' (Figure 4). These were used to label a specific measurement position in the chamber (i.e. 5A being 5 feet from the air inlet, at the position farthest from the door).

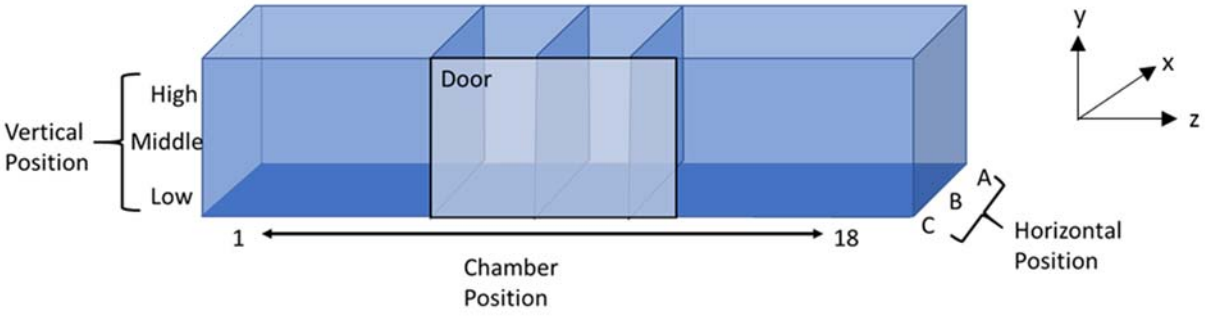

Figure 4. Chamber Measurement Locations

At each measurement location all three VelGrids were used to measure the vertical profile. Each of the stacked VelGrids was given a designation: low (1), middle (3), high (5) (Figure 5). These numbers were also used to designate a specific block within the chamber (i.e. 8B-low being 8 feet from the air inlet, at the middle position of the chamber along the x-axis, the lowest measurement point along the y-axis).

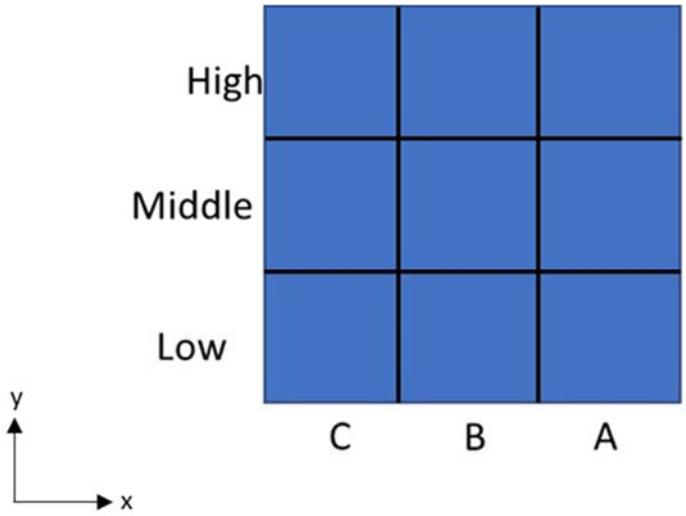

Figure 5. Plane Measurement Configuration

In the initial measurement of air velocity, the three VelGrids were stacked by clamping their poles to a ring stand. The poles were clamped at the break between the second and third sections to avoid any backwash turbulence from disturbing the velocity measurements. This was done for all measurement locations except 18 as the poles were too long so the third section was removed and the pole was clamped a third of the way from the end. The VelGrid faces were placed in the chamber at the measurement location, with each location marked with a piece of tape on the outside of the chamber to ensure alignment of the faces. For A and C positions, the middle VelGrid (called 3) was positioned to touch the wall. For B position, the lowest VelGrid (called 1) was positioned so the two cross arms were centered on the lower support bar of the chamber.

Once the VelGrids were positioned, the ADM-880c data loggers were attached and turned on to start recording data. The chamber was closed, the two sides of the door seams were sealed with tape, and the fan was turned on.

For each run, the fan was dialed up through the desired speeds using the variable frequency drive. In order to characterize the velocity across the full range of the fan, three frequencies were chosen: 60 Hz, 30 Hz, and 16 Hz. It was determined that 60 Hz would equates to an air speed of approximately 1 m/s, 30 Hz would be 0.5 m/s, and 16 Hz would be 0.2 m/s. The ADM-880c data logger had a limit of detection of 25 fpm, or 0.127 m/s. For each run, the fan was dialed to 16 Hz, then allowed to stabilize for a minute before the three-minute measurement period was started. After the three-minute measurement period, the fan was dialed to 30 Hz, given a minute to stabilize and then measured for three minutes. Finally, the fan was dialed to 60 Hz, and the stabilization and measurement periods were repeated.

Once the measurement period for 60 Hz was finished, the fan was turned off, the chamber was opened and the VelGrids were moved to the next measurement location along the x-axis. For collection of the initial set of data, the measurement locations were done sequentially (1A, 1B, 1C, 3A, 3B, 3C, etc.).

In order to validate the repeatability of measurements, certain locations within the chamber were selected for duplicate measurements on different days. For these checks, measurement locations were sequentially assigned a number and then Excel was used to generate a random number which was then used as the location. For the second round of random checks, the same locations were sampled a third time, by sequentially assigning each one a number and then using Excel to generate a random number for the sample order. One third of the original sampling locations were sampled during the random checks (14 of 39 without the flow straightener, 9 of 27 with the flow straightener in place).

In addition to the initial air speed characterization, the air velocities were measured while clean air ran through the dust generator to ensure that the introduction of another air stream did not significantly disrupt the established airflow patterns. This was measured only at four planes within the chamber: 5 and 7 without the flow straightener present, and 8 and 10 with the flow straightener in place. These measurements were repeated with two different settings on the generator, the highest and lowest flows, to ensure that neither setting had a significant effect on the established airflow patterns. Final analysis showed no impact to the established flow patterns so aerosol studies commenced.

2.2.2 Spatial Variability

Spatial variability of the chamber was examined using UltraFine Arizona Road Dust (ARD) (Particle Technology Inc., Arden Hills, MN) lofted by a rotating brush generator (RBG) 1000 dust generator (Palas GMBH, Karlsruhe, Germany) while real-time measurements were obtained with a particle counter.

Sampling probes channeled dust from the chamber to an optical particle sizer, OPS model 3330 (TSI, Inc., Shoreview, MN) to obtain particle distribution and concentration. One OPS reading was taken for two minutes, then the probe was moved to a new location (Figure 6).

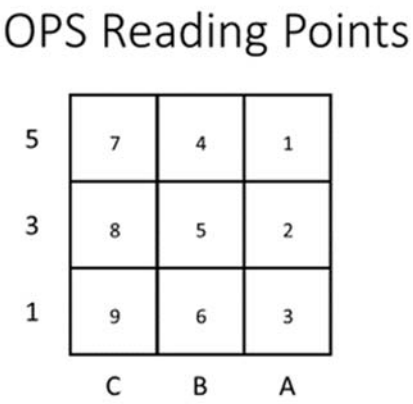

Figure 6. OPS Reading Positions in a Cross-Sectional Plane

Sampling planes were chosen based on those planes with the most consistent air velocities. Two planes were chosen which could be used without the flow straightener present (planes 5 and 7) and two planes were chosen which could be used with the flow straightener in place (planes 8 and 10).

For initial tests, the fan was set to 30 Hz. After the fan was turned on, the RBG dust generator was turned on. The compressed air line was set to 80 psi, and the pressure regulator on the RBG was set to 1 bar. The feed rate was set to 60 mm/hr. This gave a run time of approximately 40 minutes in most cases based on the amount of the reservoir filled. The brush speed was set to 1200 revolutions per minute per the manufacturer recommendation. Fifteen samples were taken per plane and experiments repeated on multiple days to capture inter-day variability.

2.3 Analysis and Results

Velocity data were visualized as contour plots using the open source software R (Version 3.6.0). Breakpoints for the velocity were chosen based on the VelGrid's precision, ± 3% + 7 fpm (Shortridge Instruments, 2009). When plotted, data for the entire chamber without a flow straightener showed unevenness of flow throughout the chamber, though the least variability was observed in the middle slice of the chamber, away from horizontal position C (Figure 7). Velocity plots for when the fan operated at 30 Hz and 60 Hz are available in Appendix E. All three fan speeds showed velocity spikes at chamber locations 9 and 12, indicating gaps in the door.

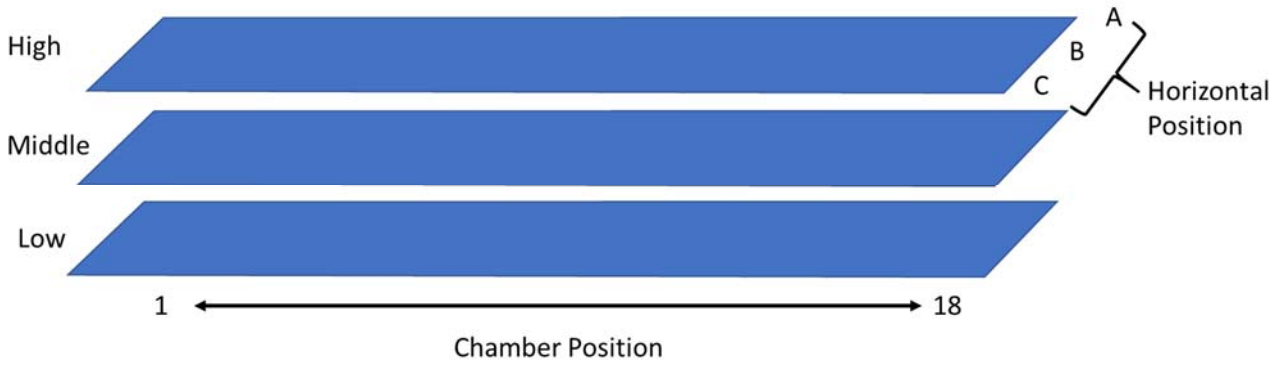

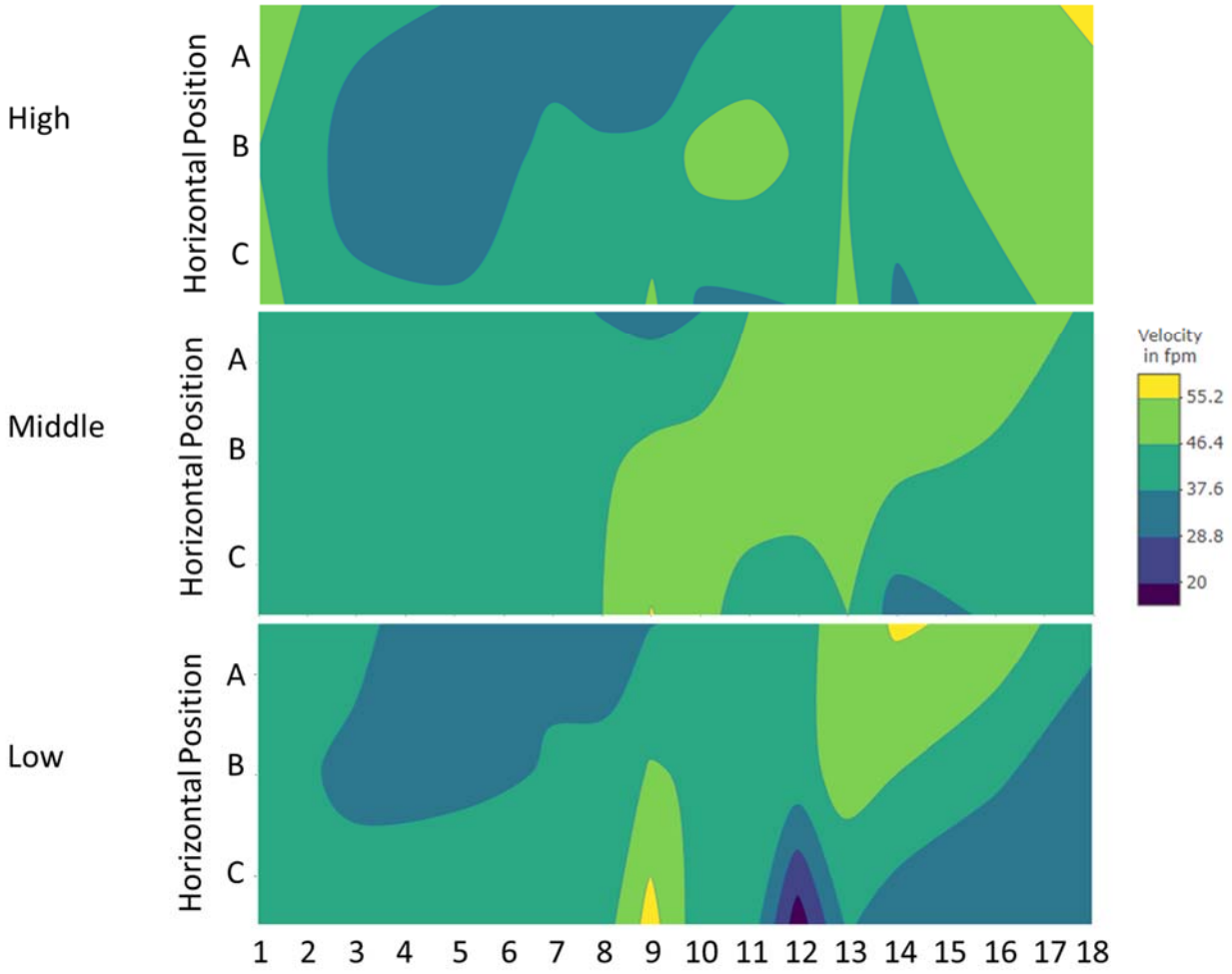

Figure 7. Vertical Velocity Profiles in the Chamber at 16 Hz, no Flow Straightener

Plotted data for flow-straightened air followed the same pattern observed without the flow straightener. The straightener was placed at chamber position 7, in hopes that it would improve stability in sections 8 – 13, allowing for experiments to take place within easy reach of the only access point, the door. Despite the flow straightener, disturbances at chamber positions 9 – 12 persisted (Figure 8). Profiles for 30 Hz and 60 Hz are available in Appendix E.

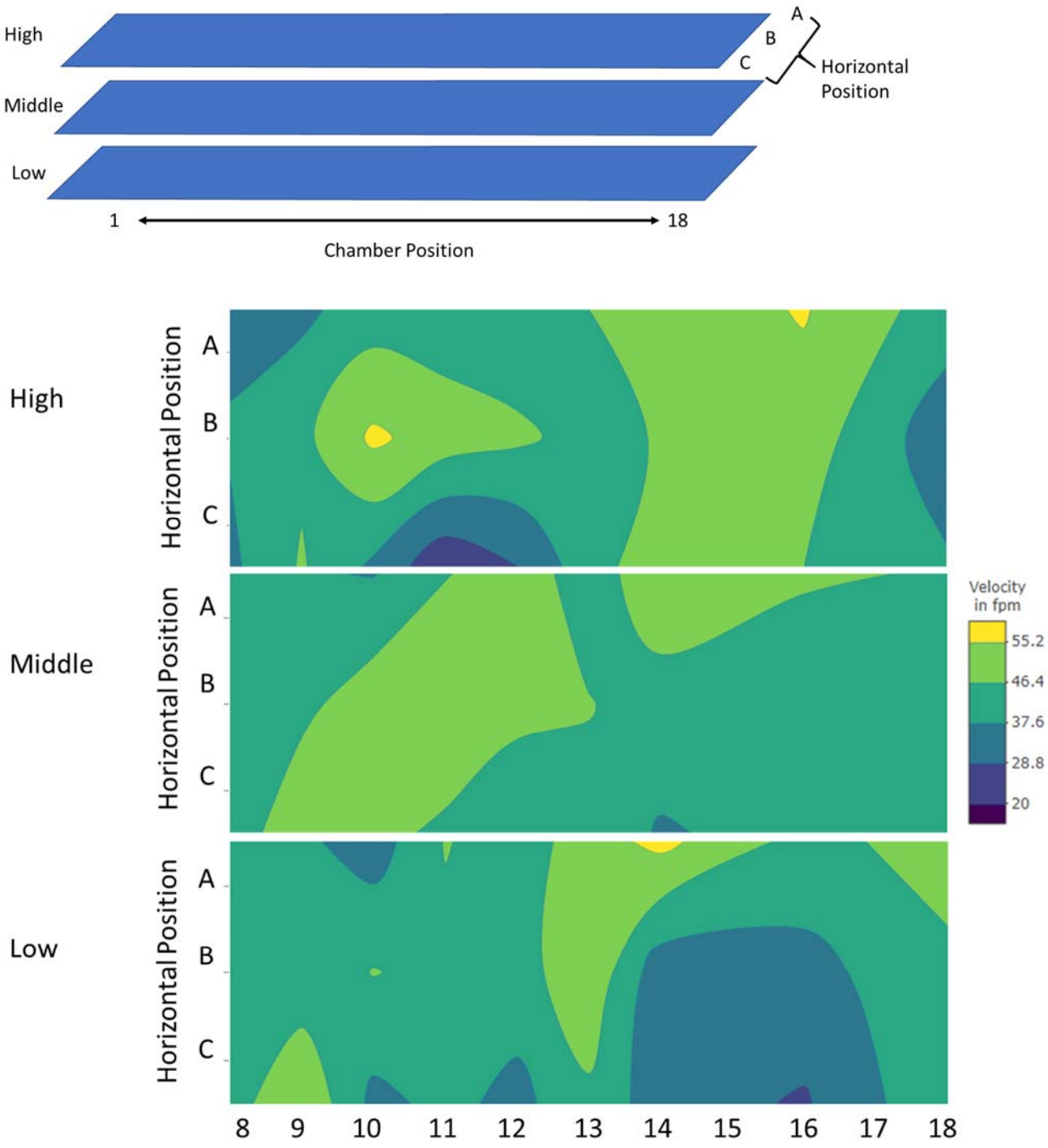

Figure 8. Vertical Velocity Profiles in the Chamber at 16 Hz, with Flow Straightener

Considering the uneven profiles collected along the chamber length, measurements were taken across different days to verify the repeatability of measurements. In Figure 9, the initial measurements are shown as black dots. Measurements collected on subsequent days are shown as red and blue dots. The pink ribbon shows the uncertainty surrounding the initial measurements. Using the Grubbs' test only one outlier, noted with a black circle, was identified. Repeated measurements at 30 Hz and 60 Hz are available in Appendix F.

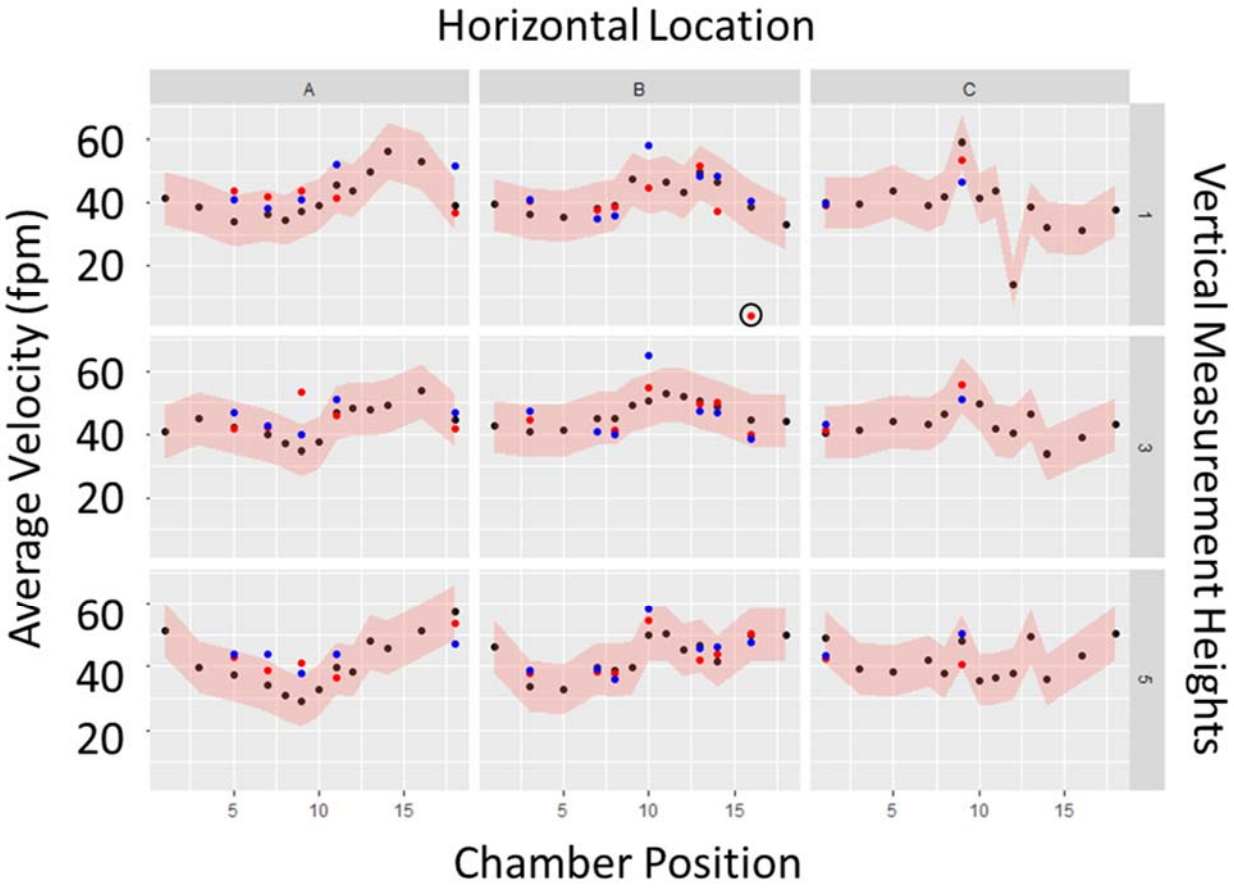

Figure 9. Day-to-Day Variability in Average Velocity at 16 Hz, no Flow Straightener

Results were similar for velocities measured with the flow straightener. Another outlier was observed at chamber position 16, suggesting transient slow velocities (Figure 10). The remaining variability plots are available in Appendix F. The variability observed was deemed controlled enough to proceed with further characterization without modification of the chamber.

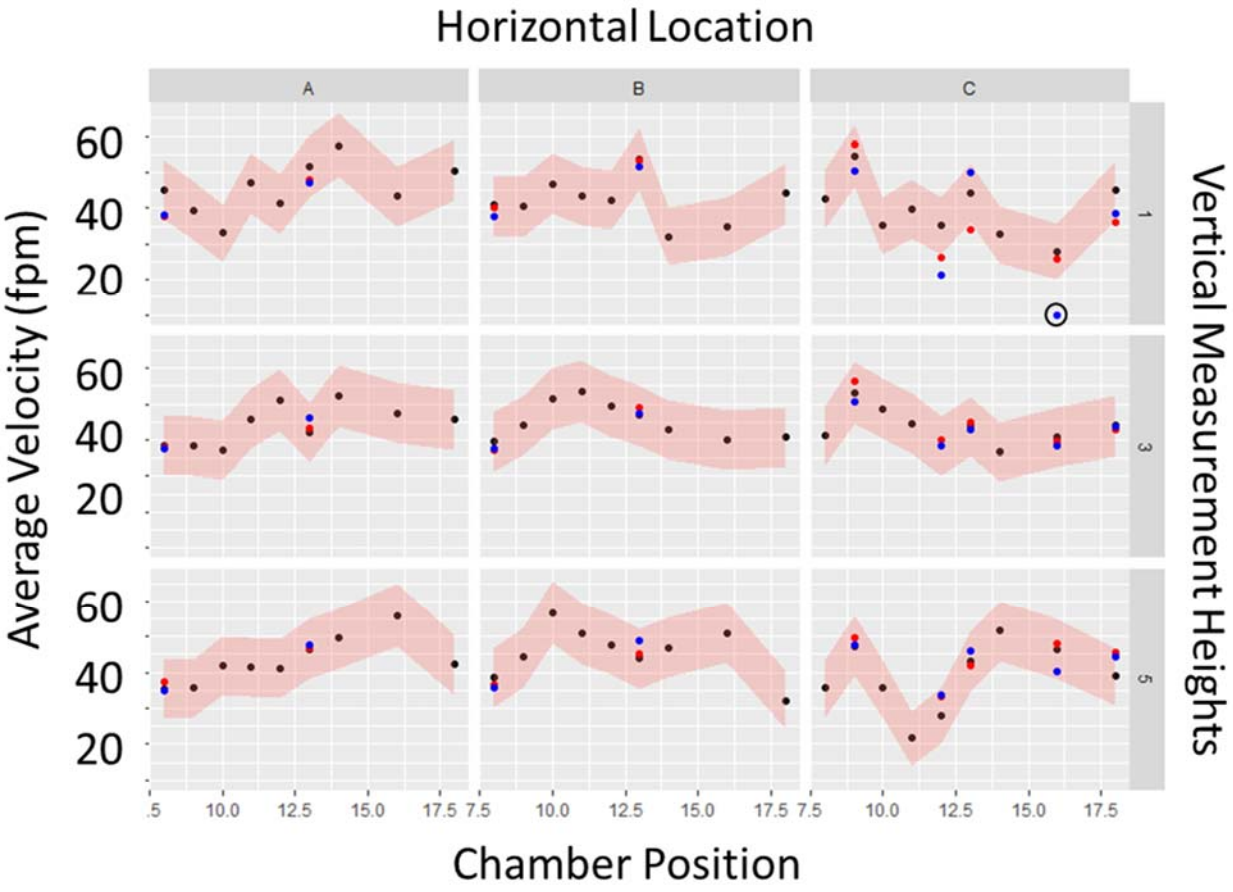

Figure 10. Day-to-Day Variability in Average Velocity at 16 Hz, with Flow Straightener

Velocity data were evaluated qualitatively and quantitatively for normality using quantile-quantile plots and the Shapiro-Wilkes test. Data collected without a flow

straightener did not behave normally; however, those collected with the flow straightener in place did behave normally (Figure 11).

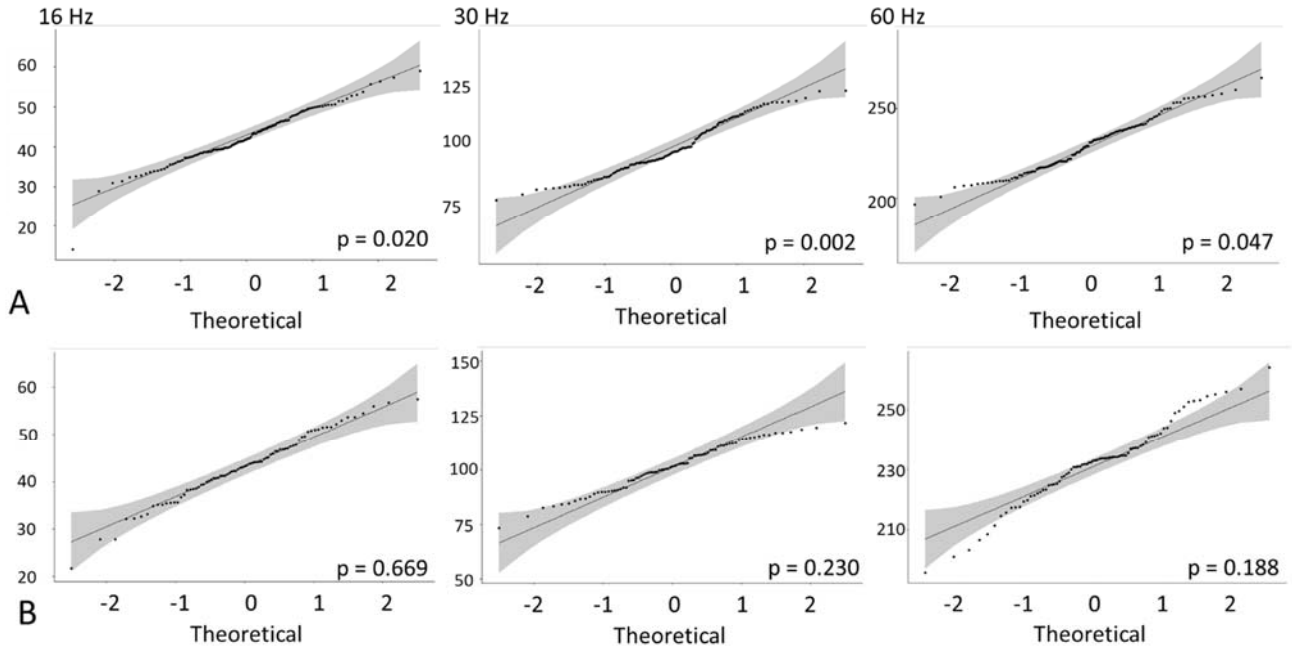

Figure 11. Quantile-Quantile Plots of Velocity Measurements: A) no Flow Straightener; B) with Flow Straightener

Data were tested for equal variance using Levene's test for data procured without the flow straightener and Bartlett's test for those procured with the flow straightener. In Levene's test, Pr(>F) should be less than the chosen cutoff value to reject the null hypothesis of equal variance. For Bartlett's test, the p-value must be less than the specified cutoff to reject the null. In this study, a significance of 0.05 was chosen as the cutoff.

Table 2 shows the results of Levene's test for a variety of conditions: the longitudinal chamber position alone, the chamber position with regard to the vertical position, the chamber position with regard to the horizontal position, and the horizontal

position with regard to the vertical position. Of these conditions, it was desirable to achieve either equal variance along the chamber length or equal variance within one plane at a specific chamber position. With respect to only the chamber position, equal variance could not be assumed for fan speeds 30 and 60 Hz. The null hypothesis could not be rejected for any fan speed when considering the horizontal and vertical position, suggesting that in a plane at a specific chamber location, equal variance exists. While equal variance for chamber position with respect to the vertical or horizontal positions failed to reject the null, these conditions were not physically meaningful as they implied a long rectangular prism with equal variance, but unequal velocities. It is unlikely any sampling scenario would rely on that specific combination of conditions.

Table 2. Results of Levene's Test for Equal Variance for Velocity Data without Flow Straightener

Fan Frequency (Hz)	Chamber Position only			Chamber Position, Vertical Position			Chamber Position, Horizontal Position			Horizontal Position, Vertical Position		
	Df	F	Pr(>F)	Df	F	Pr(>F)	Df	F	Pr(>F)	Df	F	Pr(>F)
16	12	1.7	0.077	38	0.502	0.990	38	0.502	0.990	8	0.771	0.629
30	12	3.200	0.0006	38	0.597	0.959	38	0.597	0.959	8	1.100	0.370
60	12	2.705	0.0032	38	0.528	0.984	38	0.528	0.984	8	0.558	0.810

These results for the horizontal and vertical position interaction were qualitatively evaluated through boxplots (Figure 12). The conclusion remains the same though the extent of the variances is visually more apparent.

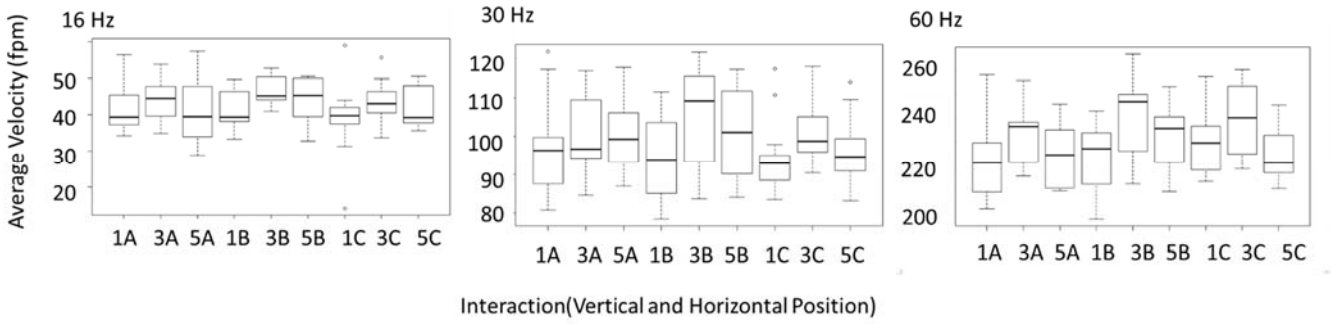

Figure 12. Variance of Velocity Profiles for without Flow Straightener Data

Data collected with the flow straightener, when analyzed with Bartlett's test for equal variance, generated results similar to those found in the data without the flow straightener. Only chamber position alone resulted in p-values that necessitated the rejection of the null hypothesis (Table 3).

Table 3. Results of Bartlett's Test for Equal Variance for Velocity Data with Flow Straightener

Fan Frequency (Hz)	Chamber Position only			Chamber Position, Vertical Position			Chamber Position, Horizontal Position			Horizontal Position, Vertical Position		
	K^2	df	p	K^2	df	p	K^2	df	p	K^2	df	p
16	14.59	8	0.067	32.42	26	0.18	25.53	26	0.489	5.59	8	0.69
30	19.43	8	0.013	34.74	26	0.12	33.58	26	0.15	0.45	8	0.99
60	31.15	8	0.0001	51.07	26	0.002	47.81	26	0.006	9.76	8	0.28

Results for the horizontal and vertical position interaction were again qualitatively evaluated through boxplots (Figure 13). Variances remained large overall.

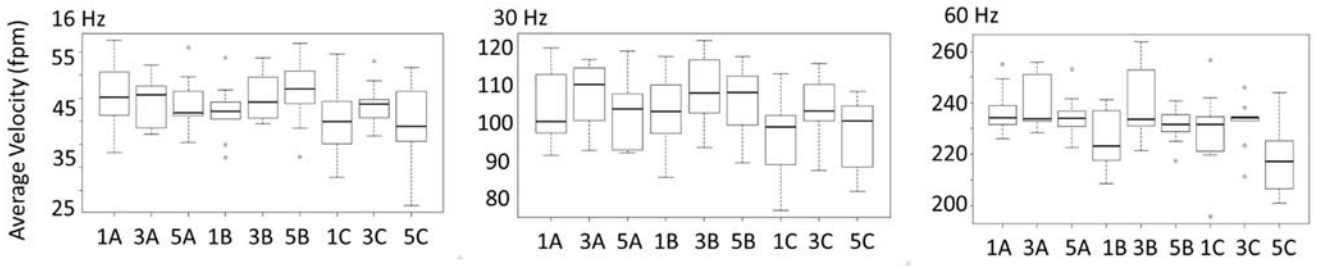

Figure 13. Variance of Velocity Profiles for with Flow Straighter Data

Planes 5 and 7 without the flow straightener and planes 8 and 10 with the flow straightener were chosen for further characterization. Every two-minute sample at a single location in the plane was transformed from raw counts to the mean mass diameter through the process described below. Next, the geometric mean of each bin was computed (Equation 4) where d_i is the midpoint of the ith bin and n_i is the number of particles in that bin. N represents the total number of bins.

Equation 4. Geometric Mean

$$\text{Geometric Mean} = \left(\prod_{i=1}^{N} d_i^{n_i}\right)^{\frac{1}{N}}$$

The midpoint for each particle size bin of the optical particle counter (OPC) was determined by averaging the extremes of the range. The volume of the particle this midpoint represented was calculated using Equation 5 where $d_{midpoint}$ is the diameter of the midpoint of the bin in meters.

Equation 5. Volume of Particle

$$\text{V}(\text{m}^3) = \frac{\pi\left(d_{midpoint} * 10^{-6}\right)^3}{6}$$

The mass the particles counted in each bin was computed with Equation 6, which assumed a particle density (ρ) of 500 kg/m^3 per the manufacturer's safety data sheet (SDS).

Equation 6. Conversion of Count to Mass per Bin

$$\text{Mass (mg)} = (\rho * count * particle\ volume) * 10^6$$

Each bin was normalized by dividing the mass by the bin width, resulting in a frequency/µm. The frequency was converted to a fraction by dividing the previous value by the total mass observed in all bins. The cumulative mass was calculated by dividing the mass per bin by the total mass of all bins.

The natural log of the midpoint diameter per bin was taken and this value multiplied by the number of particles in the bin. The average of this column was the count mean diameter (CMD) (Equation 7).

Equation 7. Calculation of CMD

$$\text{CMD (µm)} = \frac{\sum_{i=1}^{N} n_{particles,bin\ i} * \ln(d_{midpoint\ of\ bin\ i})}{N}$$

For the mass mean diameter (MMD), the natural log of the midpoint particle diameter for the bin was multiplied by the mass in the bin. The average of all the bin values was the MMD (Equation 8).

Equation 8. Calculation of MMD

$$\text{MMD (µm)} = \frac{\sum_{i=1}^{N} mass_{particles,bin\ i} * \ln(d_{midpoint\ of\ bin\ i})}{N}$$

The geometric standard deviation (GSD) for the CMD was calculated using Equation 9.

Equation 9. Calculation of GSD for CMD

$$\mathrm{GSD_{CMD}} = e^{\left(\sum_{i=1}^{N}\left(\ln\left(\frac{d_{midpoint\ of\ bin\ i}}{d_{CMD}}\right)\right)^2 * n_{particles,bin\ i})/(n_{particles,bin\ i}-1\right)^{0.5}}$$

The GSD for the MMD followed a very similar process, with the exception of substituting in the MMD and mass instead of CMD and number of particles (Equation 10).

Equation 10. Calculation of GSD for MMD

$$\mathrm{GSD_{MMD}} = e^{\left(\sum_{i=1}^{N}\left(\ln\left(\frac{d_{midpoint\ of\ bin\ i}}{d_{MMD}}\right)\right)^2 * mass_{particles,bin\ i})/(mass_{particles,bin\ i}\right)^{0.5}}$$

The MMD calculated from each reading was plotted by horizontal position, then vertical position to discern if aerosol distribution was more stable from side-to-side or top-to-bottom in the plane (Figure 14). The 30 Hz setting yielded the most consistent results though the MMD reported at any fan setting and any location only ranged from 3.5 – 4.25 μm. The boxplots for planes 7, 8, and 10 are available in Appendix H.

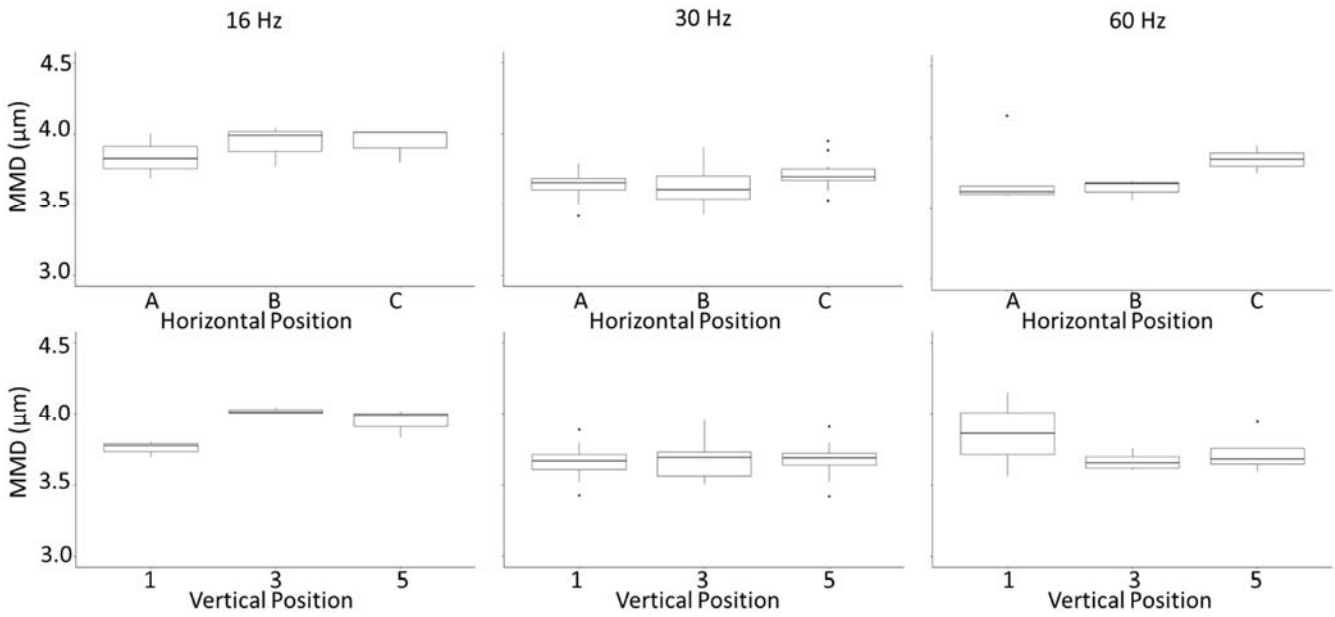

Figure 14. MMD Boxplots for Plane 5

Considering the MMD boxplots, contours of the velocity and particle count profiles were generated to visualize airflow and aerosol patterns by plane (Figure 15). These final contours served as guidelines for follow-on research sampler placement. The complete set of contour maps by plane and fan setting are found in Appendix I.

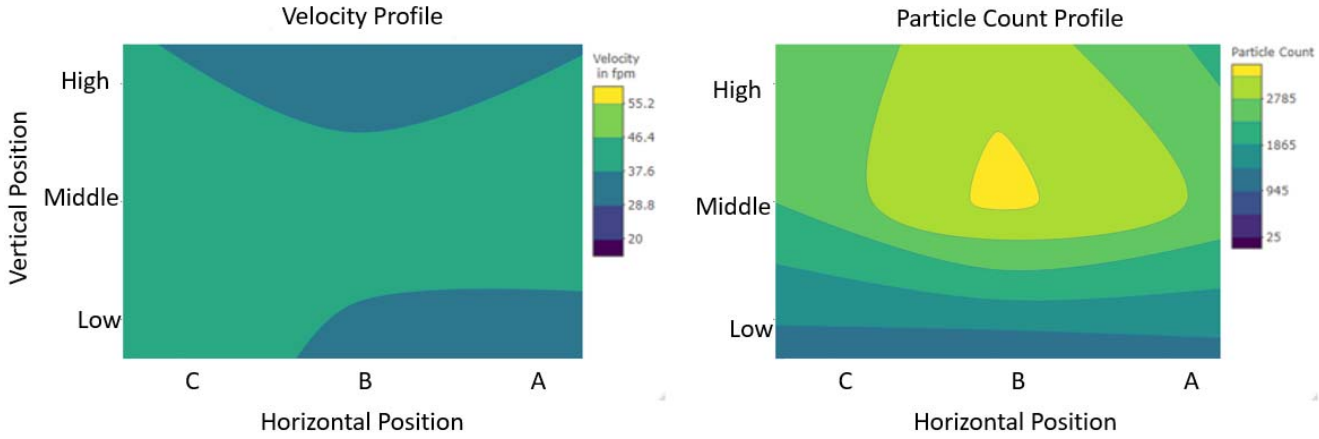

Figure 15. Velocity and Particle Count Profiles in Plane 5 at 16 Hz

All data gathered and analyzed confirmed initial design expectations, in that flow was turbulent and irregular along any plane of interest. Aerosol distribution data were encouraging as the distribution, if not the raw counts, were similar at all nine points sampled for each plane.

2.4 Conclusions and Recommendations

A 21-foot chamber with three-foot square cross-section was constructed to serve as a test space for aerosol studies. Air flow profiles were generated by measuring velocity at prescribed locations along the x-, y-, and z-axes. Aerosol size distribution profiles were created for the four planes identified as most stable with and without the flow straightener. Inter-day variability was deemed acceptable considering the limitations of the anemometer. This finding supports the use of the chamber for future studies without modification. While equal variance existed across x-y planes in the chamber, the magnitude of the variance was considerable. This considerable variance suggests researchers must either collect large sample sets to detect significance among the data or restrict their activities to a smaller, better defined subsection of a given plane.

The analysis conducted could be strengthened with a computational fluid dynamics (CFD) model. CFD could explain outlier observations (such as chamber location 16) and allow researchers to predict the impact to flow behavior when different sampling apparatus are in place prior to conducting any pilot research. It is apparent that improvements to the door's seal could be made and CFD models could inform what an improved design would look like. Finally, the flow was only characterized at three fan settings, using the aerosol behavior at a single fan speed. It stands to reason that

subsequent research may rely on intermediate velocities to achieve their research aims. A working model of the chamber could predict flow behavior that could be easily validated with judicious sampling instead of repeating the entire characterization outlined in this report. A functional CFD model would ultimately save researchers' time and funds, making it a worthwhile endeavor.

Even without a CFD model, the data collected and analyzed in this study confirm the chamber performance is stable enough for a variety of research aims. Periodic confirmation of chamber performance is recommended. Any significant changes to the setup, including the replacement of the access door require a complete recharacterization. With the present setup, researchers will need to conduct pilot studies to capture any bias inherent in the selected chamber location before proceeding to full scale studies.

Bibliography

Baldwin, P. E. J. and Maynard, A. D. (1998) 'A Survey of Wind Speeds in Indoor Workplaces', *Annals of Occupational Hygiene*, 42(5), pp. 303–313. doi: https://doi.org/10.1016/S0003-4878(98)00031-3.

Bennett, J. *et al.* (2018) 'Effect of ventilation velocity on hexavalent chromium and isocyanate exposures in aircraft paint spraying', *Journal of Occupational and Environmental Hygiene*, 15:3, pp 167-181. doi: 10.1080/15459624.2017.1401710.

Brice, T. and Hall, T. (no date) 'Vapor Pressure'. El Paso, TX: National Weather Service, NOAA.

Edge, E. (2019) *Viscosity of Air, Dynamic and Kinematic*. Available at: https://www.engineersedge.com/physics/viscosity_of_air_dynamic_and_kinematic_14483.htm (Accessed: March 2019).

Hagerman, I. *et al.* (2014) 'Effects on heart rate variability by artificially generated indoor nano-sized particles in a chamber study', *Atmospheric Environment*, 88, pp. 165–171. doi: 10.1016/j.atmosenv.2014.02.003.

Isaxon, C. *et al.* (2013) 'Realistic indoor nano-aerosols for a human exposure facility', *Journal of Aerosol Science*, 60, pp. 55–66. doi: 10.1016/j.jaerosci.2013.02.003.

Lidén, C. *et al.* (1998) 'A New Whole-body Exposure Chamber for Human Skin and Lung Challenge Experiments - the Generation of Wheat Flour Aerosols', *Annals of Occupational Hygiene*, 42(8), pp. 541–547. doi: 10.1016/S0003-4878(98)00063-5.

Lundgren, L. *et al.* (2006) 'Large Organic Aerosols in a Dynamic and Continuous Whole-Body Exposure Chamber Tested on Humans and on a Heated Mannequin', *Annals of Occupational Hygiene*, 50(7), pp. 705–715. doi: 10.1093/annhyg/mel027.

Lundgren, L. (2006) *Large organic aerosols in a human exposure chamber: Applications in occupational dermatology and lung medicine*. Karolinska Institutet. Available at: https://openarchive.ki.se/xmlui/bitstream/handle/10616/39694/thesis.pdf?sequence=1&isAllowed=y.

NATO (2013) 'NATO Standard AMedP-2.1, Stretchers, Bearing Brackets and Attachment Supports'. North Atlantic Treaty Organization NATO Standardization Agency, pp. 1–22.

de Nevers, N. (2005) *Fluid Mechanics for Chemical Engineers*. 3rd edn. New York, NY: McGraw-Hill Companies.

Pieretti, L. F. and Hammad, Y. Y. (2018) 'Performance of a whole-body human dust inhalation challenge exposure chamber', *Toxicology Reports*, 5, pp. 793–799. doi: 10.1016/j.toxrep.2018.07.004.

Rønborg, S. M. *et al.* (1996) 'Exposure chamber for allergen challenge: The development and validation of a new concept', *Allergy: European Journal of Allergy and Clinical Immunology*, 51(2), pp. 82–88. doi: 10.1111/j.1398-9995.1996.tb04562.x.

Shortridge Instruments. (2009). Airdata Multimeter ADM-8800 Operating Instructions. Scottsdale, AZ: Shortdige Instruments, Inc.

Toolbox, E. (2004) *Relative Humidity in Air*. Available at: https://www.engineeringtoolbox.com/relative-humidity-air-d_687.html (Accessed: 3 January 2020).

III. Aerosol Characterization of Abrasive Blasting Operations

Chapter Overview

The purpose of this chapter is to characterize the aerosol properties of particulate generated during abrasive blasting. Samples were collected from the field by industrial hygienists at Hill AFB. This chapter seeks to answer research aims one and two.

The target journal for this paper is Aerosol Science and Technology.

3.1 Introduction

It is well established that particulate matter in the work place poses health hazards to unprotected workers. Like gas and vapor contaminants, the concentration and composition of the particulate matter determine the severity of the hazard; however, the distribution of particle sizes also contributes to potential health effects (Mirowsky, 2013; Lippmann, 1999; Kan, 2018). Due to the increasingly narrow branches that make up the lower respiratory tract, only particles up to 4 μm can penetrate the alveolar region of the lungs (Phalen, 1999). Coarse particles ≤10 μm penetrate the thoracic region and particles larger than 10 μm up to 100 μm penetrate primarily to the upper airways and nose (Phalen, 1999).

Particle size selective (PSS) samplers are designed to mimic the penetration of particles in the respiratory system by abiding by a 50% cut point at 4 μm, 10 μm, and 100 μm for respirable, thoracic, and inhalable particles respectively (Raabe, 1999; Vincent, 1999). It is policy for the American Conference of Governmental Industrial Hygienists

(ACGIH) to include PSS guidance for new threshold limit values for aerosol contaminants.

ACGIH recently recommended sampling for hexavalent chromium using a sampler that adheres to the inhalable convention since large chromium containing particles that deposit in the nose can cause painful ulcers (ACGIH, 2018). In the Department of Defense (DoD), hexavalent chromium exposure is most often found in corrosion control operations during painting and depainting aircraft and their components (Carlton, 2003; Bennett, 2016; Bennett, 2018). While aerosol size and composition during painting operations have been established, little data are available on the characteristics of the dust generated during abrasive blasting procedures, with estimates of particle size ranging from 1 – 1000 μm (Carlton, 1997; Sabty-Daily, 2005; Carlton, 2000).

Aircraft maintenance and associated processes impact a large workforce and generate a high volume of samples. The bulk of prior exposure data was collected using 37-mm closed-face cassettes (CFCs). These cassettes, designed prior to PSS practice, do not adhere to any health-based size convention but instead have efficiencies that drop precipitously at larger particles sizes, with a reported efficiency of 7% at 38.7 μm compared to the 55% dictated by the inhalable convention (Witschger, 2004; Vincent, 1999). This is in stark contrast with the performance of the best-known inhalable sampler, the Institute of Medicine (IOM) sampler, which closely approximates the inhalable convention. In order to compare historical data with data obtained using an IOM, it has been proposed that industrial hygienists apply a correction factor to account for the under sampling inherent in the CFC's design (Vincent, 2007). The issue with this

assumption is that it is based on additional assumptions, including consistent composition of the particulate across the entire size distribution. As the Air Force considers adopting inhalable sampling for corrosion control operations, it would be prudent to verify some of the underlying assumptions associated with the standard correction factor so as not to over- or under-estimate past exposures.

This study focused on characterizing the dust generated during abrasive blasting procedures using real time particle size distribution data, IOM samples, and a bulk dust grab sample. The samples fed a multipronged analytical approach which included microscopic imaging, energy dispersive X-ray spectroscopy (EDS), elemental composition through inductively coupled plasma (ICP), and real-time size distribution data based on optical particle counting.

3.2. Methods

Two types of discrete samples, a single bulk dust sample and five IOM filters, were imaged using a scanning electron microscope (SEM) and evaluated with EDS to determine particle size distribution and surface composition. The bulk dust sample was also evaluated using ICP for elemental chromium.

3.2.1 Bulk Dust Analysis

A 44.4 g bulk dust samples was taken from an abrasive blasting booth and sieved (Precision e-forming, Cortland, NY) into five fractions: >126 µm, 80 – 125 µm, 60 – 79 µm, 40 – 59 µm, and 20 – 39 µm. Each section was weighed and transferred to plastic cylinders compatible with acid digestion. The samples were digested at a third-party lab and run through an ICP for elemental chromium (i.e. all valence states).

Prior to digestion the researcher took a representative sample of the dust from each fraction and mounted them on SEM stubs with conductive carbon tape. As the blasting media was primarily composed of plastic, a nonconductive material, it was expected that a "charging" effect, where electrons load on the surface and fail to dispel causing areas of white, would be observed (Shaffner, 1970). The stubs were sputter coated with 10 nm of gold to provide a continuous conductive surface to minimize charging while imaging. Imaging of each stub included four non-overlapping sections at a consistent magnification. Due to the polydispersity of the largest size fraction, three samples were mounted. From each of these stubs, three images were taken and the nine images were processed together.

3.2.2 IOM Filter and Dust Analysis

A researcher prepared five IOMs with polycarbonate filters. Each cassette was pre-weighed then sent out for collection. During five abrasive blasting operations, researchers calibrated the samples for 2 LPM and collected air for 30 minutes. The samples were shipped back to the lab and the post-weights recorded for the filter and the dust retained on top of the filter.

The filters were returned with details surrounding the conditions under which they were collected (Table 4). Four of the five samples collected were from booths that used plastic beads as the abrasive material and one sample was taken in a booth with steel media.

Table 4. IOM Filter Collection Parameters

Filter ID	Blasting Media	Number of Blasters	Sample Collection Time (min)
A	Plastic	1	31
C	Plastic	2	34
D	Steel	2	30
F	Plastic	1	34
G	Plastic	2	29

While the bulk on top of the filters did not appreciably differ between the plastic media samples, the steel media produced a powdery gray solid which was in stark contrast to the plastic media bulk (Figure 16).

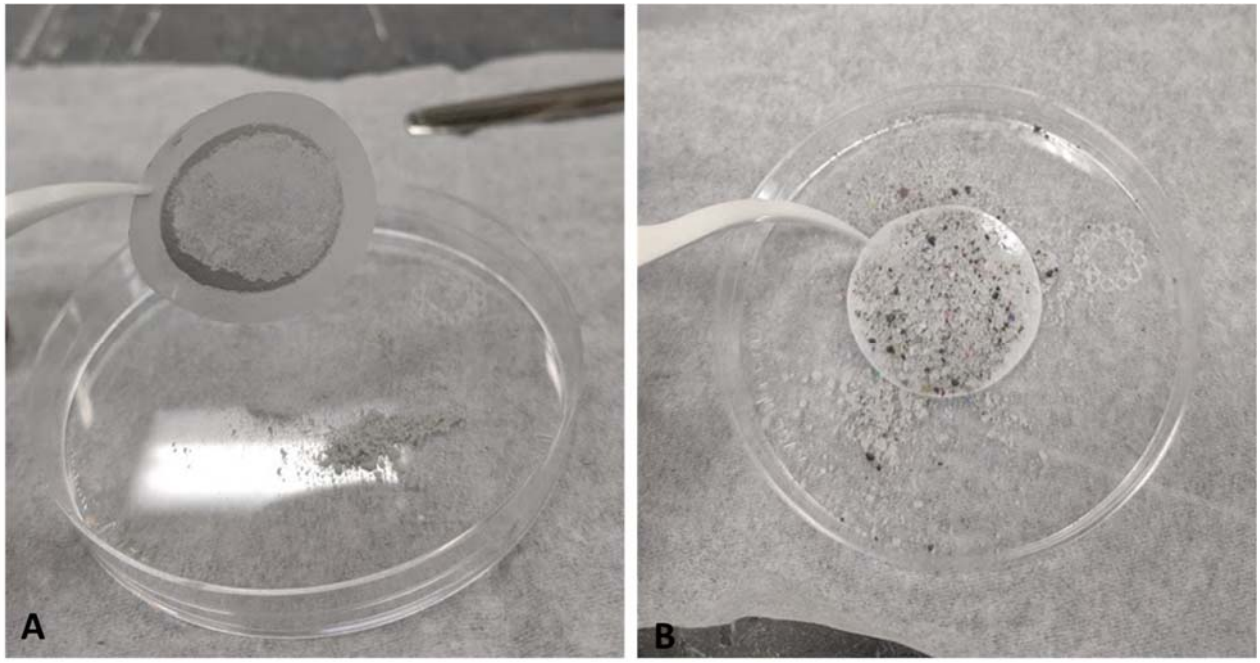

Figure 16. IOM Filters and Bulk Media. A) Bulk Material from Steel Media; B) Bulk Material from Plastic Media

The filters were sputter coated with 10 nm of gold and the imaged using EM-Tec F25 filter sample holder (Rave Scientific, Somerset, NJ) which allowed for processing the entire filter instead of an excised portion.

3.2.3 Image Analysis

All samples were analyzed on a JSM-IT500 (JEOL, Tokyo, Japan) scanning electron microscope. Bulk dust samples were loaded on 10 mm aluminum stubs with conductive carbon tape. Whole filters were mounted on a 25-mm disk holder (Rave Scientific, Somerset, NJ).

3.2.4 Bulk Dust

The researcher processed all SEM images with open-source software ImageJ (NIH) using the pre-packaged application Fiji (v. 1.52q).

For images gathered from the bulk dust stubs, automatic particle processing was not possible. The auto-characterization function relies on the ability to turn any image into binary, which itself depends on strong contrast between the particle edge and the background. Despite the layer of gold coating the stub, charging was an issue during imaging which resulted in areas of pure white juxtaposed with areas of varying shades of grey. Despite the researcher's bests efforts to manually set thresholds and the use of auto-thresholding techniques available in the ImageJ package, it was not possible to capture crisp outlines for most particles.

Instead of turning each image to binary, the researcher manually outlined each particle using the freehand selection tool, used ImageJ's measurement tool, then filled in each particle with white to prevent the accidental characterization of the same particle twice.

The built-in measurement function allowed for great flexibility in capturing unique parameters associated with an individual particle. The researcher selected eight measurements: area, circularity, Feret's diameter, Feret's angle, the minimum Feret diameter, aspect ratio, roundness, and solidity. The definition of each of these parameters is available in Appendix J.

3.2.5 Filters

Due to the more homogenous surface of the small particles on the filters, the 10 nm layer of gold greatly reduced charging effects. This reduction in charging allowed for higher contrast images which, in turn, allowed for automated image processing using the ImageJ as described above. Due to the 0.8 μm pores of the polycarbonate, an artificial lower size cut off of 0.5 μm^2 was used to prevent ImageJ's automatic particle identification feature from incorrectly classifying pores as particles.

The grey particulate on top of the Filter D was dense enough that individually resolving particles was impossible, therefore the filter was excluded from imaging analysis. Filter A was damaged during specimen mounting, leading to a wrinkled surface that proved impossible to image leading to its exclusion from the size distribution analysis. It was possible to conduct EDS analysis for all five filters.

3.2.6 EDS Analysis

All samples were analyzed on a JSM-IT500 (JEOL, Tokyo, Japan) scanning electron microscope equipped with an X-max^N 80 EDS (Oxford Instruments, Concord, MA). Each imaged stub was also analyzed for elemental composition. Point analysis was used as the gold coating dominated the response for mapping. A minimum of 100 random points spread out over the surface of the stub were analyzed for each size fraction or IOM

sample. While EDS was performed on the same area as the imaging, all imaging locations were randomly selected. The microscope included a feature where previously visited spots were marked to ensure no overlap in images or EDS. The percent of measured points containing an element were determined by dividing all points containing the element of interest by the total number of particles measured for the filter.

3.2.7 Size Distribution

Using the projected area estimated from the ImageJ processed images, the physical diameter of the particles was estimated using the equation below (Equation 11) (Fan, 1998) where A is the area of the particle.

Equation 11. Particle Physical Diameter

$$D_p = 2\sqrt{\frac{A}{\pi}}$$

Once the physical diameter was calculated, histograms for each sieve section or filter were generated. For sieved fractions, bins were generated in five micrometer intervals until counts dropped off. For filter samples, bin intervals varied from 0.8 – 10 μm. Bins were then normalized by their range, then these normalized values converted to frequency/μm by dividing by the total number of particles counted.

The count median diameter (CMD) was calculated by first determining the cumulative fraction of particles by bin. The 50^{th} percentile was interpolated from the nearest fractions. The geometric standard deviation (GSD) for each fraction was determined using Equation 12 (Hinds, 1999).

Equation 12. Aerosol GSD

$$\text{GSD} = \frac{50th\ percentile}{16th\ percentile}$$

3.3 Results

While charging was an issue with the bulk dust samples, the micrographs generally did not have areas of brightness indicating metals (Figure 17a). Combined with EDS results, it was concluded that most bulk dust was comprised of the plastic media used in blasting instead of paint chips. In contrast, the particles on the IOM filters, when viewed with the SEM, did show areas of brightness that when analyzed with EDS showed evidence of metal compounds (Figure 17b). The brightness of these smaller, metallic particles is due to their greater ability to backscatter electrons as they have a higher atomic number.

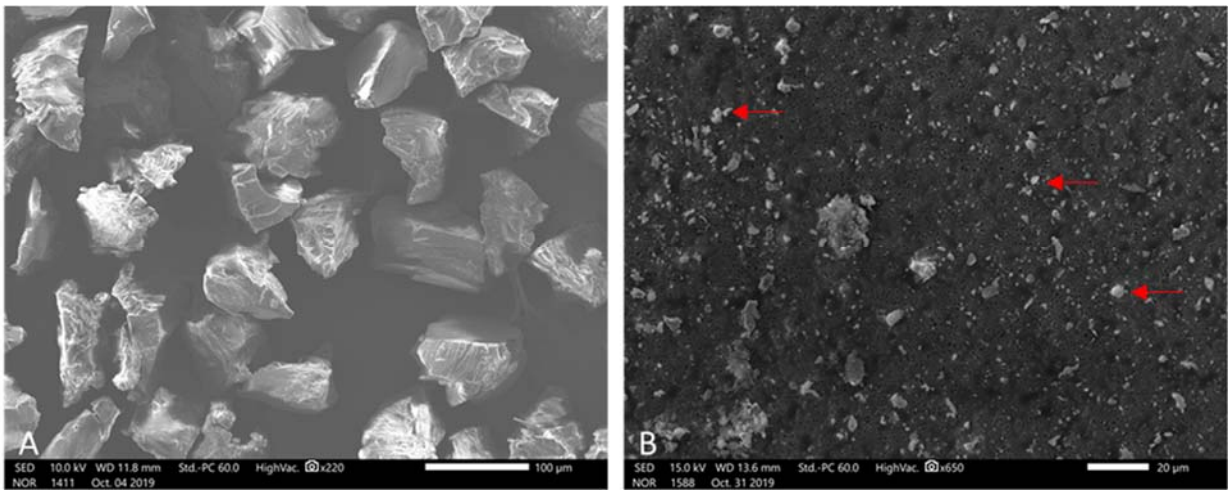

Figure 17. Micrographs: A) Bulk Dust; B) IOM Filter F, Red Arrows Showing Bright Particles

The distribution for each bulk dust size fraction is shown in Figure 18. Significant overlap exists between all size fractions, as sieving relied on separation based on physical diameter rather than aerodynamic diameter.

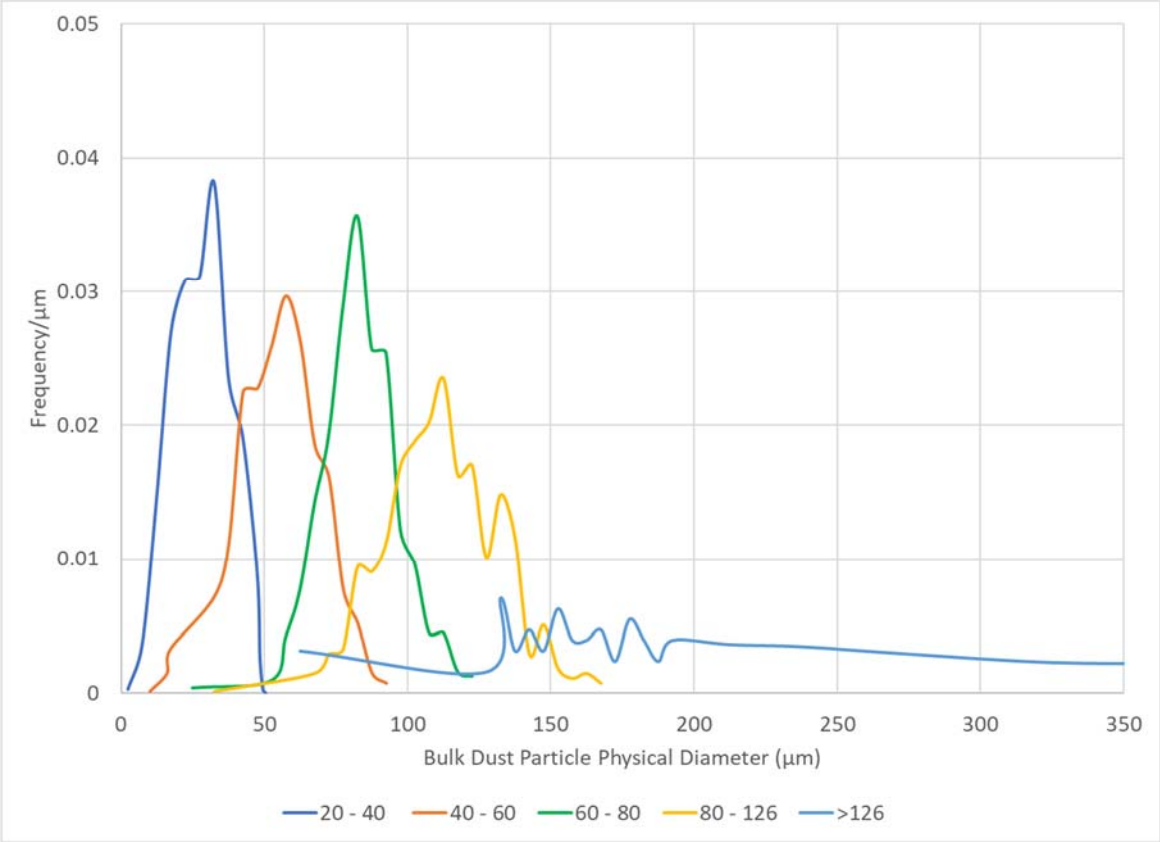

Figure 18. Size Distribution for Each Sieve Fraction

The CMD and GSD for the bulk dust was determined by fraction (Table 5). All GSD's were below two, indicating a relatively tight distribution, despite the heterogeneous appearance of the particles in each fraction. While the shape of the largest size fraction (>126µm) was unusual, when the log transformed frequency/µm values were evaluated using the Shapiro-Wilkes test, the results indicated a lognormal distribution. This finding validates the calculation method for finding the CMD and GSD.

Table 5. CMD and GSD for Bulk Dust Size Fractions

Size Range (µm)	CMD (µm)	GSD
20-40	26.3	1.8
40-60	53.4	1.4
60-80	80.4	1.2
80-126	108.7	1.2
>126	244.1	1.6

The sieved fraction of bulk dust sent off for percent chromium content through ICP analysis showed an increase in chromium as particle size decreased (Table 6). Particles were sieved, placed in flat-bottomed tubes, then weighed.

Table 6. Elemental Cr Content of Sieve Fractions by Metals by ICP

Size (µm)	Result (mg/kg)	Total Mass of Fraction (g)	Mass of Cr (mg)	Percent Cr
>126	64	43	2.752	0.006%
80-126	550	1.3	0.715	0.055%
60-80	2400	0.13	0.312	0.240%
40-60	2900	0.05	0.145	0.290%

EDS identified 25 elements in total among the sieved fractions (Figure 19a). Results from EDS of the primary compound of concern found in aircraft primer, strontium chromate, showed the highest percent of chromium was associated with the highest percent of strontium (Figure 19b). The percentages shown correspond to the number of particles sampled that had a positive match for the element normalized by the total number of particles sampled for sieved fraction.

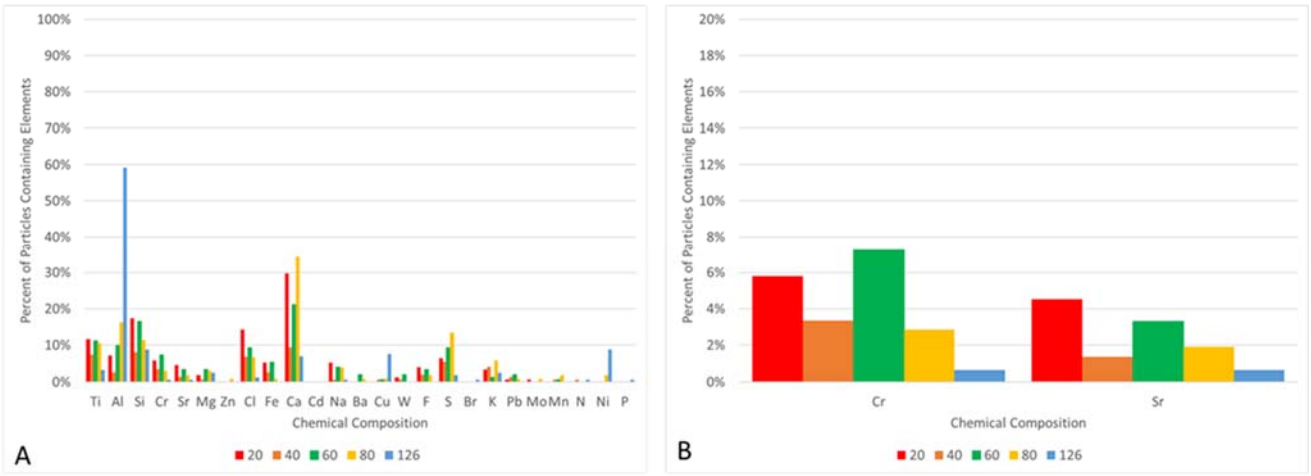

Figure 19. EDS Results of Bulk Dust: A) All Identified Elements; B) Elements Known to Exist in Aircraft Primer

The distributions for filters C, F, and G are shown in Figure 20. All distributions were truncated due to the cutoff introduced through image analysis. Due to the incomplete distribution, the CMD and GSD were not calculated. The CMD and GSD are predicated on knowing the median particle size. Without seeing the full distribution, which should resemble a skewed normal curve, it isn't possible to assert where the median lies.

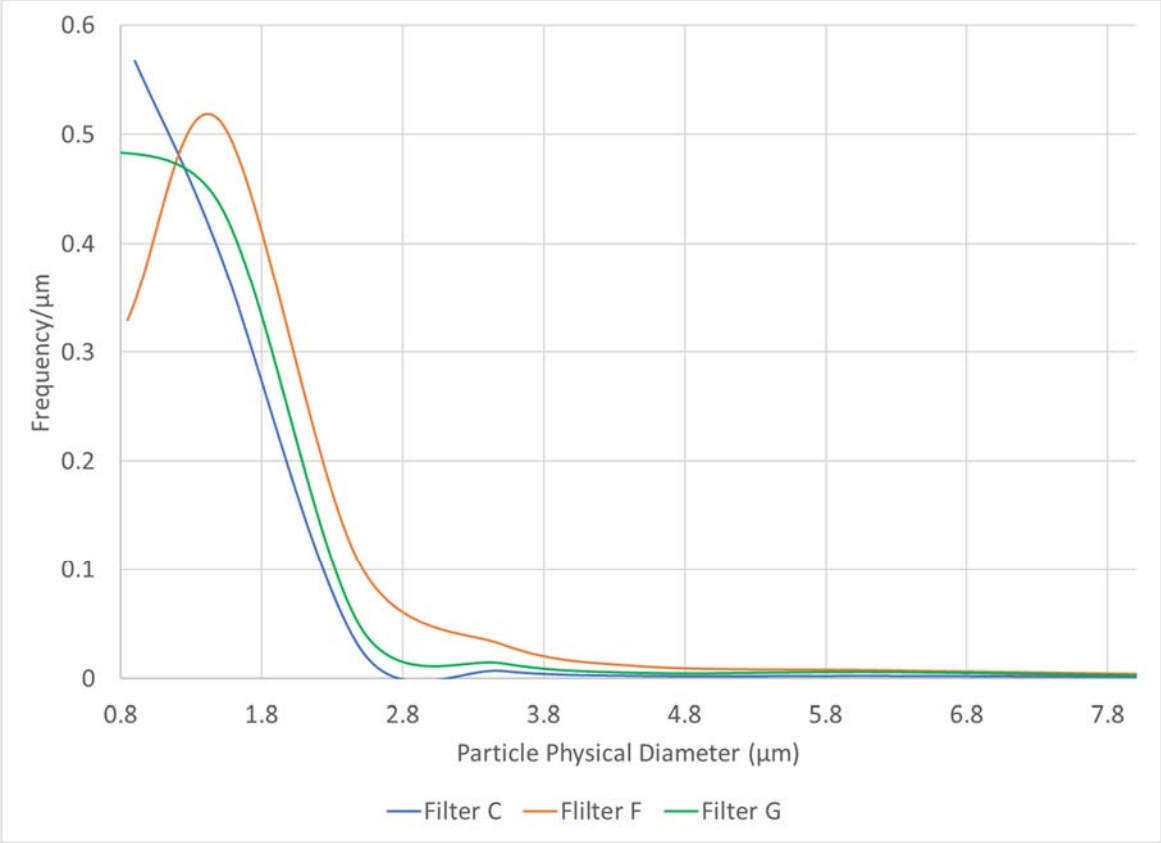

Figure 20. Size Distribution for Filters C, F, and G (Plastic Blast Media Depainting Operations)

As with the bulk samples, EDS identified 25 elements in total among the five filters (Figure 21a). The percent chromium identified did not correlate with the strontium (Figure 21b). It is of interest to note no chromium or strontium was found on Filter D the only IOM sampled from a blasting booth using steel media. It seems likely the part being blasted did not contain a layer of primer.

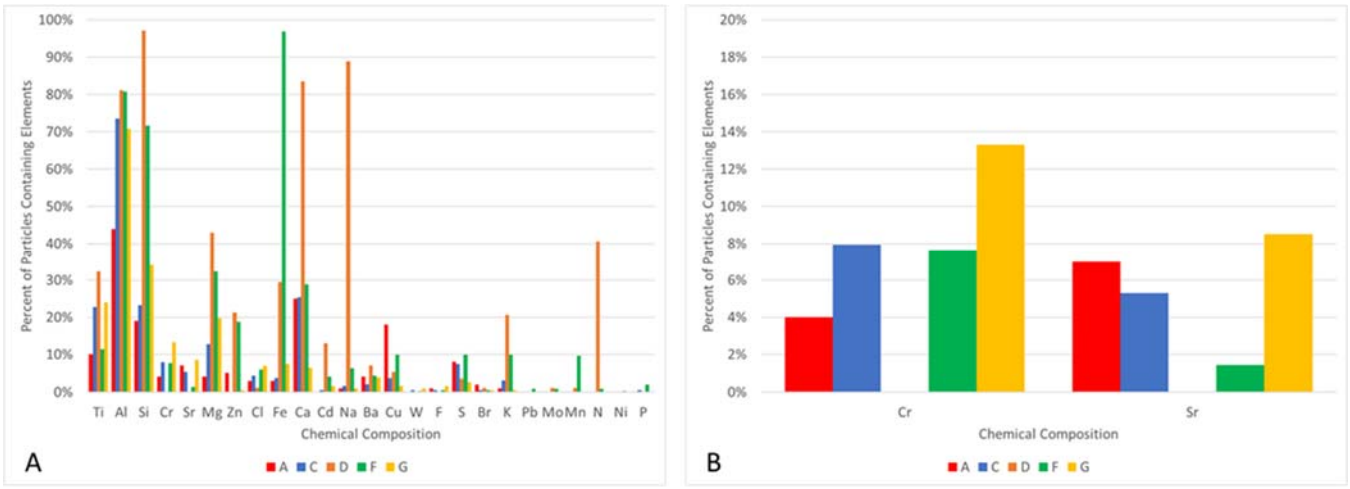

Figure 21. Elemental Analysis of IOM Samples via EDS: A) All Elements Identified; B) Elements of Concern in Aircraft Primer

3.4 Discussion

A potential weakness of this study was the bulk analysis which hinged on a single grab sample. At present, it is not appropriate to extrapolate the composition and distribution profile across all blasting booths or processes; however, the results obtained do indicate that chromium is likely adhered to large particles and those large particles have been observed in the IOM capsule. While a correction factor could not be obtained from the single bulk sample, the ICP analysis indicates that elemental chromium concentration is not linear across all particle sizes nor proportional in a predictable way.

The impact of the limitation introduced during image processing for determining the particle size distribution for those particles adhered to the IOM filter was evident. A more appropriate technique would be to separate particles via a cascade impactor to remove the very large particles, then follow the impactor outlet with an electrometer in order to count and deposit the small particles on a TEM filter. The increased resolution

and negligible pore size of the TEM filter would allow for image processing of submicron particles without relying on an artificial area cutoff.

Only a single filter was available from a steel blast media process and the particulate generated was significantly different in size, shape, and composition from the particulate in plastic blast media samples. While the lack of chromium and strontium in the EDS analysis suggests the particular operation sampled didn't involve primer, if other steel blasting operations do involve depainting, the plastic media distributions and composition would not be generalizable.

All methods used to analyze for chromium did not evaluate valence state, only presence of elemental chromium. While in principle it was more conservative to use this approach, future research should include a validation that hexavalent chromium is the only valence present.

Future research that includes a larger study sample size and impactor samples would improve understanding surrounding abrasive blasting processes and build on the findings presented here.

3.4 Conclusion

The size distribution of particulate matters when it comes to potential health effects. For hazardous compounds with detrimental impacts to the nose and upper airways, aerosol sampling using an inhalable sampler is appropriate to measure exposure. The findings from this project indicate abrasive blasting aerosols are heterogeneous and complex. A simple correction factor to convert historical CFC values is likely inappropriate and would overestimate prior exposures.

For an organization as large as the Department of Defense, the decision to move to inhalable sampling represents an enormous commitment of time and resources both for samplers and analysts. To avoid losing decades of exposure data when making this change in sampling, efforts should be made to equate prior CFC data with what an IOM would have collected. The impulse to use a convenient conversion factor should be scrutinized, however, as it could unreasonably bias estimates. The voluntary switch to the more conservative TLV represents an admirable intent to protect workers. It would be a disservice to the spirit of the endeavor to overcorrect past samples if a reasonable alternative exists. Using the methods outlined in this study with the addition of a few key pieces of equipment, a larger study could answer the distribution question and provide an evidence-based correction factor.

Bibliography

ACGIH. Chromium and Inorganic Compounds in TLV Documentation. (2018).

Bennett, J. S., Marlow, D. A., Nourian, F., Breay, J., Hammond, D. Hexavalent chromium and isocyanate exposures during military aircraft painting under crossflow ventilation. *Journal of Occupational and Environmental Hygiene, 13*(5), pp 365-371. (2016).

Bennett, J. S., Marlow, D., Nourian, F., Breay, J., Feng, A., Methner, M. Effect of ventilation velocity on hexavalent chromium and isocyanate exposures in aircraft paint spraying. *Journal of Occupational and Environmental Hygiene, 15*(3), pp 167-181. (2018).

Carlton, G. N., Flynn, M. R. Influence of Spray Painting Parameters on Breathing Zone Particle Size Distributions. *Applied Occupational and Environmental Hygiene, 12*(11), pp 744-750. (1997).

Carlton, G. N., England, E. C. Assessing Worker Exposures During Abrasive Blasting: Industrial Hygiene Field Guidance for Bioenvironmental Engineers. *United States Air Force IERA*. Report IERA-RS-BR-TR-2000-0001. (2000).

Fan, L., Zhu, C. Size and Properties of Particles. In Principles of Gas-Solid Flows (Cambridge Series in Chemical Engineering, pp. 3-45). Cambridge: Cambridge University Press. (1998). doi:10.1017/CBO9780511530142.002

Hinds, W. C. Aerosol Technology: Properties, Behavior, and Measurement of Airborne Particles, 2nd Ed. New York, NY: John Wiley & Sons. (1999)

Igathinathane, C., Pordesimo, L. O., Columbus, E. P., Batchelor, W. D., Sokhansanj, S. Sieveless particle size distribution analysis of particulate materials through computer vision. *Computers and Electronics in Agriculture, 66,* pp 147 – 158. (2009).

Lippmann, M. Rationale for Particle Size-Selective Sampling. In J. H. Vincent (Ed.), *Particle Size-Selective Sampling for Particulate Air Contaminants* (pp. 3-26). Cincinnati, OH: ACGIH. (1999).

Kan, H., Pan, D., Castranova, V. Engineered nanoparticle exposure and cardiovascular effects: The role of a neuronal-regulated pathway. *Inhalation Toxicology, 30*(9-10), pp 335-342. (2018).

Mirowsky, J., Hickey, C, Horton, L., Bloustein, M., Galdanes, K., Peltier, R. E., Chillrud, S., Chen, L. C., Ross, J., Nadas, A., Lippmann, M., Gordon, T. The effect of particle size, location and season on the toxicity of urban and rural particulate matter. *Inhal Toxicol, 25*(13), pp 747-757. (2013).

Phalen, R. F. Airway Anatomy and Physiology. In J. H. Vincent (Ed.), *Particle Size-Selective Sampling for Particulate Air Contaminants* (pp. 29-49). Cincinnati, OH: ACGIH. (1999).

Raabe, O. G., Stuart B. O. Sampling Criteria for the Thoracic and Respirable Fractions. In J. H. Vincent (Ed.), *Particle Size-Selective Sampling for Particulate Air Contaminants* (pp. 73-95). Cincinnati, OH: ACGIH. (1999).

Sabty-Daily, R. S., Harris, P. A., Hinds, W. C., Froines, J. R. Size Distribution and Speciation of Chromium in Paint Spray Aerosol at an Aerospace Facility. *Ann. Occup. Hyg. 49*(1). pp 47-59. (2005).

Shaffner, T. J., Ved, R. D. V. 'Charing' effects in the scanning electron microscope. *Journal of Physics E: Scientific Instruments 4*(9). (1970).

Takashimizu, Y., Iiyoshi, M. New parameter of roundness R: circularity corrected by aspect ratio. *Progress in Earth and Planetary Science,* 3(2). (2016).

Vincent, J. H. Sampling Criteria for the Inhalable Fraction. In J. H. Vincent (Ed.), *Particle Size-Selective Sampling for Particulate Air Contaminants* (pp. 51-72). Cincinnati, OH: ACGIH. (1999).

Vincent, J. H. Aerosol Samplers in Workplaces In *Aerosol Sampling* (pp. 544-545). Hoboken, NJ: John Wiley & Sons Ltd. (2007).

Witschger, O., Grinshpun, S. A., Fauvel, S., Basso, G. Performance of Personal Inhalable Aerosol Samplers in Very Slowly Moving Air When Facing the Aerosol Source. *Ann. Occup. Hyg. 48*(4), pp 351-368. (2004).

IV. Impact of IOM Flow Rate on Capture Efficiency

Chapter Overview

Chapter IV is composed of a comparison of IOM capture efficiency when operated side-by-side at 2 and 6 L/min. This research answers research objective three.

The Journal of Occupational and Environmental Hygiene is the target publication for this paper.

4.1. Introduction

The recent lowering of the American Conference of Governmental Industrial Hygienists (ACGIH) threshold limit value (TLV) and requirement for inhalable fraction sampling for hexavalent chromium presents a technical challenge for industrial hygiene practitioners (ACGIH, 2018). The new limit, 0.2 $\mu g/m^3$, requires an extremely low limit of detection (LOD) for analytical laboratories to achieve. In order to circumvent this, it has been suggested that industrial hygienists simply increase the flow rates of common inhalable samplers to allow more mass to be deposited on the filter in the same eight-hour window. The most commonly employed inhalable sampler, the Institute of Medicine (IOM), was initially designed to operate at a flow rate of 2 L/min. Several research teams have explored the impact to sampler efficiency at much higher flow rates, upwards of 10.6 L/min as it represents the maximum achievable flow with current personal sampling pumps.

Using computational fluid dynamics (CFD), researchers compared different inlet designs for the 37-mm cassette in order to better match the inhalable curve (Anthony *et al*, 2016). The design used a freestream velocity of 0.2 m/s, a sample flow rate of 10

L/min, and with the samplers forward-facing as this represented the maximum aspiration efficiency of all orientations. The results of the study indicated an inlet of 15-mm was most desirable, which corresponds to the inlet diameter of the IOM.

Zhou and Cheng (2009) compared sampling efficiencies of IOMs operated at 2 L/min and 10.6 L/min in a wind tunnel with particles ranging from 2 – 100 µm generated by a vibrating orifice aerosol generator (VOAG). Samplers were mounted on the front, side, and back of a full sized manikin. The orientation average concentrations were not statistically different for the two flow rates tested.

An another study, Stewart *et al* (2017) tested the modified IOM sampler described by L'Orange *et al* (2016) in a wind tunnel using both flow rates of 2 L/min and 10 L/min. Six samplers, three at each flow rate, were mounted on a rotating manikin in the chamber, then exposed to a monodisperse aerosol with MMAD of 32.7, 12.8, 9.5, and 4.9 µm. Using the Wilcoxon signed rank test, no statistical difference in sampler performance was detected.

The Zhou and Cheng study (2009) did not include enough samples to allow for more than descriptive statistics which makes it difficult to determine if the affect described in their results is due to a true difference or an artifact of a small sample size. The Stewart study (2017) used particles with relatively small diameters (<33 µm) which means the larger particles more relevant to the IPM were not evaluated. None of the studies mentioned above included flow rates between 2 and 10.6 L/min. Considering higher flow rates result in faster depletion of pump batteries and increase the likelihood of pump faults, it is prudent to evaluate sampler efficiency impact as a lower flow rate closer to what is practicable in the field. With these limitations in mind, there is room to

study the impact of sample flow rate on IOM behavior at the top of the IPM range with a large enough sample set to allow for parametric statistics.

In this study, IOMs operating at 2 L/min and 6 L/min were paired and exposed to Arizona Road Dust (ARD) with a mean aerodynamic diameter of 70 µm. A larger aerodynamic diameter was chosen as any effect was expected to occur at the extreme of the inhalable size range. Collected filters were weighed and the concentration calculated. Concentration means were compared to determine if a difference of 25% existed between sampling flow rates.

4.2 Methods

The IOM cassettes were assigned a number and labeled with permanent marker. After labeling, the filters were allowed to equilibrate in the laboratory for 24-hours, then pre-weighed (Figure 22). Each filter was massed three times, then loaded back into the IOM body in preparation for sampling. For each round of experiments, five blanks were equilibrated, pre-weighed, and loaded into IOM cassettes. During experiments, the blanks were left open in the research space. At the conclusion of the experiments, the blanks were closed and transported with the samples back to the laboratory space. Samples were allowed to equilibrate for a minimum of 24-hours, then the post-weights collected in triplicate. The difference in the blank average was used to correct the samples.

Figure 22. IOM Disassembled and Ready for Equilibration

Researchers conducted experiments in a 3’ x 3’ x 21’ aerosol chamber, previously characterized (described in Chapter II) (Figure 23). A rotating brush generator (RBG) (Model: 1000, Palas, GMBH, Karlsruhe, Germany) aerosolized pre-sieved Arizona road dust (ARD) (Particle Technology Inc, Arden Hills, MN) with a particle distribution centered around an aerodynamic diameter of 70.4 µm. ARD was fed into the generator via a motorized stage. The reservoir was emptied at a rate of 120 mm/h. The ARD was then expelled into the airstream with the brush rotating at 1200 RPM.

The dust was transported through a hard-plumbed stainless-steel tube from the outlet of the generator to the chamber. To maximize mixing with the incoming clean air, the aerosol inlet was pointed into the airstream.

IOMs were positioned between planes 5 and 7, labeled as “sampling planes” in Figure 23, to mitigate large particle loss due to settling prior to encountering the

samplers. The variable frequency drive of the centrifugal fan was set to 30 Hz, a setting that pulled air through the system with a velocity of 0.5 m/s.

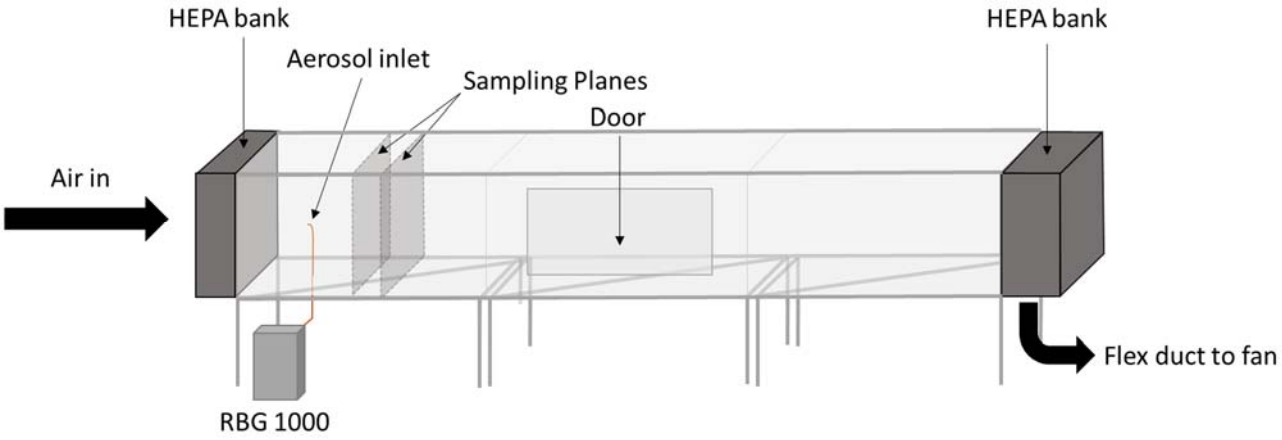

Figure 23. Aerosol Chamber Setup

Incoming and outgoing air passed through high-volume, high-throughput banks of HEPA filters to prevent outside contamination of the airstream and to avoid exposing researchers to ARD. During chamber characterization, the efficacy of the HEPA bank was verified by particle counts using an optical particle counter. The data showed incoming air was essentially particle free, so any mass registered on filters in these experiments can be assumed to originate from the ARD.

For the experiments, IOMs were paired such that one IOM was attached to a pump calibrated to two L/min and the other IOM attached to a pump calibrated to six L/min. The IOMs were hung in a pre-determined pattern in the aerosol chamber and their pumps turned on. The chamber door was sealed and the fan set to 30 Hz. The RBG 1000 was turned on and dust fed was to the chamber. The dust reservoir was refilled twice over the course of one experiment, to ensure the mass collected was well above the signal-to-noise ratio from the variability of the filter weights.

Once the final volume of dust was expended, the RBG 1000 and fan were turned off, the chamber unsealed, and the pumps halted. The IOM dust covers were inserted over the IOM faces and the samplers removed from the chamber. The pump volumes were recorded for each IOM. The chamber floor was cleaned with a HEPA shop vacuum, a new batch of IOMs loaded, and the experiment repeated. Two experiments were carried out a day, each experiment generating four paired samples. In total, ten experiments were accomplished, resulting in 40 paired samples. One pair was discarded when it was discovered the sampling line detached from one of the pumps at an unknown point. The remaining 39 pairs were analyzed for a 25% difference in the means.

4.3 Results

4.3.1 Pilot Studies

Generally, it is preferable to operate industrial (protective) ventilation in such a way that the contaminant is moved away from the worker, such that the worker's back is to the direction of air flow or perpendicular to the airflow. In the pilot studies, two

configurations were considered, both with the faces of the IOMs at 90° to the direction of air flow in the chamber (Figure 24).

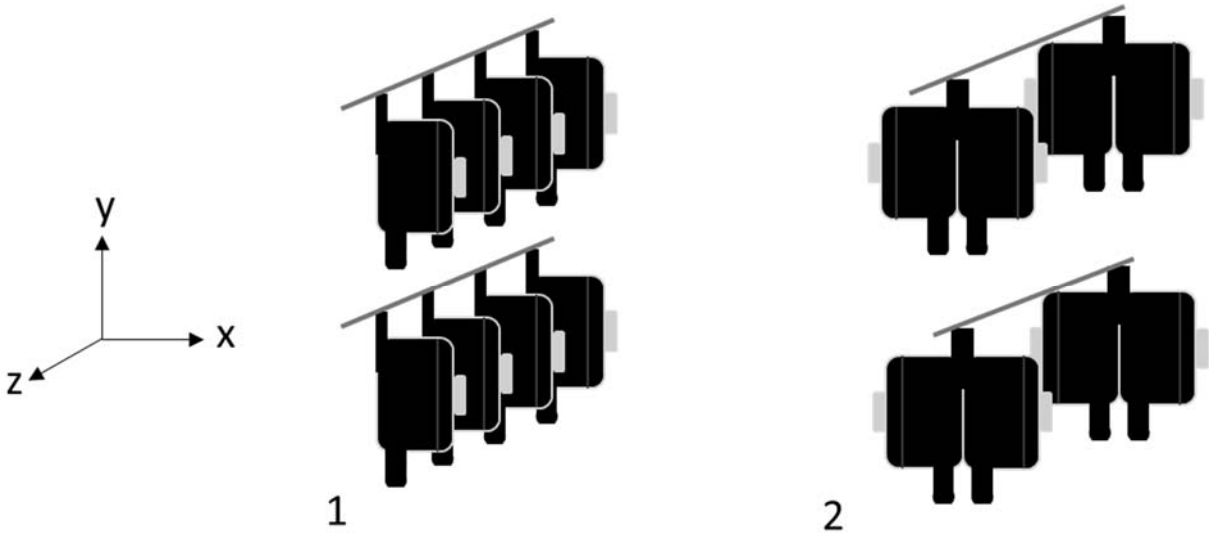

Figure 24. IOM Sampler Configuration: 1) All Eight IOMs Facing the Same Direction; 2) IOMs Paired Back-to-Back

In configuration 1, the goal was that the four samplers on the same level could be pooled and compared against one another. In configuration 2, the samplers could not be pooled but pairing was made more explicit through true collocation in the z- and y-axes. Final setup is shown in Figure 25.

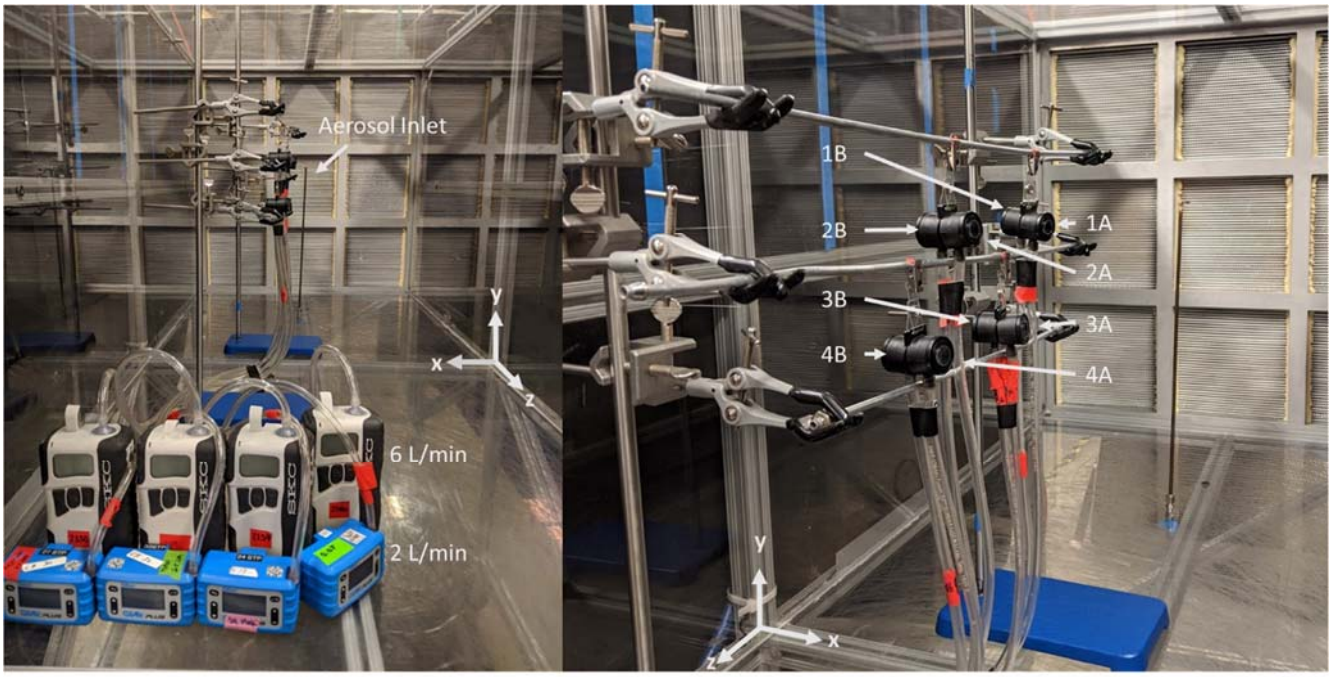

Figure 25. Final Experiment Setup in Aerosol Chamber

4.3.2 Power Analysis

One of the aims of this study is to inform practitioners considering increasing the flow rate to their IOM samplers in an effort to meet analytical LODs. In order for the findings to have relevance, their power must be known. For this study, an alpha of 0.05 and a beta of 0.8 were chosen as acceptable risks for under- and overestimating exposure. The number of samples necessary to ensure sufficient power was determined using the relative standard deviation from the pilot study in Equation 13.

Equation 13. Calculation of Number of Samples Needed for Power

$$\mathrm{n} = \frac{\left(t_{n-1,\frac{\alpha}{2}} + t_{n-1,\beta}\right)^2}{d^2}$$

where,

$\alpha = 0.05$

$\beta = 0.2$

$$d = \frac{difference\ in\ samples}{standard\ deviation} = \frac{Mean\ conc.\ 2LPM - 75\%\ of\ mean\ conc.\ 2LPM}{Mean\ experiment\ SD}$$

Using a range of relative standard deviations (0.19 – 0.68), the number of samples needed to achieve the desired power fell between 29 and 39. Since four pairs could be collected in one run, ten sets of experiments were planned for the full-scale study.

4.3.3 Full Scale Study

Pilot studies confirmed that IOMs paired back-to-back at two heights had a reasonable relative standard deviation and the power analysis resulted in a number of samples that were feasible to obtain.

Ten experiments with four paired samplers were carried out. In an effort to avoid local eddy effects, the pattern of flow rates was varied each experiment (Figure 26). Note the z-axis points into the page.

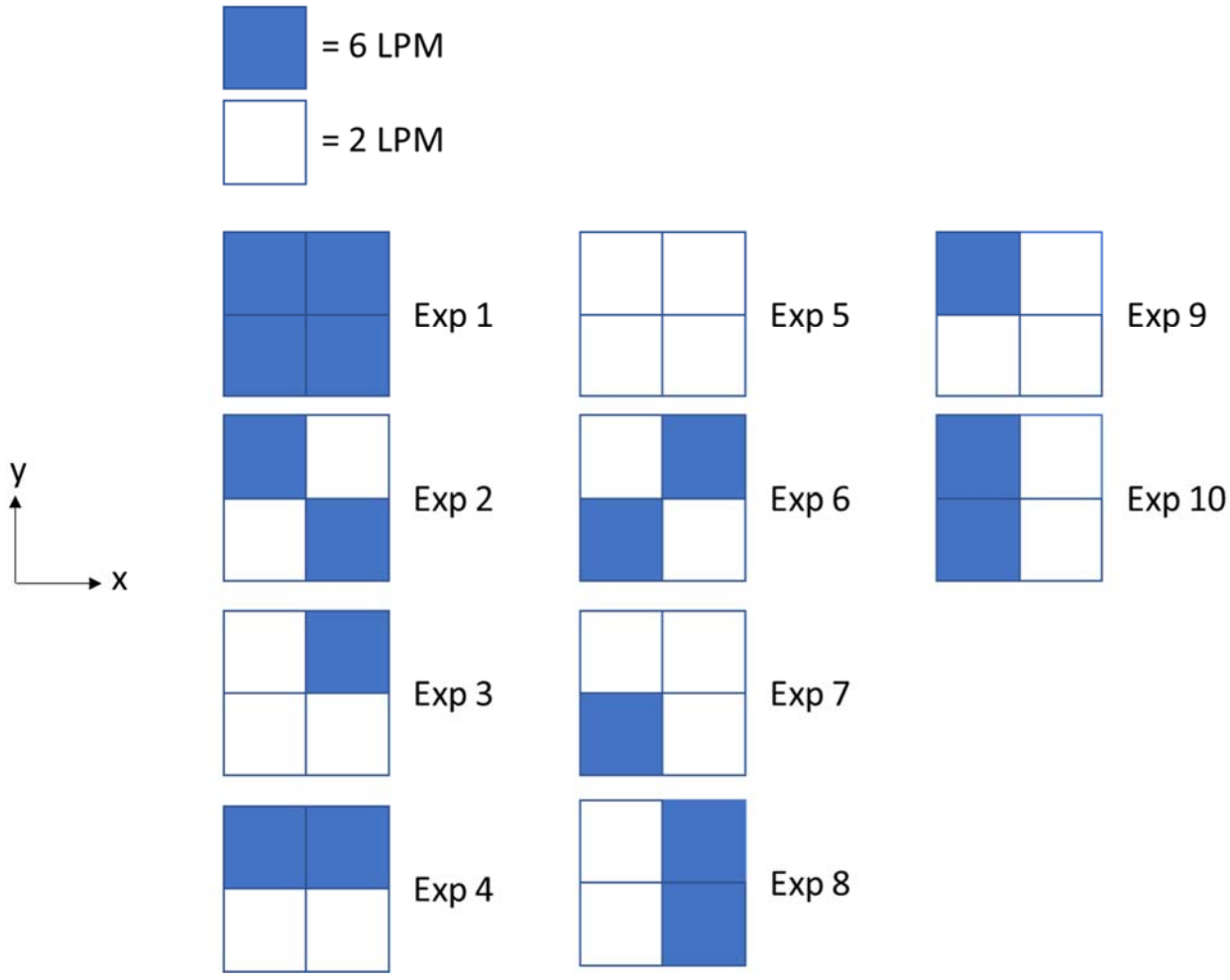

Figure 26. Configuration of IOMs by Flow Rate on Side A

Differences in the sample concentrations were plotted to determine visually if any outliers were likely. In Figure 27, the blue line represents the sample means and the orange lines represent three standard deviations. Only one potential outlier, outlined in red, was identified.

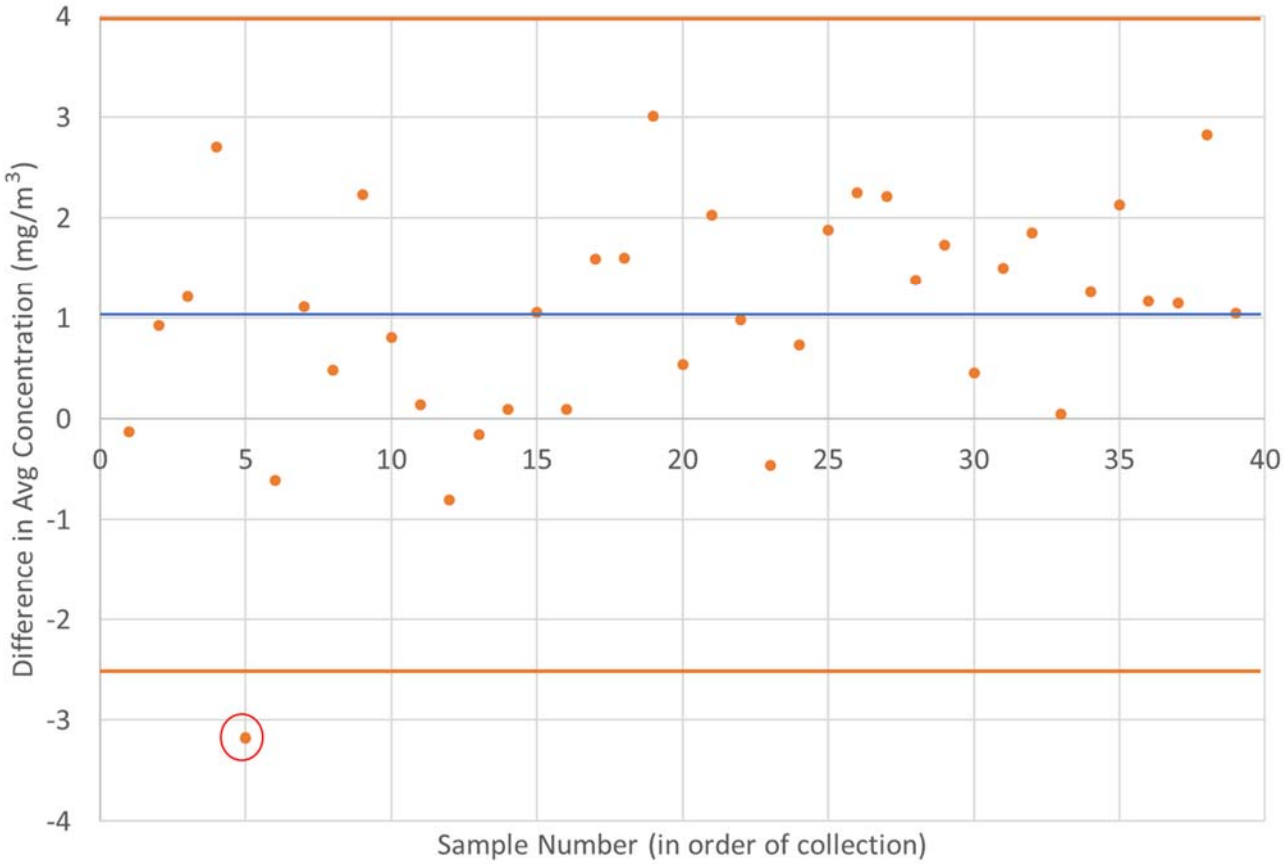

Figure 27. Control Chart for 39 Paired Samples

A two-sided Grubbs test was used to determine if the highlighted point represented a true outlier ($\alpha = 0.05$, $N = 39$) (Equation 14). N represented the total number of pairs and t is the appropriate value from the Grubbs' critical value table.

Equation 14. Grubbs' Test Statistic

$$G > \frac{N-1}{\sqrt{N}} \sqrt{\frac{(t_{\frac{\alpha}{2N},N-2})^2}{N-2+(t_{\frac{\alpha}{2N},N-2})^2}}$$

As the outlier exceeded the critical G value (3.025), samples from experiment 2 position 1 were excluded from subsequent analysis. Upon reviewing experiment notes, no cause was identified to explain the unusually large difference in concentration.

The mean concentration reported across all ten experiments for all four locations by side was computed with error bars (Figure 28). The side A concentration was not statistically different from the side B concentration, suggesting that data collected are not biased by the side of the apparatus they were collected on.

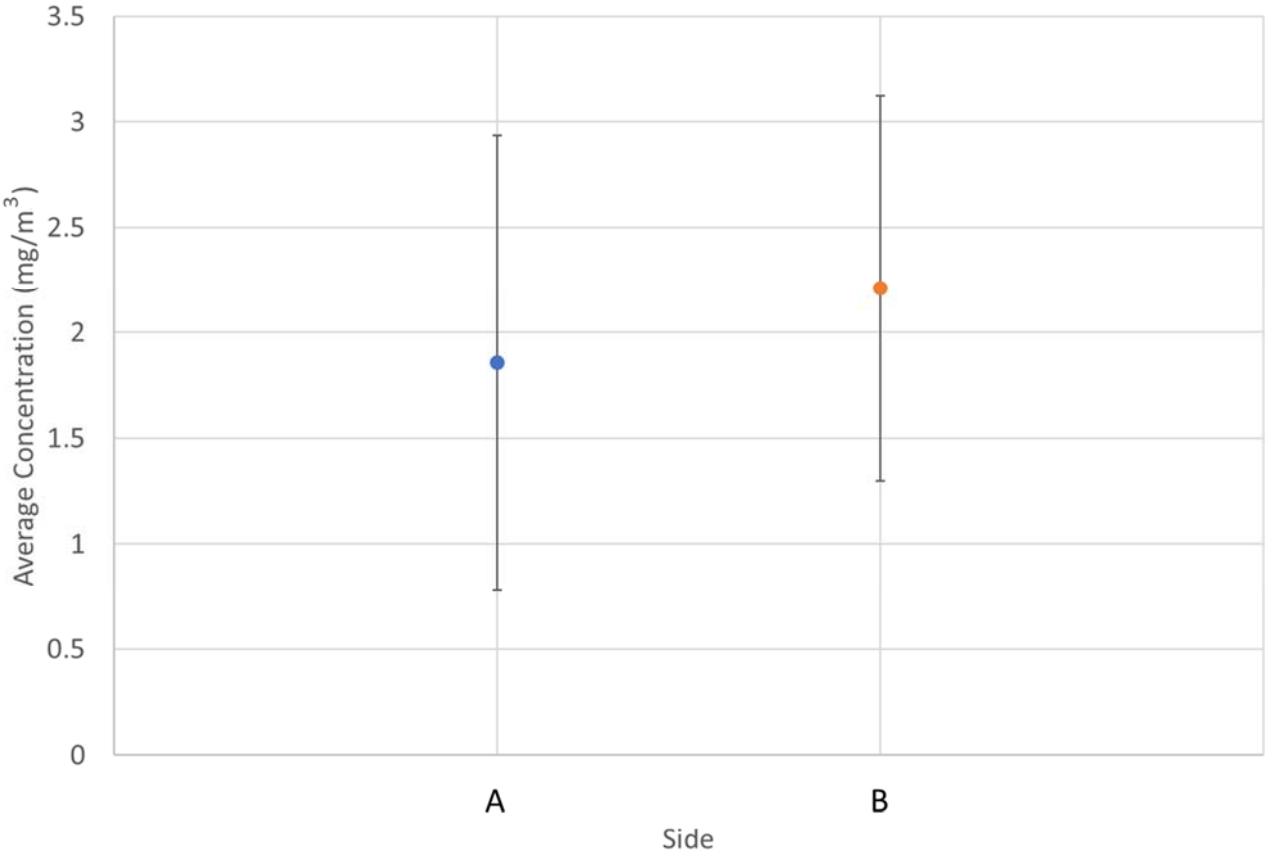

Figure 28. Average Concentration by Side

The mean concentration for each position and side was computed and error bars added to determine if any location reported statistically different concentrations (Figure 29). While locations 1A and 3B are statistically significant, the data were not pooled so at no point was concentration data at 1A compared to 3A. Instead, data show that all paired locations (i.e. 1A and 1B, 2A and 2B, etc.) are not statistically different from one another. This is an important feature to have to provide confidence that the result from the paired-t test is measuring true differences in behavior due solely to the flow rate, not to the location in the setup.

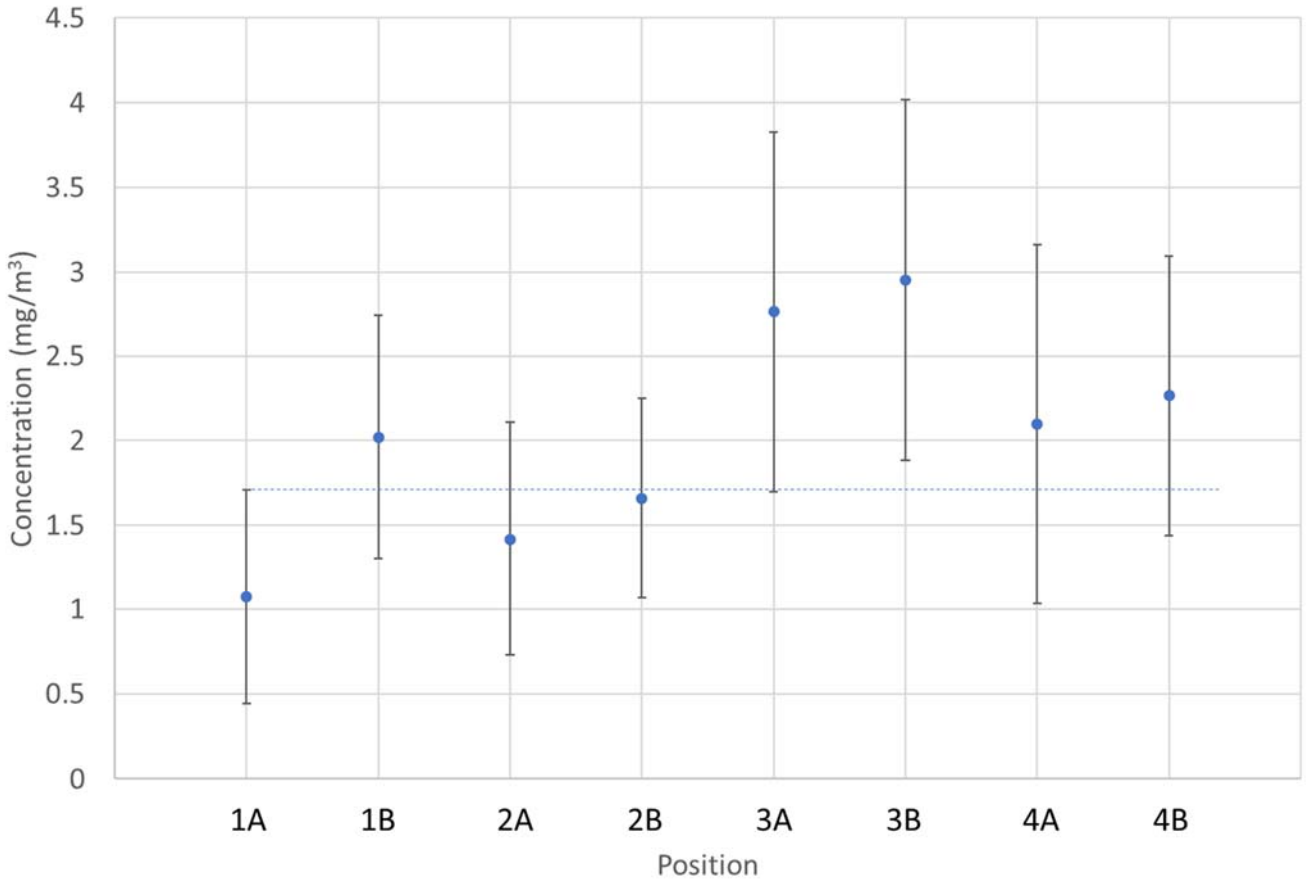

*dotted line shows the lowest average upper range to compare against other positions

Figure 29. Average Concentration by Position

A Tukey Honestly Significant Difference (HSD) test was conducted for each of the eight positions to determine quantitatively what differences existed (Table 7). While no paired positions significantly differed from each other, there were significant differences between some unpaired positions. While this result does not negate the relevance of the paired t-test, it does continue to support the conclusion that the samples collected among all experiments cannot be pooled based on flow rate.

Table 7. Tukey Test for Difference between Position Means

	1A	1B	2A	2B	3A	3B	4A	4B
1A		0.285	0.900	0.789	0.001*	0.001*	0.175	0.064
1B			0.764	0.900	0.479	0.310	0.900	0.900
2A				0.900	0.013*	0.005*	0.626	0.358
2B					0.071	0.033*	0.900	0.730
3A						0.900	0.560	0.812
3B							0.383	0.643
4A								0.900
4B								

* statistically significant differences between locations

Prior to conducting the paired-t test to determine if a 25% difference in the concentration existed between paired samples, the differences were evaluated for normality. A histogram was generated and the Shapiro-Wilk test conducted, both of which conclude the data are normally distributed (Figure 30).

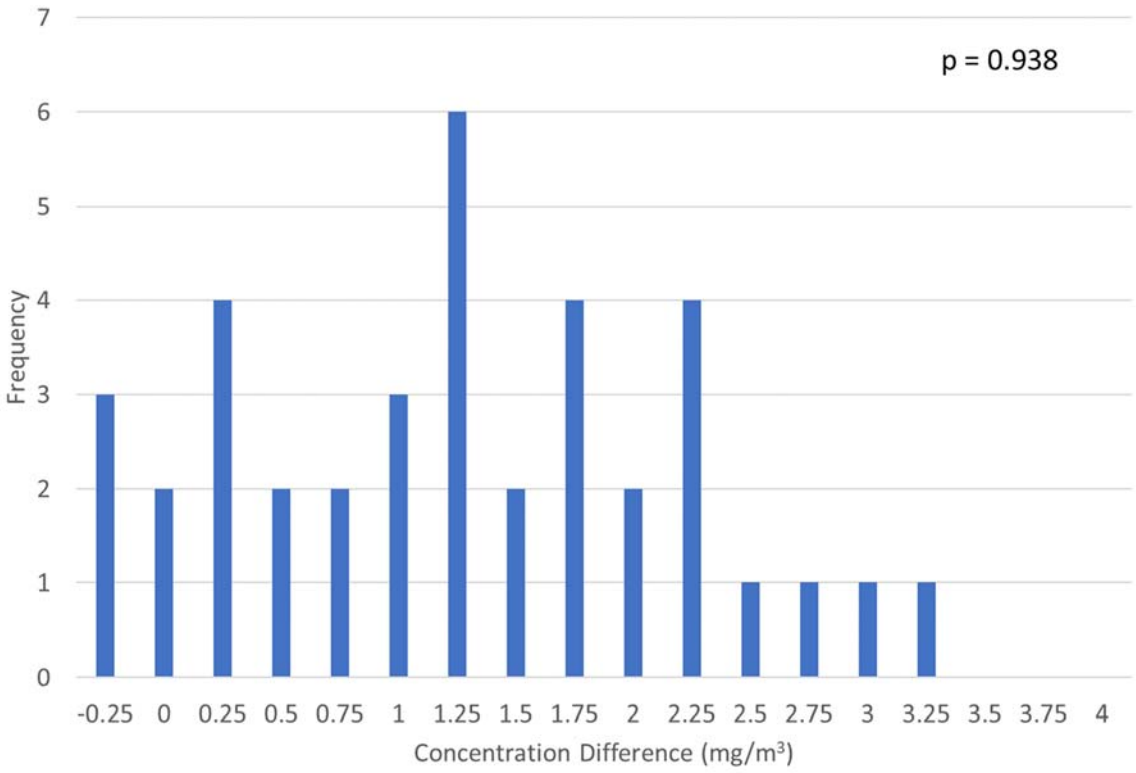

Figure 30. Distribution of Paired Differences (High Flow – Low Flow)

With normal distribution confirmed, a power analysis of all full-scale data was run using Equation 13, which yielded 34 as the minimum sample size. Even excluding the one outlier, more than the minimum number of samples were taken through the ten experiments.

The thirty-eight samples were analyzed with a paired two sample for means t-test. The hypothesized mean difference chosen was the difference between the average concentration for IOMs operating at 6 L/min minus 75% of that value. Based on the two-tailed p-value, the null hypothesis was rejected (Table 8).

Table 8. Paired t-test Results for IOM Data

IOM Operating Flow Rate	*6 L/min*	*2 L/min*
Mean	2.58	1.48
Variance	0.93	0.52
Observations	38	38
Pearson Correlation	0.37	
Hypothesized Mean Difference	0.67	
df	37	
t Stat	2.79	
P(T<=t) one-tail	0.004	
t Critical one-tail	1.69	
P(T<=t) two-tail	0.008	
t Critical two-tail	2.03	

The difference between the 6 L/min and 2 L/min sample concentration means is statistically significant up to 30%. This exceeds the NIOSH guidance for new method development. Based on the results of this study, sampling with a higher flow rate introduces a positive bias in particle collection.

4.4 Discussion

The study outlined by Zhou and Cheng most closely matches the parameters of this study, though the results do not agree with one another. A key difference between the studies is that the prior study did not have both flow rates sampling simultaneously. Instead, a single condition was tested at one flow rate and the results compared to the collocated reference samplers then the other flow rate tested and compared to its reference sample values. No study power was stated nor were the total number of repetitions per condition, so it is difficult to ascertain what level of significance can be attributed to the results.

In the case of Stewart *et al* (2017), neither the particle distribution nor the statistical testing was the same as the conditions in this study. In Stewart *et al*, the largest particle size tested had a MMAD of 32.7 μm. While a large particle, it is a fraction of the size of the 50% cut point for the inhalable convention. Based on aerosol principles, if differences in performance can be observed, they are most likely to appear in the upper region of the inhalable particle size distribution. Additionally, the use of non-parametric statistics due to non-normal data could not deliver the same sensitivity as a parametric test. While this study does not invalidate the findings of Stewart's study, it does go a step beyond what was possible given the constraints of their low velocity (0.2 m/s) wind tunnel.

In one regard, this study attempted to minimize any complicating factors by forgoing a manikin and the effect of a bluff body on sampler performance. While the researchers decided this method would allow for the comparison of sampler performance at its most fundamental, the design prevents it from strict comparisons to other sampler studies which more closely mimic real-world conditions. It is possible that the effect shown in this study is dwarfed by the influence of changes in flow characteristics due to a person wearing the sampler.

The lack of orientation averaged results is another short-coming of this study. It is well documented that sampler capture efficiency depends on a great many factors, including carrier wind speed, particle size, and sampler inlet orientation. The results presented here cannot be extrapolated to forward or rear facing samplers. An improvement could be made if the pairs were rotated in a way that allowed all orientations be sampled equally over the course of the test.

Finally, due to time constraints, a single air velocity was chosen. While this velocity was grounded in a real-world condition, follow on studies should confirm the trends found continue under new conditions. At minimum, the lower velocity limit (0.2 m/s) and upper velocity limit (1 m/s) should be tested as they represent the calm office environment documented by Maynard and it is anticipated that a higher flow rate will increase differences between the means based on data in literature (Zhou, 2009).

For the industrial hygiene practitioner, the results of this study indicate a positive bias will be introduced if the IOM is operated at 6 L/min instead of 2 L/min for large particles. This represents an increase in Type II bias, which can have real-world impacts. In practice, this could drive unnecessary personal protective equipment (PPE) changes if the new flow rate is used and the assigned protection factor (APF) for respiratory protection is no longer protective. However, this method may be suitable for screening a process to demonstrate definitively that a hazard does not exist or monitoring the effectiveness of a control treatment.

4.4 Conclusion

In this study, IOMs operating at design flow rate and triple the design flow rate were paired and the mass collected on the filters compared. Thirty-eight pairs were analyzed with a paired t-test, the results of which show a greater than 25% difference in the sample means, with the 6 L/min IOMs collecting more mass than their 2 L/min counterparts. These results indicate a positive bias inherent in the IOMs operating at 6 L/min effectively oversampling particles in the coarse inhalable size range and could lead

practitioners to overly conservative results. Follow-on work should include orientation averaged sampling and free stream air velocities both higher and lower than 0.5 m/s.

Bibliography

ACGIH. Chromium and Inorganic Compounds in TLV Documentation. (2018).

Anthony, T. R., Sleeth, D., Volckens, J. Sampling Efficiency of Modified 37-mm Sampling Cassettes Using Computational Fluid Dynamics. *J Occup Environ Hyg. 13*(2), pp 148 – 158. (2016).

L'Orange, C., Anderson, K., Sleeth, D., Anthony, T. R., Volckens, J. A Simple and Disposable Sampler for Inhalable Aerosol. *Annals of Occupational Hygiene 60*(2), pp 150 – 160. (2016).

Stewart, J., Sleeth, D. K., Handy, R. G., Pahler, L. F., Anthony, T. R., Volckens, J. Assessment of increased sampling pump flow rates in a disposable, inhalable aerosol sampler. *J Occup Environ Hyg. 14*(3), pp 207-213. (2017).

Titus, E., Steele, M. Aerosol Test Chamber Characterization. AFIT-ENV-MS-20-M-242. (2020).

Zhou, Y., Cheng, Y.S. Evaluation of IOM Personal Sampler at Different Flow Rates. *J. Occup. Environ. Hyg. 7*(2), pp 88 – 93. (2009)

V. Conclusions and Recommendations

5.1 Conclusions of Research

The first objective of this work, to determine if use of an IOM was justified in sampling abrasive blasting processes, was confirmed. Analysis of bulk dust showed that chromium was presented even on particles larger than 100 μm. As those large particles will be captured and add to the total mass a worker could be exposed to, an inhalable sampler is most appropriate.

To answer the second research objective, which was to better characterize the aerosols generated during abrasive blasting, IOM filters and bulk dust were imaged with

microscopy and their composition analyzed with EDS. Results show that chromium concentration does not follow a linear trend with particle size and that a wide distribution of particles exist.

The final research objective, which asked if the capture efficiency of an IOM differed when operated at 2 L/min and 6 L/min was tested through side-by-side operation in an exposure chamber. Results showed the 6 L/min IOM oversampled by 30%, suggesting use in the field would have a positive bias.

5.2 Significance of Research

The DoD has decided to adopt the ACGIH hexavalent chromium TLV in an effort to better protect service members. The TLV represents more than a 10-fold decrease in the allowed exposure level and was derived from levels reported to be associated with nasal irritation. By itself, this lowering of the TLV may cause changes in required PPE. In combination with the change from a total dust sampler (CFC) to a sampler that meets the IPM convention (IOM), it is highly likely that respiratory protection will need to be increased since a higher assigned protection factor will be needed. This change is not necessarily driven by new, increased risk to workers. Without evidence of nasal irritation in the exposed population, there is no reason to believe those exposed are suddenly more vulnerable and in need of increased protective equipment.

The adoption of the IOM as the hexavalent chromium sampler and the reality that operating the sampler at its design flow rate provides insufficient mass for the analytical lab creates a quandary. Based on this research, operating the IOM at the lowest flow rate

that still ensures sample viability results in a positive bias. This would make processes sampled using this higher flow rate seem more contaminated than they are.

Reevaluating all processes, training personnel in the use of the IOM, providing new PPE, and adding workers to a respiratory protection program are all actions that are costly both in terms of monies and man hours. This research gives insight into the issues surrounding something as simple as changing the flow rate on a pump. Ultimately, there are many considerations that feed into a decision such as adopting the new TLV, but it is the duty of researchers to provide facts supported by evidence.

5.3 Recommendations for Action

The researcher recommends the Air Force review health records for those who worked in occupations with chromium exposure and assess whether evidence of nasal irritation existed historically. Under 29 CFR 1910.1026 (2012), occupationally exposed workers must have their nasal cavities and skin monitored by a physician for sores so health records should be reliable for showing evidence of exposure. If this epidemiological study shows no significant trend in nasal irritation among the exposed population, the DoD should reevaluate if their aim in providing the best protection for their service members will be served by accepting the lowered TLV. The decision to embrace the TLV will have other consequences, such as decreased productivity for workers required to wear higher and higher levels of PPE, and will require a substantial allocation of resources. Resources spent on hexavalent chromium exposures could mean other potentially hazardous exposures receive less funding or attention. The results of this study indicate positive bias is likely if the IOM is operated at a higher flow rate.

Considering the lower TLV is already highly conservative, the results captured in the field may give the picture of a more hazardous situation than what truly exists.

5.4 Recommendations for Future Research

Some questions raised in this work remain open. While a promising start, abrasive blasting aerosol characterization is far from complete. Future work should widen the breadth of processes sampled and include other bases where blasting processes are common. In particular, pairing IOM sampling and real-time particle sizing equipment with impactors would allow for density calculations and finer binning of the super-micron particles as the real-time instruments only measure a single bin from 30 – 75 μm. Composition analysis of samples was only undertaken for elemental chromium as at the time it was considered more conservative.

The IOM study only included a single orientation (90° to the freestream air) and only a single velocity for the freestream. Not all operations use ventilation at 0.5 m/s and workers are not stationary. To ensure results hold true over a wider variety of conditions, experiments should be repeated at higher and lower air velocities and incorporate several orientations to allow for an orientation averaged estimate of differences between the two sample flow rates. Orientation averages are typically presented in literature, so future experiments would allow for a more direct comparison of values to those offered by other researchers.

Appendix A

Health Effects from Hexavalent Chromium

I. Introduction

Chromium (Cr) is the 20th most abundant element in Earth's crust by mass fraction (Bertini, 2007). As a transition metal, it can exist in a variety of valence states. Cr does not exist as a pure element, Cr(0), in nature but instead as complexes most often as Cr(III) or Cr(VI). Historically, Cr(III) was regarded as an essential micronutrient tied to insulin regulation, though current analysis has rejected this assertion on the basis that no human biomolecules have been identified as interacting with Cr(III) for transport or metabolism (Vincent, 2013). Though no longer considered essential, the consensus is Cr(III) represents a low toxicity risk to humans, in part because of its low absorption potential (Vincent, 2013). Cr(VI) has a long history as a known carcinogen and mucous tissue irritant. Due to its presence in many industrial processes, the toxicity of Cr(VI) is of interest to safety professionals and industrial hygienists. The Occupational Safety and Health Administration (OSHA) set the permissible exposure level for Cr(VI) at 5 $\mu g/m^3$ (OSHA, 2006). In 2016, the American Conference of Governmental Industrial Hygienists (ACGIH), a non-regulatory body recommended a threshold limit value of 0.2 $\mu g/m^3$ for the inhalable fraction of particles containing Cr(VI) (ACGIH, 2018). This lowered value was based on epidemiological data that tied exposure levels lower than 5 $\mu g/m^3$ to dermal sensitization and severe irritation of the nasal passages (ACGIH, 2018). The toxicological and epidemiological data surrounding Cr(VI) are outlined in the following sections of this report.

II. Toxicokinetics in Humans

Generally, Cr is poorly absorbed through digestion and is not considered a major occupational exposure concern (Barceloux, 1999). Both inhalation and dermal exposure are critical routes of entry. Though the fraction absorbed through the lungs is not well characterized, Cr(VI) is absorbed through phagocytosis or by permeating the cell membranes (Barceloux, 1999). Dermal irritation is widely reported and sensitization from exposure to both Cr(III) and Cr(VI) is possible (Avina, 2002).

Once inhalation exposure occurs, there are two important cellular uptake pathways for Cr(VI): active transport through anion channels and phagocytosis (Avina, 2002). Soluble Cr(VI) compounds are often reduced to Cr(III) by extracellular fluids but insoluble compounds often attach to cell walls, dissolve into chromium oxyanions, and are transported through anion channels into cells (Singh, 1999). Once inside the cell, several different enzymes are capable of reducing Cr(VI) to Cr(III). There is evidence of a transient valence state, Cr(V), and free radical production, which can cause a wide array of damaging effects from forming Cr-DNA adducts, to causing cross-linkage of DNA or even membrane lipid peroxidation (Singh, 1999). The stress can lead to cell carcinogenesis, cessation of the cell cycle, or even apoptosis (Singh, 1999).

As far as cellular absorption in the epidermis, Cr(VI) is highly cytotoxic to HaCaT kerantinocyte cells, even at concentrations as low as 10 μM (Ermolli, 2001). When not toxic, 28-57% of the dosed Cr(VI) absorbs into the nucleus and cellular membrane with the balance present in the cytoplasm, a stark difference from Co or Ni which preferentially absorb in the cytoplasm (Ermolli, 2001). The HaCaT cells concentrated Cr(VI) up to 170 times the initial dose over a 24-h period (Ermolli, 2001).

Regardless of valence state, studies have shown that cells have no reliable means of ridding themselves of Cr which invariably leads to build up (Avina, 2002). The highest concentration of Cr in the body is found in the lungs, followed by the liver and kidneys (Barceloux, 1999). Cr is primarily excreted through urine and feces with approximately 10% excreted through the biliary system (Barceloux, 1999).

III. Respiratory Toxicity

Intermediate and chronic exposure to chromium particles are tied to a variety of symptoms. One of the most thorough epidemiology studies of chromium workers looked at 70,000 air samples collected over two decades at a chromate production factor and compared the average exposure concentration to lung cancer incidence among the workers (Gibb, 2000b; Gibb, 2015). Gibb found a dose-response relationship between the chromate exposure and incidence of cancer, which laid the foundation for Cr(VI)'s classification as a known carcinogen (ATSDR, 2012).

Even short-term exposure to chromium particles is linked to negative respiratory responses. Gibb found that among the same group of workers, the company physician frequently diagnosed nasal irritation or perforation for workers with less than ninety days on the job (2000a). A cross-sectional study of 20 chrome plating companies within the United Kingdom (UK) found that 17% of surveyed workers had active nasal inflammation and 23% had some permanent effect to the nasal passages, such as perforation, though no correlation with concentration was made (Williams, 1996). A health hazard evaluation (HHE) was conducted by NIOSH investigators in 1975 at a chrome plating facility in Columbus, Ohio, where of the 11 men evaluated by a

physician, four workers had evidence of current or past nasal ulcers and five had evidence of septal perforation (Lucas, 1975).

IV. Dermal Toxicity

The dermal irritation from Cr has been documented as early at the 1860's as deep sores found on dye workers' hands (Christison, 1845). Further study of Cr sores was made by Dr. DaCosta, who found that tanners who worked with their hands in tanning solution often developed sores that had very little lateral spread but penetrated deeply into the tissue, at times so deeply that bone was visible (DaCosta, 1916). These sores only formed when the skin was already compromised in some way and only resolved once the worker no longer used the tanning solution. In the Lucas HHE, nine out of the eleven workers evaluated had evidence of past ulcers that had healed (1975).

Dermatitis and sensitization is frequently reported in literature for workers exposed to Cr(VI). Williams reported during a cross-sectional study that 23% of workers had active dermatitis, 34% had evidence of healed ulcers, and 13% had active ulcers (1996). In a pre-exposed population, Nethercott determined that 10% of the minimum elicitation threshold to for allergic response was 0.089 $\mu g/cm^3$ (1994).

V. Ingestion Toxicity

While generally a poor route of exposure, it is possible for poisoning to occur if a sufficient amount of Cr(VI) is ingested. Gad affirmed that while acute effects from ingesting a large amount of Cr(VI) was possible, it was most often used in a suicide attempt, not as accidental exposure through an occupational setting (1989). Recent review of meta data available from studies which reported Cr(VI) exposure and stomach cancer concluded no concrete association was present between the two (Suh, 2019).

A summary of key human studies and their health effects is available in Table A1.

Table A1. Health Effects in Humans from Cr(VI) Exposure

Route	Exposure Duration	Effect	Mean Concentration of Exposure (mg/m^3)	Study
Inhalation	<90 days	irritated/ulcerated nasal septum	0.02 (as CrO_3)	Gibb et al. 2000a
Inhalation	Chronic	lung cancer	≥ 0.03 (as CrO_3)	Gibb et al. 2000b
Inhalation	Chronic	irritated/ulcerated nasal septum	0.004	Lucas, 1975
Dermal	Chronic	ulcerated skin	0.025 (as CrO_3)	Gibb et al. 2000a
Dermal	Chronic	burns	0.022 (as CrO_3)	Gibb et al. 2000a
Dermal	Chronic	ulcerated skin	0.004	Lucas, 1975
Dermal	<1 day	allergic response	0.089 $\mu g/cm^2$	Nethercott, 1994

VI. Ubiquity in Industry

Cr exposure occurs frequently in a variety of industries, including electroplating, stainless steel manufacture and welding, textile manufacturing and leather tanning, paint and pigment manufacturing, printing ink manufacturing, catalyst producing, and wood preservation. (National Toxicology Program, 2019; NIOSH, 2013). It was estimated in 2006 that over half a million workers in the United States were exposed to Cr(VI) as part of their job duties (NIOSH, 2013).

Cr exposure is a concern for the Air Force in corrosion control, as the primer that is used to bond bare metal to paint contains Cr(VI) (Aizenberg, 2000). Any operation where primer is applied or disturbed, such as sand blasting in preparation for a repainting operation, has the potential to expose workers to Cr(VI) particulate. Since 2008, over 9,100 air samples for Cr(VI) have been loaded into the Defense Occupational and Environmental Health Readiness System (DOEHRS). Generally, the DOEHRS samples marked welding were not over the OEL, however; an HHE of welding at a shipyard where air samples were collected yielded results above the limit of detection, suggesting that Cr can be freed during arc welding processes at an appreciable amount (Kiefer, 1998).

Considering the health effects seen at low concentrations of Cr(VI), accurate sampling of occupational environments is necessary to recommend appropriate PPE. In light of the lowered TLV proposed by ACGIH, confirmation that the IOM can be operated at a higher flow rate without compromising its adherence to the inhalable particle convention is critical.

Bibliography

ACGIH. Chromium and Inorganic Compounds in TLV Documentation. (2018).

Aizenberg, V., England, E., Grinshpun, S., Carlton, G., Willeke, K. Metal Exposure Among Abrasive Blasting Workers at Four U. S. Air Force Facilities. *Applied Occupational and Environmental Hygiene, 15*(10), pp 766-772. (2000).

Anthony, T. R., Sleeth, D., Volckens, J. Sampling Efficiency of Modified 37-mm Sampling Cassettes Using Computational Fluid Dynamics. *J Occup Environ Hyg. 13*(2), pp 148 – 158. (2016).

ATSDR. Toxicological Profile for Chromium. Atlanta, GA: Agency for Toxic Substances and Disease Registry. (2012).

Avina, L., Codd, R., Killon, C. T., Lay, P. A. Chapter 2: Chromium in Biology: Toxicology and Nutritional Aspects in *Progress in Inorganic Chemistry, 51*, pp 145-250. Hoboken, NJ: John Wiley and Sons, Inc. (2003).

Barceloux, D. G., Barceloux, D. Chromium. *Journal of Toxicology: Clinical Toxicology 37*(2), pp 173-194. (1999).

Bertini, I., Gray, H. B. Stiefel, E. I., Selverstone, J. Biological Inorganic Chemistry - Structure and Reactivity. University Science Books. (2007). Retrieved from https://app.knovel.com/hotlink/toc/id:kpBICSR00H/biological-inorganic/biological-inorganic

Christison, R. *A Treatise on Poisons in relation to Medical Jurisprudence, Physiology, and the Practice of Physic*, 4th Edition. London, England: Adam and Charles Black. (1845). Available from: https://collections.nlm.nih.gov/ocr/nlm:nlmuid-61910390R-bk.

DaCosta, J. C., Jones, J. F. Tanners' Ulcer. *Annals of Surgery, 63*(2), pp 155-166. (1916).

Ermolli, M., Menné, C., Pozzi, G., Serra, M. A., Clerici, L. A. Nickel, cobalt and chromium-induced cytotoxicity and intracellular accumulation in human hacat keratinocytes. *Toxicology, 159*, pp 23-31. (2001).

Gad, S. C. Acute and Chromic Systemic Chromium Toxicity. *The Science of the Total Environment, 86,* pp 149-157. (1989).

Gibb, H. J., Lees, P. S. J., Pinsky, P. F., Rooney, B. C. Lung Cancer Among Workers in Chromium Chemical Production. *American Journal of Industrial Medicine, 38*, pp 115-126 (2000a).

Gibb, H. J., Lees, P. S. J., Pinsky, P. F., Rooney, B. C. Clinical Findings of Irritation Among Chromium Chemical Production Workers. *American Journal of Industrial Medicine, 38*, pp 127-131 (2000b).

Gibb, H. J., Lees, P. S. J., Wang, J., O'Leary, K. G. Extended Followup of a Cohort of Chromium Production Workers. *American Journal of Industrial Medicine, 58*, pp 905-913 (2015).

Kiefer, M., Trout, D., Wallace, M. E. Avondale Shipyards Health Hazard Evaluation. Cincinnati, OH: NIOSH Publications Office. HETA 97-0260-2716. (1998).

Lucas, J. B., Kramkowski, R. S. HHE determination Report of Industrial Platers, Inc. Cincinnati, OH: NIOSH Publications Office. HHE-74-87-221. (1975).

National Toxicology Program. Hexavalent Chromium. Retrieved 4 April 2019 from https://www.niehs.nih.gov/health/materials/hexavalent_chromium_508.pdf.

NIOSH. Criteria for a Recommended Standard Occupational Exposure to Hexavalent Chromium. Cincinnati, OH: Department of Health and Human Services. (2013).

Nethercott, J., Paustenbach, D., Adams, R., Fowler, J., Marks, J., Morton, C., Taylor, J., Horowitz, S., Finley, B. A study of chromium induced allergic contact dermatitis with 54 volunteers: implications for environmental risk assessment. *Occupational and Environmental Medicine, 51*, pp 371-380. (1994).

OSHA. Occupational Safety and Health Standards, 29 CFR §1910.1026—Chromium (VI) (2006).

Rock, J. C. A comparison between OSHA-compliant criteria and action-level decision critera. *American Industrial Hygiene Association Journal 43*(5), pp 297-313. (1982).

Singh, J., Pritchard, D. E., Carlisle, D. L., Mclean, J. A., Montaser, A., Orenstein, J. M., Patierno, S. R. Internalization of Carcinogenic Lead Chromate Particles by Cultured Normal Human Lung Epithelial Cells: Formation of Intracellular Lead-Inclusion Bodies and Induction of Apoptosis. *Toxicology and Applied Pharmacology, 161*, pp 240-248. (1999).

Stewart, J., Sleeth, D. K., Handy, R. G., Pahler, L. F., Anthony, T. R., Volckens, J. Assessment of increased sampling pump flow rates in a disposable, inhalable aerosol sampler. *J Occup Environ Hyg. 14*(3), pp 207-213. (2017).

Suh, M., Wikoff, D., Lipworth, L., Goodman, M., Fitch, S., Mittal, L., Proctor, D. Hexavalent chromium and stomach cancer: a systematic review and meta-analysis. *Critical Reviews in Toxicology.* (2019).

Vincent, J. B. Chromium: is it essential, pharmacologically relevant, or toxic? *Metal ions in Life Sciences, 13*, pp 171-198. (2013).

Williams, N. A survey of respiratory and dermatological disease in the chrome plating industry in the West Midlands, UK. *Journal of Occupational Medicine 46*(6), pp 432-434 (1996).

Appendix B

LOD and LOQ Calculations for Hexavalent Chromium Sampling

New proposed ACGIH TLV-TWA-8hr = 0.0002 mg/m^3 = 0.2 µg/m^3

New proposed STEL = 0.0005 mg/m^3 = 0.5 µg/m^3

The current LOD of the analytical lab is 30 ng. Assuming a desired LOQ of 10% the new OEL, the general equation for calculating the LOQ is shown below.

$$\text{LOQ (µg)} = \text{OEL} * 0.1 * time\ sample\ (min) * flow\ rate\left(\frac{L}{\text{min}}\right)$$

$$\text{LOQ (µg)} = 0.0002\frac{mg}{m^3} * (8hr * 60\ \text{min}) * 2\left(\frac{L}{\text{min}}\right) = 0.192\ \mu g$$

Assuming the LOD is three times the signal-to-noise ratio and the LOQ is ten times the signal-to-noise ratio, the LOD can be calculated from the LOQ by multiplying by three tenths.

Table shows the necessary LOQs and LODs by the sample flow rate.

Table B1. Necessary LOQ by Flow Rate

Flow Rate (L/min)	LOQ (µg)		LOD (µg)	
	TWA-8h	STEL	TWA-8h	STEL
2	0.0192	0.0015	0.00576	0.00045
4	0.0384	0.0030	0.01152	0.00090
6	0.0576	0.0045	0.01728	0.00135
8	0.0768	0.0060	0.02304	0.00180
10	0.0960	0.0075	0.02880	0.00225
12	0.1152	0.0090	0.03456	0.00270

The assumptions above are based in best practices but it is apparent from that quantification necessary is difficult to achieve in practice, as in many cases less than 10

nanograms of chromium would be present. A more realistic approach would be to assume a desired LOQ of 50% of the OEL, the results of which are shown in Table B2.

Table B2. Revised necessary LOQ by flow rate

Flow Rate (L/min)	LOQ (µg)		LOD (µg)	
	TWA-8h	STEL	TWA-8h	STEL
2	0.096	0.0075	0.0288	0.00225
4	0.192	0.0150	0.0576	0.00450
6	0.288	0.0225	0.0864	0.00675
8	0.384	0.0300	0.1152	0.00900
10	0.480	0.0375	0.1440	0.01125
12	0.576	0.0450	0.1728	0.01350

By assuming 50% of the OEL for the LOQ, it could be determined if the action limit had been exceeded. The magnitude of the value below the action limit, while of research interest, does not necessarily add to the decision-making process. Therefore, in the interest of feasibility, a target LOQ of 50% of the applicable OEL can be used without compromising workers' health.

Appendix C

Empirical Model for Cassette Capture

I. Introduction

As the bodies of toxicological and epidemiological knowledge grow, there is a trend for exposure standards to decrease to better protect workers' health. For contaminants with a large exposure base, this process leads to new sampling for groups previously exposed below levels of concern and increased sampling of groups who are now considered overexposed. Two contaminants of concern, beryllium and hexavalent chromium, have large exposure bases in both civilian and military settings. Both contaminants have recently had their recommended exposure levels lowered from 2 $\mu g/m^3$ to 0.02 $\mu g/m^3$ for beryllium and 5 $\mu g/m^3$ to 0.2 $\mu g/m^3$ for chromium (Brisson, 2005; ACGIH 2017). On top of the lowering of recommended exposure thresholds, both have had particle size selective (PSS) sampling added.

ACGIH is reevaluating threshold limit values with an aerosol component to determine if PSS is warranted (ACGIH, 2018). Of the three conventions outlined by ACGIH, the one with the largest range of size of particles collected is the inhalable. Traditional 'total dust' sampling with closed face cassettes (CFCs) were not designed for any particle size fraction, though several studies have demonstrated CFCs have a cut point of ~ 20 μm which is much lower than 100 μm as required for the inhalable convention. While several inhalable PSS samplers exist, the IOM remains popular, due to its availability and the strength of its claim to follow the inhalable convention.

Taken together, ever lowering exposure limits and particle selective criteria, there is a struggle to collect enough mass to meet the limit of detection for a method. While

tinkering with a method is the purview of analytical scientists, industrial hygienists contribute to sample mass through the flow rate set for the sampler. The temptation exists to simply increase the sample flow rate to gain more mass without considering the impact to aspiration efficiency of the device for different sized particles.

The aspiration efficiency is one of the primary measures of sampler performance. It is a measure of how many of the particles in the free stream make it into the inlet of the sampler. In isokinetic sampling, the free stream velocity and angle are matched with the sampling velocity and the concentration of particles outside the sampler matches the concentration of particles aspirated through the inlet. In the real-world isokinetic sampling is rarely achievable. A mismatch of flow or the effect of a blunt object on the flow streams around the sampler inlet conspire to introduce bias into the sampling process.

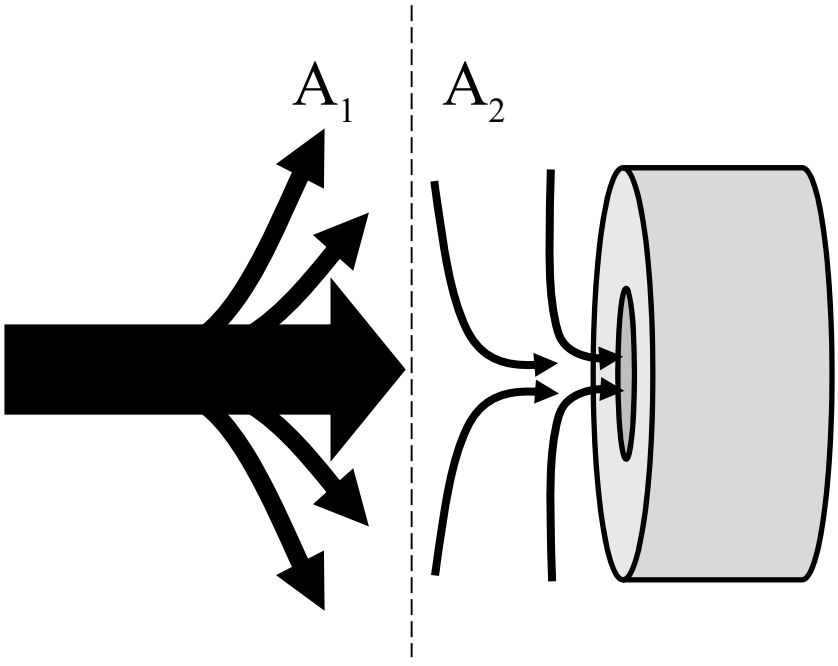

Figure C1. Flow Regimes for a Blunt Sampler

For a blunt sampler, two flow regimes can be visualized (Figure C1). The first is the effect the blunt body has on the flow streams, causing the streams to diverge from their path to go around the object. The second regime is where the suction of the sampler influences those diverging flow lines and pulls them into the inlet. These two forces have different efficiencies, A_1 and A_2. The overall efficiency of the sampler is the product of the efficiencies from the two different regimes.

The relationship between the freestream air velocity (U), sampling air velocity (U_S), aerodynamic particle diameter (d_{AE}), and aspiration efficiency of a disk-shaped sampler was refined by Paik and Vincent (2002). Their empirical model for aspiration efficiency had an R^2 of 0.80 when fitted to historical data and explained 97% of the variability observed between samples (Paik, 2002).

While at times it is necessary to increase sample flow rates to meet LODs, practitioners should be cognizant of the effect these increases have on the cut points of their devices. Two commonly used samplers, the CFC and IOM, are evaluated in different flow conditions using empirical aspiration efficiency equations to illustrate impact to sampler performance.

II. Methods

Aspiration efficiency can be thought of as a function of the Stokes number (St), the sampler inlet diameter, and the ratio of air velocities. Table C1 shows the parameters explored in the simulation. Both the closed face cassette (CFC) and IOM were modelled separately.

Table C1. Simulation Parameters

Parameter	Values
U_S	2, 4, 6, 8, 10 (LPM)
U	0.1, 0.5, 1.0 m/s
d_{AE}	5, 10, 15, 20, 30, 40, 50, 60, 70, 80, 90, 100 μm
δ_{IOM}	0.015 m
δ_{CFC}	0.004 m
D_{IOM}	0.028 m
D_{CFC}	0.041

To begin, the St number was calculated for a variety of particle sizes using Equation 15 (Paik, 2002). The Cunningham slip correction factor was not included since the particles of interest were >1 μm.

Equation 15. Stokes' Number

$$\mathrm{St} = \frac{d_{ae}^2 * \rho_p * U}{18 * \eta * \delta}$$

In the A_1 regime, the modified St number is given in Equation 16, using the dimensional number, ϕ_A, which represents the ratio of the sampling flow rate to the flow incident on the face of the sampler (Paik, 2002).

Equation 16. Stokes 1

$$\mathrm{St}_1 = \mathrm{St}\left(\frac{r}{\phi_A^{\frac{1}{3}}}\right)$$

The efficiency due to impaction, β_1, is described in Equation 17, where G_1 and G_2 were empirical coefficients determined through non-linear least-squares regression (Paik, 2002).

Equation 17. Efficiency due to Impaction

$$\beta_1 = 1 - \left(\frac{1}{1 + G_1\left(\frac{R}{r}\right)^{G_2}\mathrm{St}_1}\right)$$

Finally, the aspiration efficiency for the first regime was calculated using Equation 18 (Paik, 2002).

Equation 18. First Regime Aspiration Efficiency (A_1)

$$A_1 = 1 + \beta_1(\phi_A^{-\frac{1}{3}} - 1)$$

Equations 5 – 7 mirror those above, though they represent the second regime influenced by the suction of sampler inlet (Paik, 2002).

Equation 19. Stokes' 2

$$\mathrm{St}_2 = \mathrm{St}\phi_A^{\frac{1}{3}}$$

Equation 20. Efficiency due to Suction

$$\beta_1 = 1 - \left(\frac{1}{1 + G_2\mathrm{St}_2}\right)$$

Equation 21. Second Regime Aspiration Efficiency

$$A_2 = 1 + \beta_2 \left(\left(\frac{r}{\phi_A^{\frac{1}{3}}} \right)^2 - 1 \right)$$

The overall aspiration efficiency for the sampler is shown in Equation 22 (Paik, 2002).

Equation 22. Overall Sampler Efficiency

$$A = A_1 A_2$$

III. Results

The following plots are the result of the calculations described in section II. Figure C2 shows a general trend of under sampling for the CFC, with the trend increasing as the freestream velocity increases. The IOM is more complex as some freestream velocities demonstrate over sampling at low pump velocities and under sampling at higher pump velocities. Inflection points can be seen in both the 0.5 m/s and 1 m/s freestream plots as the A_1 efficiency effect dwindles and A_2 begins to dominate.

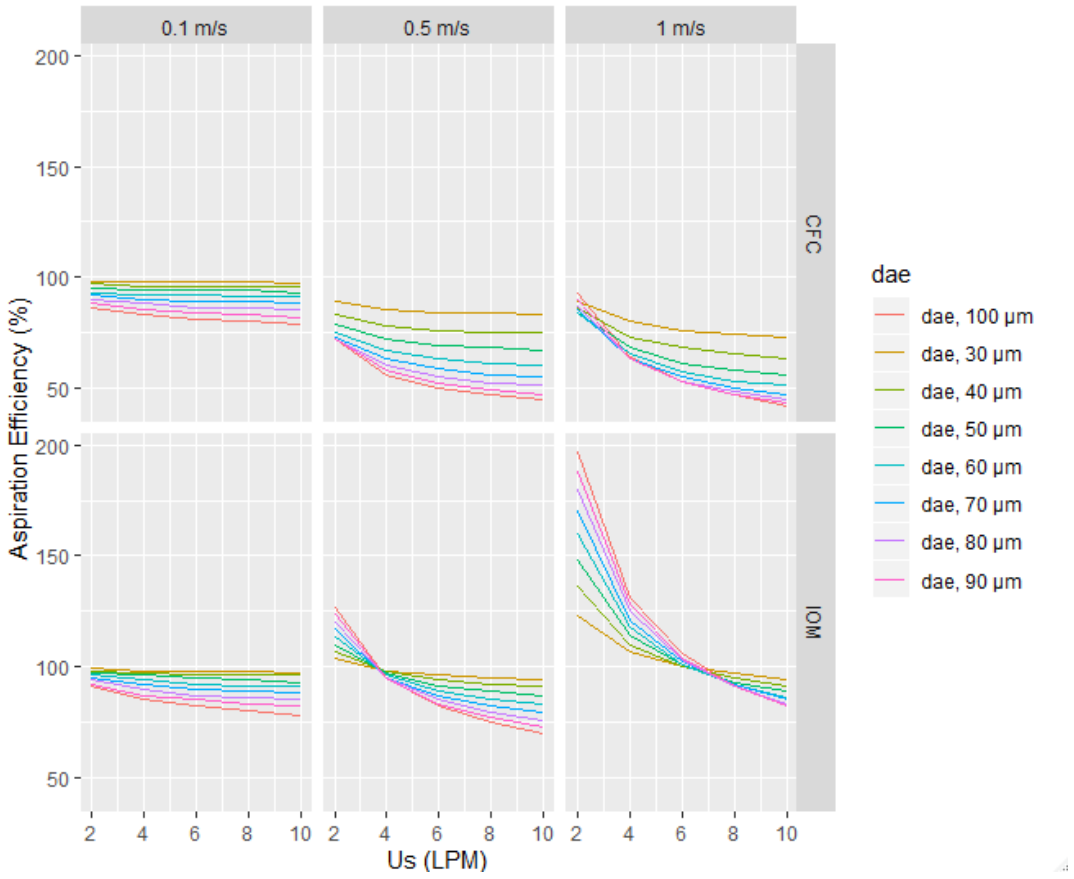

Figure C2. CFC and IOM Aspiration Efficiency for Varying Particle Diameters

The results from the CFC simulation support what has been found in the field, namely that the CFC under samples large particles in most conditions, more so than the IOM. The ease of use and familiarity practicing IHs have with CFCs should not be discounted but there are serious drawbacks in performance that must be understood before using one. This simple model underscores how even idealized conditions result in poor performance.

Earlier calculations indicated to meet the laboratory's 30 ng LOD, the minimum flow rate necessary to collect enough volume during eight hours was 6 LPM. Based on these results, under sampling large particles is likely for 0.1 and 0.5 m/s free stream

velocity when the pump flow rate is 6 LPM or higher. Near isokinetic conditions occur around 6 LPM when the free stream velocity is 1 m/s. Free stream velocities higher than 1 m/s would likely result in oversampling large particles.

These results serve two purposes. One is to illustrate how seemingly small variations in the sampling environment can have a large impact on the sample result. The other is to benchmark what the expected aspiration efficiency is at a given condition so that during experiments the bias of the samplers can be evaluated.

Bibliography

ACGIH. Chromium and Inorganic Compounds in TLV Documentation. (2018).

ACGIH. Appendix C: Particle Size-Selective Sampling Criteria for Airborne Particulate Matter in *2018 TLVs and BEIs.* pp 80 – 81. Cincinnati, OH: ACGIH Signature Publications. (2018).

Brisson, M. J., Ashley, K. Sampling and Analysis Issues Relating to the ACGIH Notice of Intended Change for the Beryllium Threshold Limit Value in Analytical Performance Criteria. DOE Contract: DE-AC09-96SR18500. (2005).

Paik, S. Y., Vincent, J. H. (2002). Aspiration efficiency for thin-walled nozzles facing the wind and for very high velocity ratios. *Journal of Aerosol Science 33*(5), pp 705-720.

Vincent, J. H. (2007). Aerosol Sampling: Science, Standards, Instrumentation and Applications. West Sussex, England: John Wiley & Sons Ltd

Appendix D

Chamber Characterization Data Processing

In order to know where the three-minute measurement period started and ended in the Excel file, the data line off the ADM-880c display was recorded. The data line was recorded in an Excel sheet both when the thee-minute timer was started and when it finished.

For the initial measurements, data was downloaded from the ADM-880c after every plane (the location was known because locations were always sampled A to C). For the random measurements, data was downloaded after every location in order to maintain data integrity. Downloaded files were named by the location (distance from inlet, horizontal letter, and height, i.e. 18A-3).

There were several steps taken during the data processing. First, the CSV files retrieved from the ADM-880c were converted to Excel files and the unused columns were deleted (mainly those for other ADM-880c recording functionalities). Then the data file was cross-referenced with the data lines recorded during measurement and the measurement rows were highlighted. During this process the time for the first and last measurements were compared to ensure that a 3-minute window had been recorded. In all cases at least a 3-minute window was recorded. In a couple of instances, the end timer was not heard due to noise in the surroundings and more than 3-minutes of data were collected. In these cases, the start time was used to determine an end row of 3-minutes.

After all of the measurement rows were marked, they were copied to a third Excel workbook to consolidate all data in one place. The location and fan setting information

were input manually from the file name and then all data were copied to the new workbook. The columns containing only units were deleted as they were captured in the column headings.

Next, the recorded velocities were corrected for the relative humidity of the workspace. This was done by inserting 7 columns between the existing Temperature (°F) column and the Abs Pres (in Hg) column. These were used to convert temperature to degrees Celsius, calculate the Saturation Vapor Pressure (P_{sat}) and Vapor Pressure (P_{vapor}), contain the relative humidity data, and then calculate the corrected velocity (Equations 3, 4, 5). The relative humidity data was copied from the downloaded Kestrel data sheet or from manually recorded points. The Kestrel was set to log data every 20 minutes. The following convention was used to assign relative humidity data to velocity readings. If a Kestrel reading was taken at 9:20:00, it was associated with ADM-880c readings between 9:20:00 and 9:39:59. Then the Kestrel reading for 9:40:00 was associated with velocity readings taken between 9:40:00 and 9:59:59. In addition, a column was added to capture the difference between the original value and the corrected value. Relevant equations are shown (Equation 23). The calculation of P_{sat} was done by using the equation behind the National Weather Services Vapor Pressure Calculator (Equation 23) (Brice and Hall, no date). After the saturation vapor pressure was calculated, it was used to calculate the vapor pressure by the relationship between relative humidity and P_{sat} (Equation 24) (Engineering Toolbox, 2004). Finally, the barometric pressure (Abs Pres, recorded by the ADM-880c), recorded velocity, and vapor pressure were used to determine the corrected velocity (Equation 25).

Equation 23. Saturation Vapor Pressure

$$\mathrm{P_{sat}} = 6.11 * 10^{\frac{7.5*T}{237.3+T}},\ \ P_{sat} = [mbar]$$

$$\mathrm{P_{[inHg]}} = 0.0295300 * P_{[mbar]}$$

Equation 24. Relative Humidity, Vapor Pressure, and Saturation Vapor Pressure Relationship

$$\mathrm{RH} = \left(\frac{P_{vapor}}{P_{sat}}\right) * 100\% \rightarrow P_{vapor} = \left(\frac{\mathrm{RH}}{100}\right) * P_{sat}$$

Equation 25. Corrected Velocity for Moist Air

$$\mathrm{V_{moist\ air}} = \frac{P_b * V_{dry}}{P_b - P_{vapor}},$$

Where:

$V_{moist\ air}$ = velocity corrected for moist air

P_b = local barometric pressure,

V_{dry} = velocity corrected for local density (T & barometric pressure)

P_{vapor}=vapor pressure

Appendix E

Velocity Profiles at 30 and 60 Hz

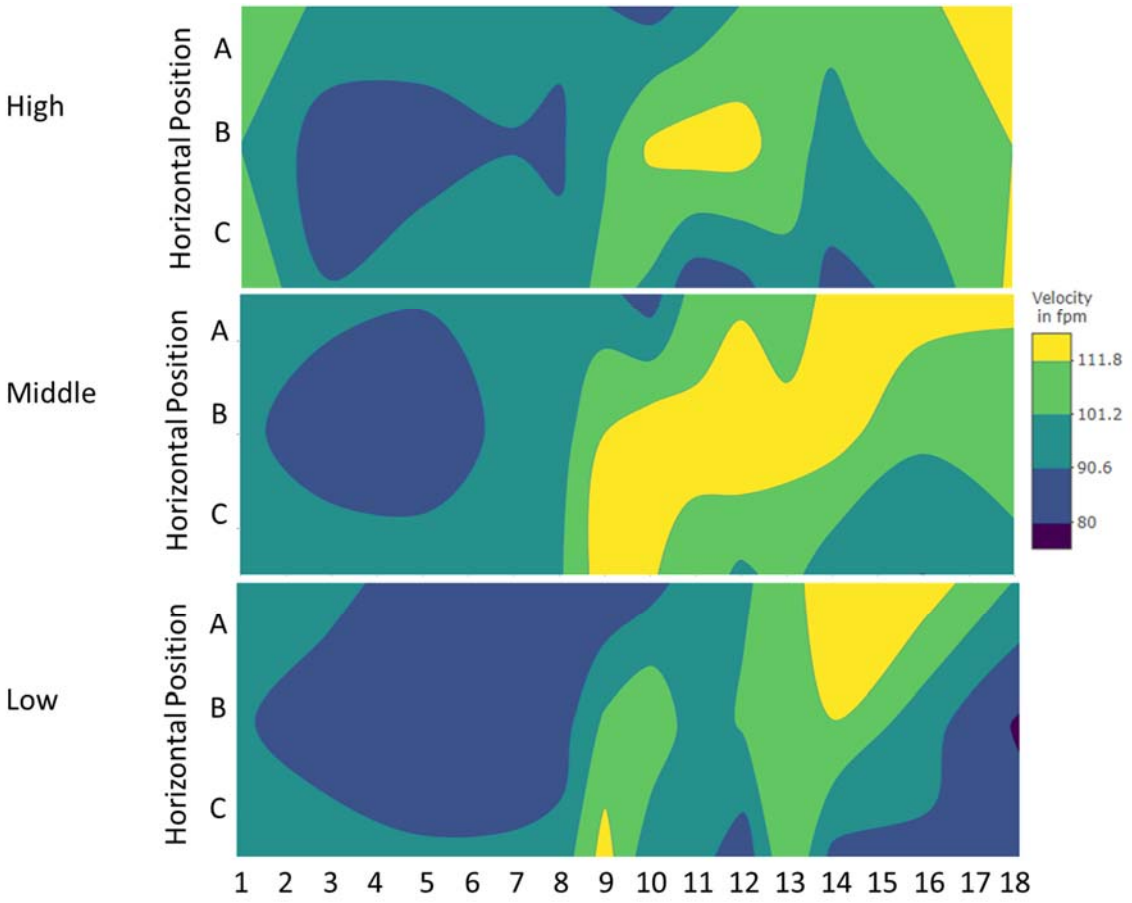

Figure D1. Vertical Velocity Profile of the Chamber at 30 Hz, no Flow Straightener

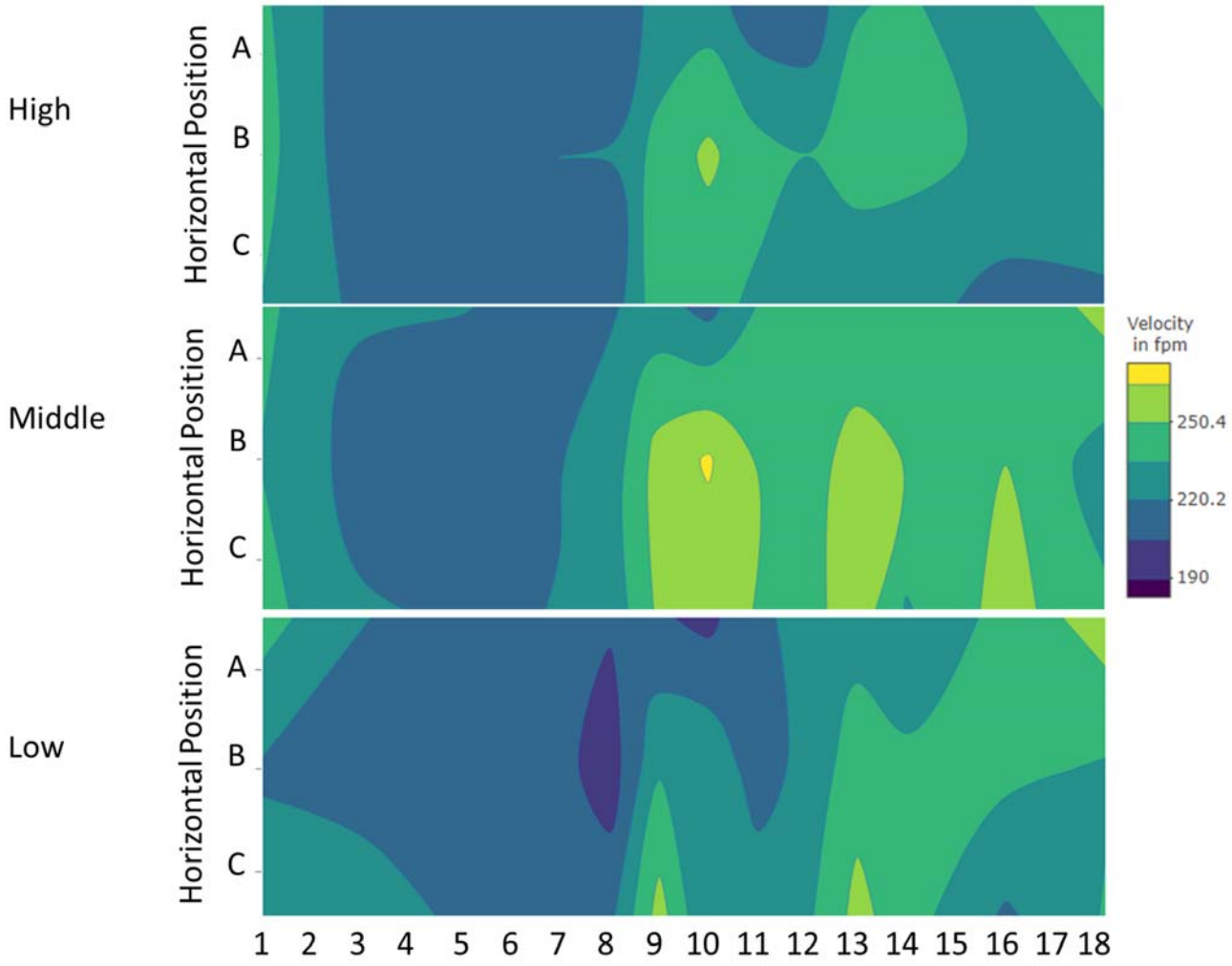

Figure D2. Vertical Velocity Profile of the Chamber at 60 Hz, no Flow Straightener

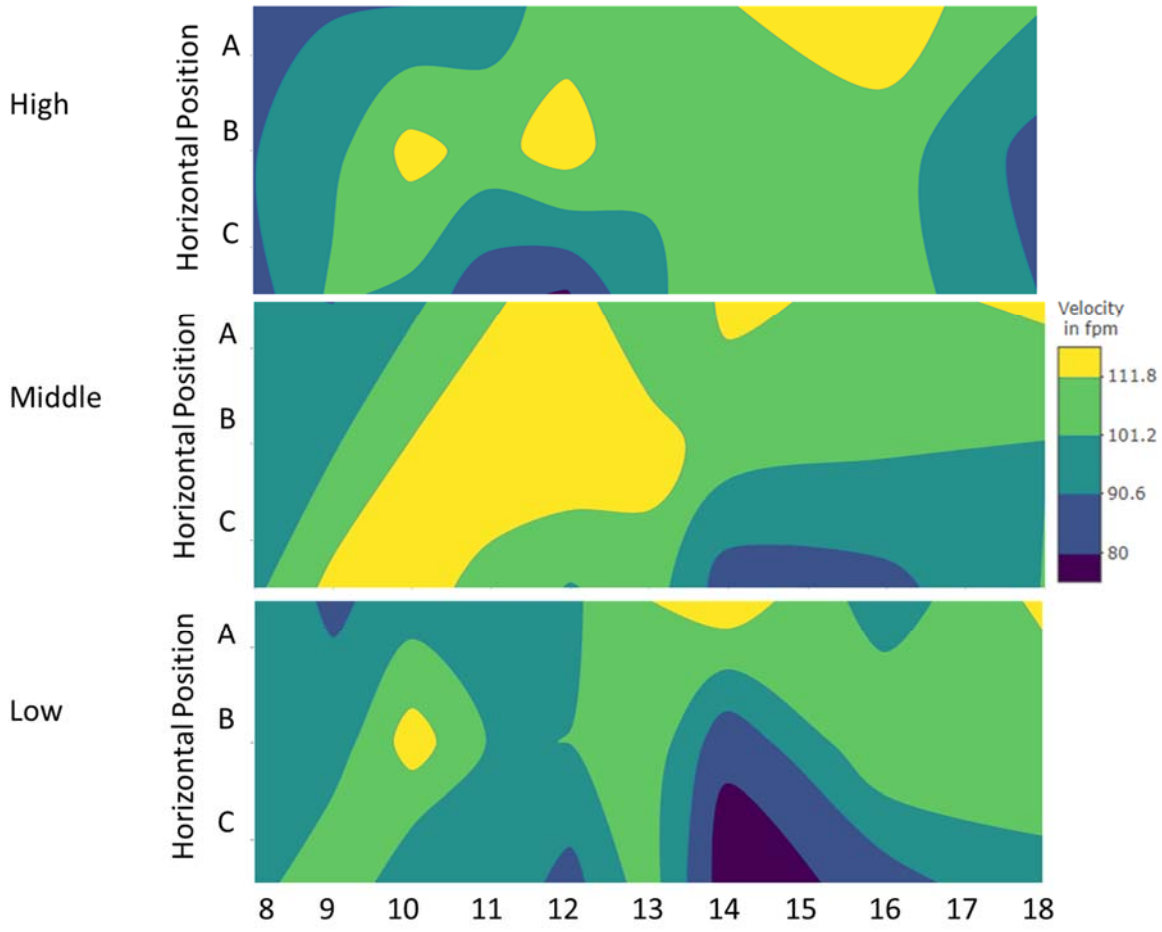

Figure 31. Vertical Velocity Profile of the Chamber at 30 Hz, with Flow Straightener

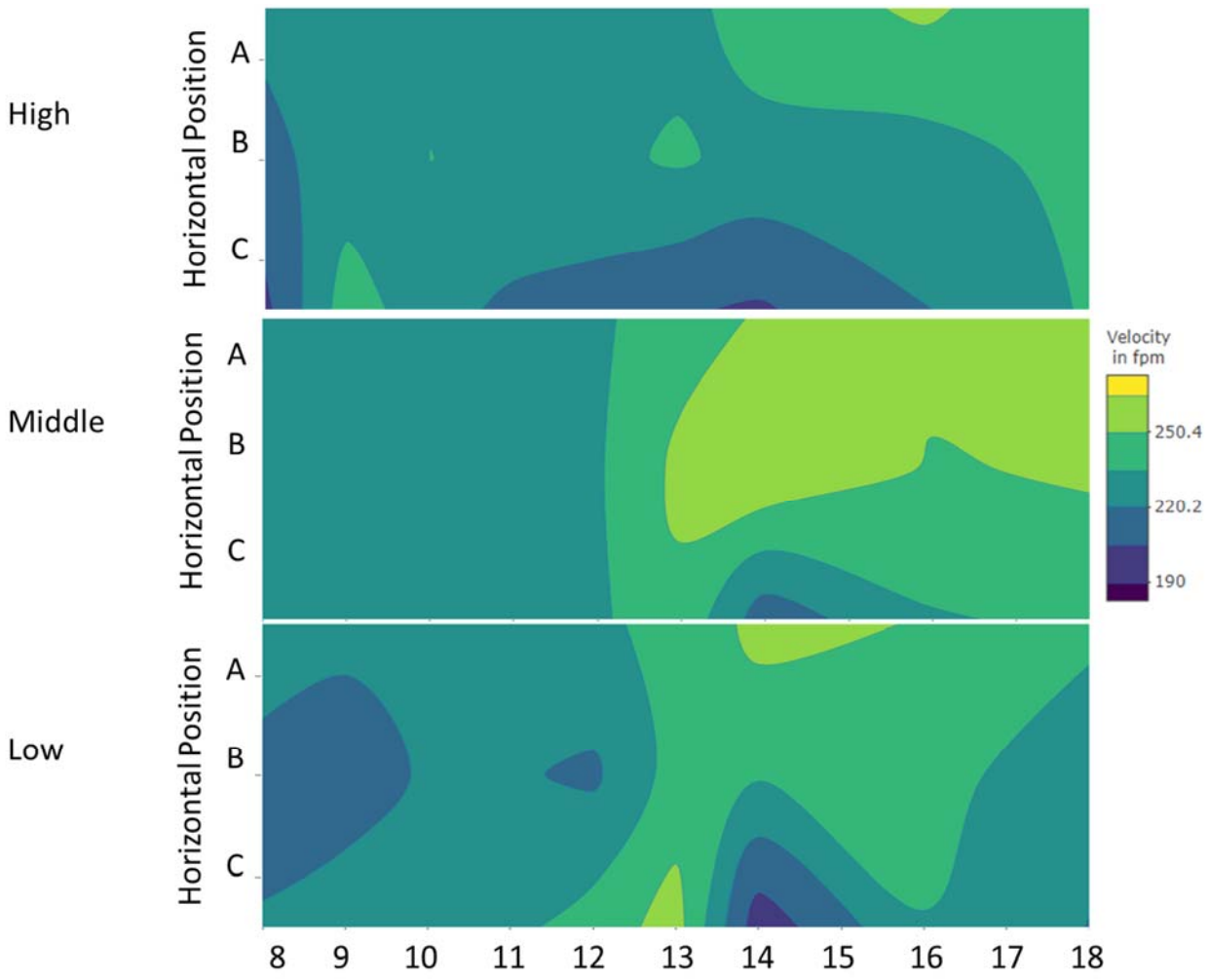

Figure D4. Vertical Velocity Profile of the Chamber at 60 Hz, with Flow Straightener

Appendix F

Day-to-Day Variability in Velocity Measurements

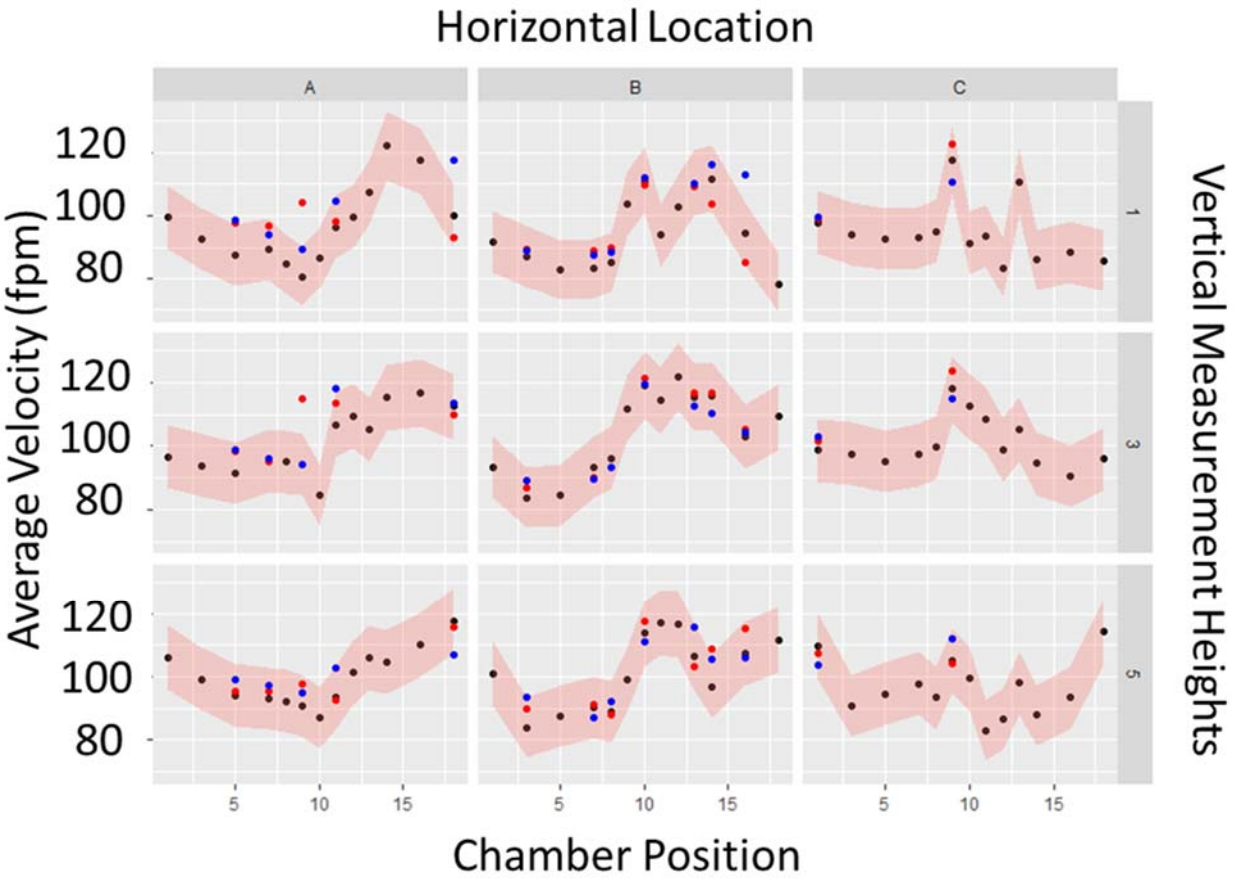

Figure F1. Day-to-Day Variability in Average Velocity at 30 Hz, no Flow Straightener

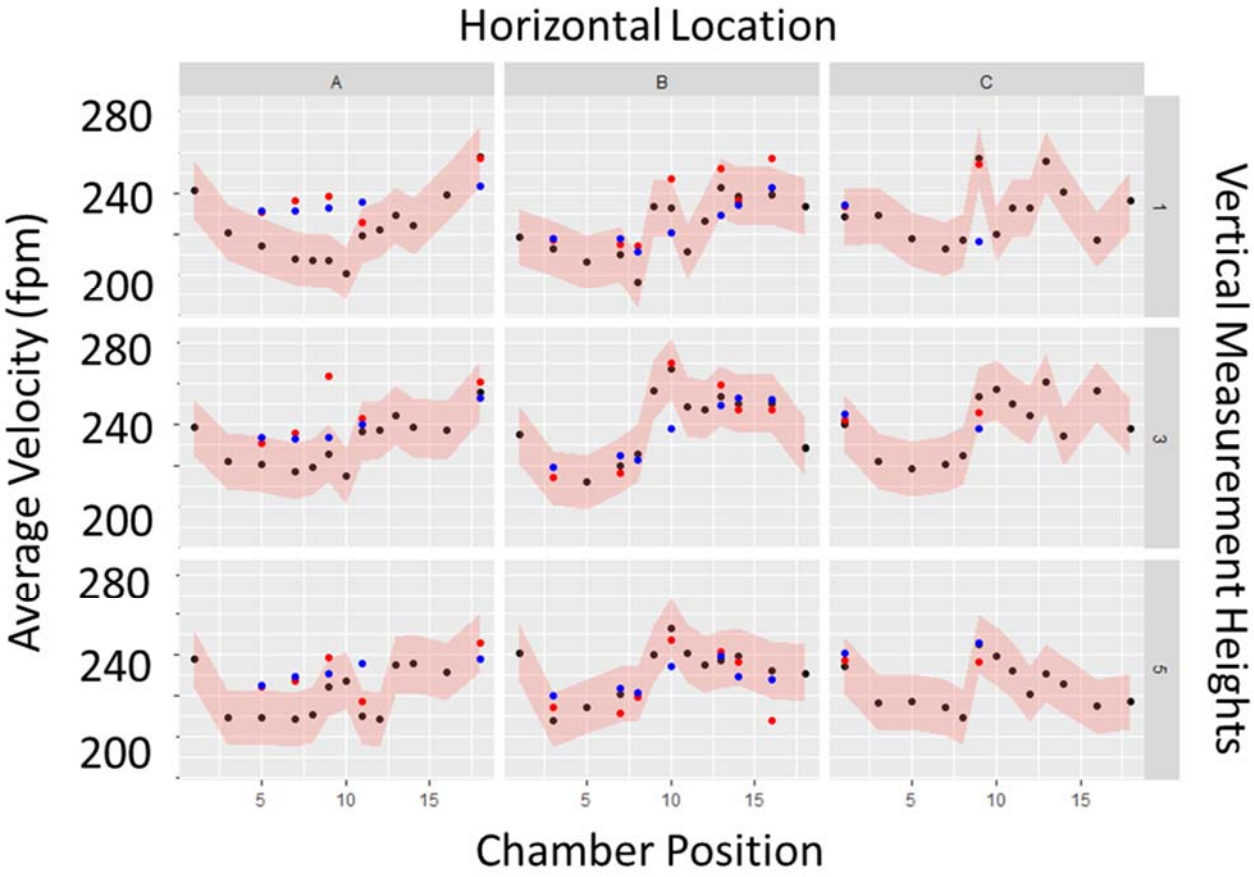

Figure F2. Day-to-Day Variability in Average Velocity at 60 Hz, no Flow Straightener

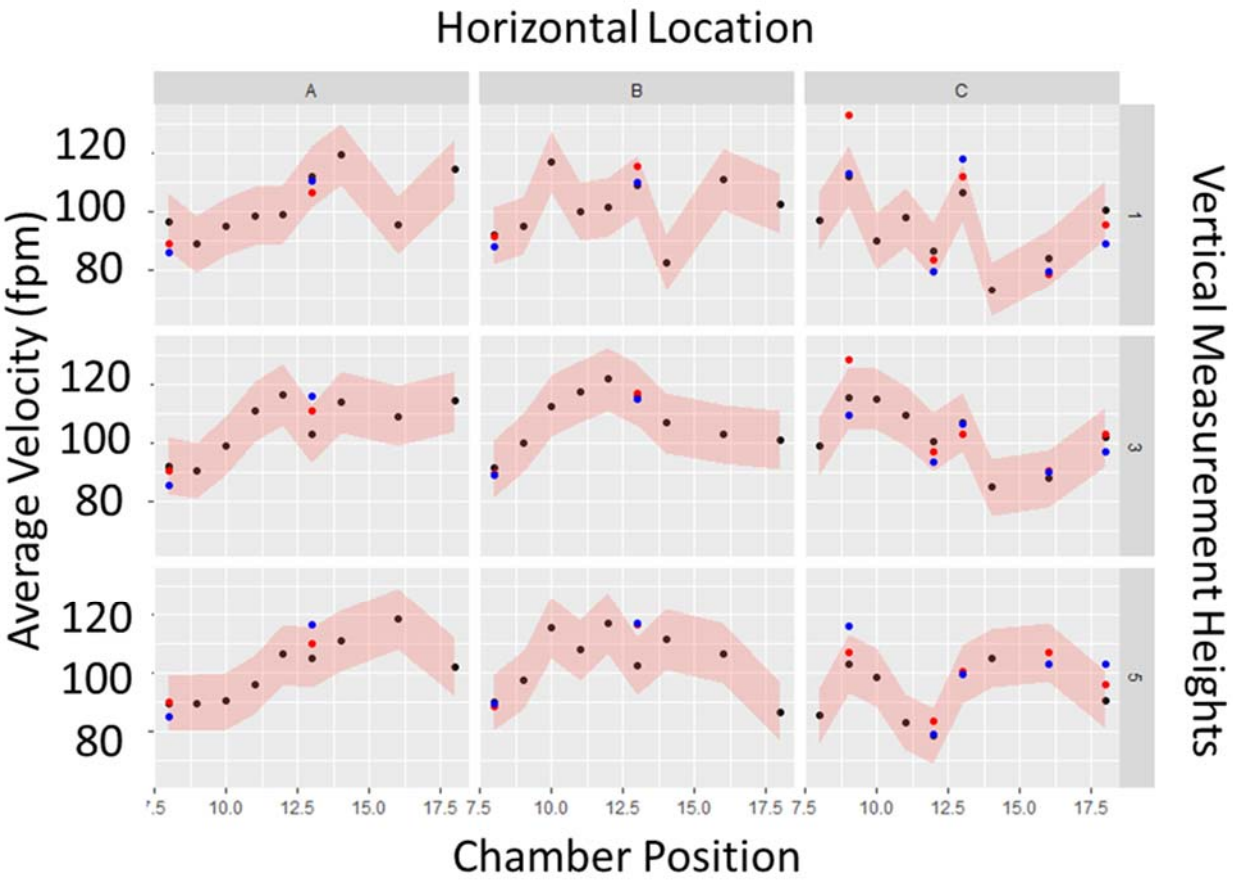

Figure F3. Day-to-Day Variability in Average Velocity at 30 Hz, with Flow Straightener

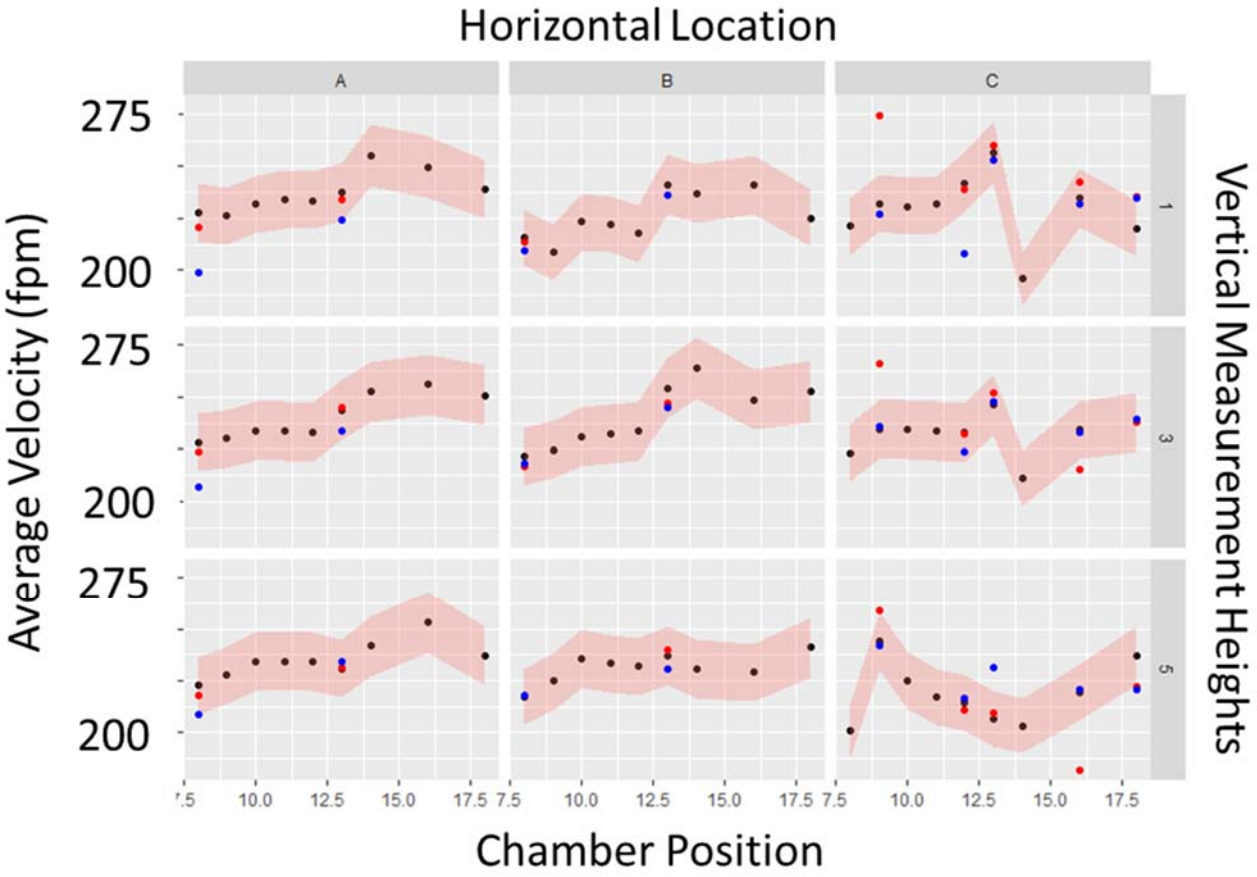

Figure F4. Day-to-Day Variability in Average Velocity at 60 Hz, with Flow Straightener

Appendix G

Example Determination of CMD, MMD, and GSD for Aerosol Data

Table G1. Size Distribution Calculations of Aerosol Data

Bin Width	Size Range (µm)	Midpoint	Volume (m^3)	Count	Mass (mg)	Frequency/µm	Fraction/ µm	Cumulative Mass	LN(d_i)	n_i*LN(d_i)	d_i/d_g	CMD	CMD (d_i/d_g)
0.074	0.3 - 0.374	0.337	2.00E-20	21789	2.18E-07	2.95E-06	0.119	1%	-1.09	-2.37E-07	1.20E-06	-23699.3	2802.2
0.091	0.374 - 0.465	0.420	3.87E-20	11158	2.16E-07	2.37E-06	0.095	2%	-0.87	-1.87E-07	9.79E-07	-9692.5	217.6
0.114	0.465 - 0.579	0.522	7.45E-20	5694	2.12E-07	1.86E-06	0.075	3%	-0.65	-1.38E-07	7.75E-07	-3701.6	35.5
0.142	0.579 - 0.721	0.650	1.44E-19	1951	1.40E-07	9.88E-07	0.040	3%	-0.43	-6.04E-08	4.02E-07	-840.5	173.6
0.176	0.721 - 0.897	0.809	2.77E-19	637	8.82E-08	5.01E-07	0.020	4%	-0.21	-1.87E-08	1.92E-07	-134.9	170.2
0.220	0.897 - 1.117	1.007	5.35E-19	2408	6.44E-07	2.93E-06	0.118	6%	0.01	4.49E-09	1.01E-06	16.8	1304.7
0.274	1.117 - 1.391	1.254	1.03E-18	1077	5.56E-07	2.03E-06	0.082	8%	0.23	1.26E-07	5.96E-07	243.7	982.8
0.341	1.391 - 1.732	1.562	1.99E-18	688	6.85E-07	2.01E-06	0.081	11%	0.45	3.05E-07	4.56E-07	306.4	948.7
0.424	1.732 - 2.156	1.944	3.85E-18	990	1.90E-06	4.49E-06	0.181	19%	0.66	1.27E-06	6.78E-07	657.8	1922.4
0.529	2.156 - 2.685	2.421	7.43E-18	722	2.68E-06	5.07E-06	0.204	30%	0.88	2.37E-06	3.82E-07	638.6	1879.7
0.658	2.685 - 3.343	3.014	1.43E-17	407	2.92E-06	4.43E-06	0.179	41%	1.10	3.22E-06	7.31E-08	449.1	1366.6
0.819	3.343 - 4.162	3.753	2.77E-17	256	3.55E-06	4.33E-06	0.174	56%	1.32	4.69E-06	1.31E-08	339.0	1078.9
1.020	4.162 - 5.182	4.672	5.34E-17	154	4.12E-06	4.04E-06	0.163	72%	1.54	6.36E-06	3.23E-07	238.1	796.2
1.269	5.182 - 6.451	5.817	1.03E-16	68	3.49E-06	2.75E-06	0.111	86%	1.76	6.14E-06	8.69E-07	119.2	419.7
1.580	6.451 - 8.031	7.241	1.99E-16	21	2.07E-06	1.31E-06	0.053	95%	1.98	4.10E-06	1.07E-06	41.2	152.9
1.969	8.031 - 10	9.016	3.84E-16	2	4.50E-07	2.28E-07	0.009	96%	2.20	9.89E-07	3.95E-07	5.2	20.1
10.000	10 - 20	15.000	1.77E-15	1	8.84E-07	8.84E-08	0.004	100%	2.71	2.39E-06	1.85E-06	2.7	11.8
			TOTAL:	48023	2.48E-05								

Appendix H

MMD Distribution Boxplots

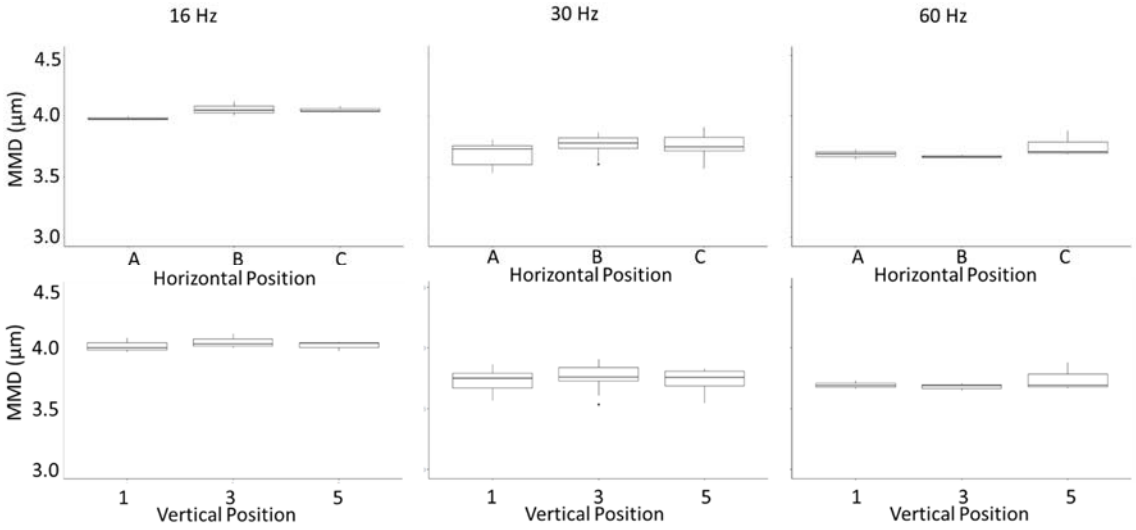

Figure H1. MMD Boxplots for Plane 7

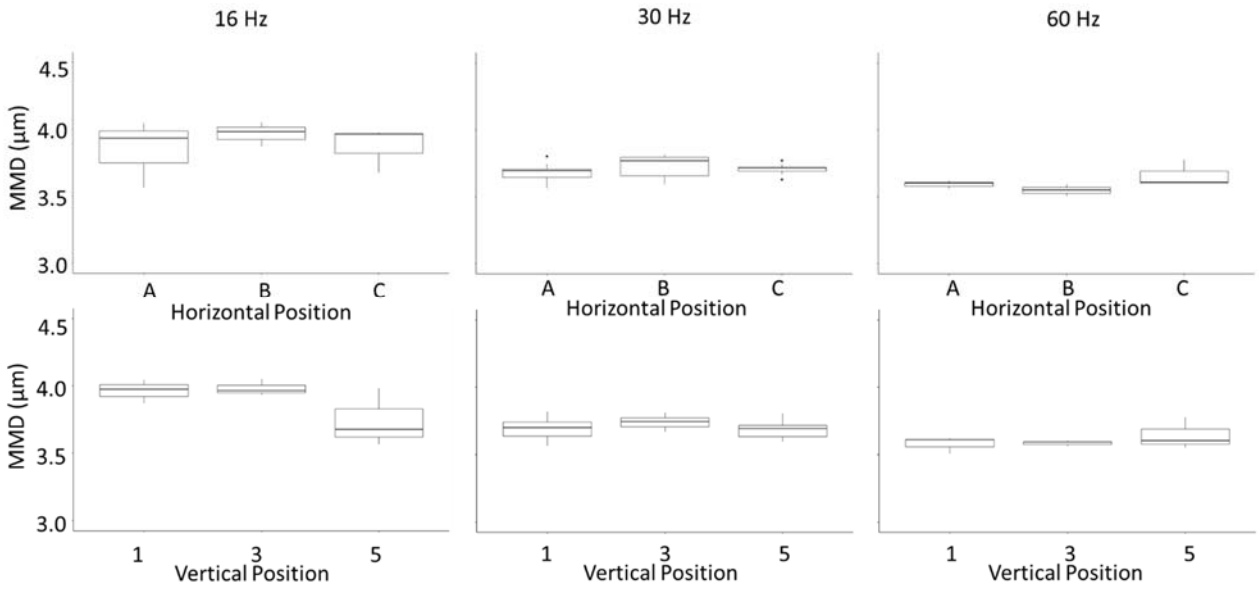

Figure H2. MMD Boxplots for Plane 8

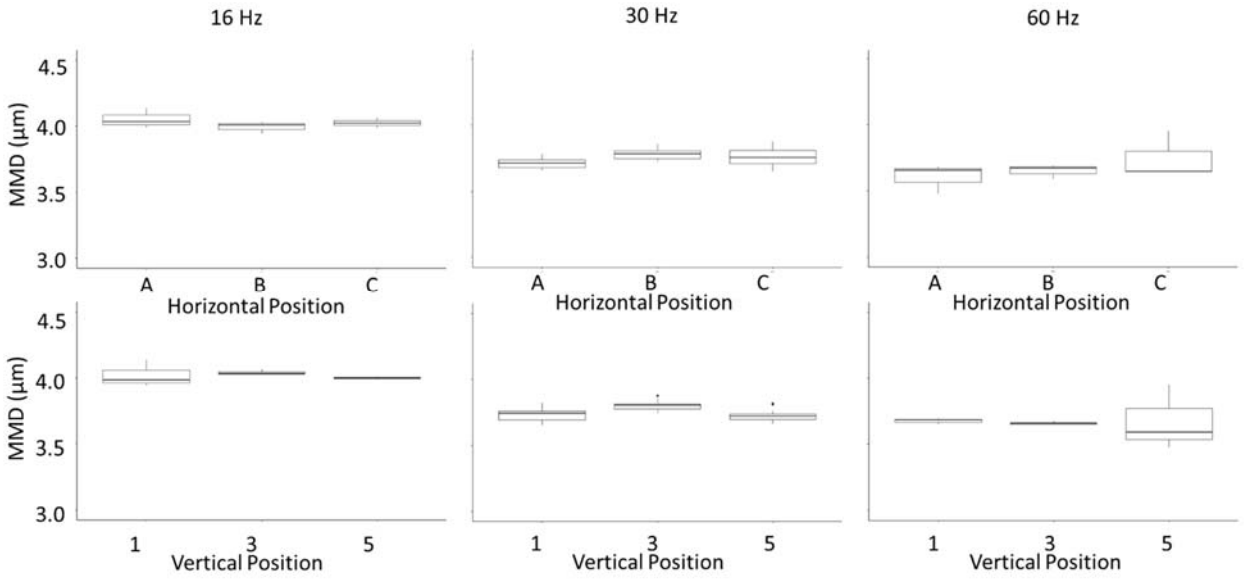

Figure H3. MMD Boxplots for Plane 10

Appendix I

Velocity and Particle Count Profiles

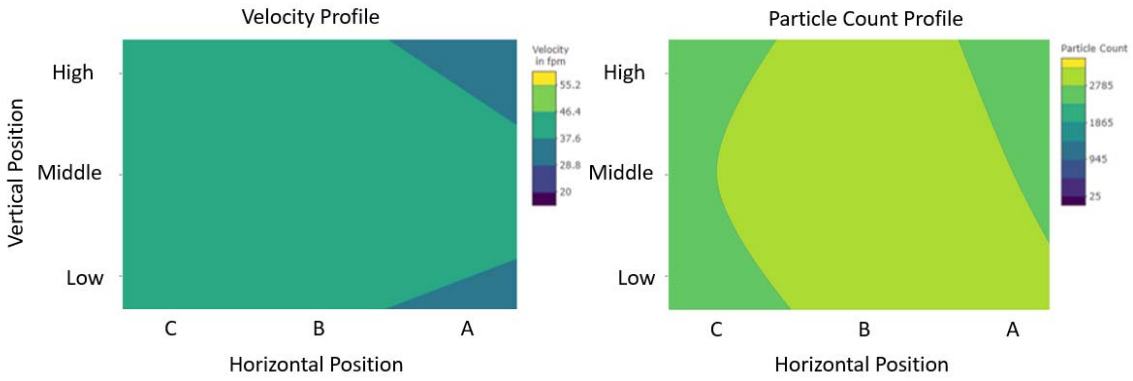

Figure I1. Velocity and Particle Count Profiles in Plane 7 at 16 Hz

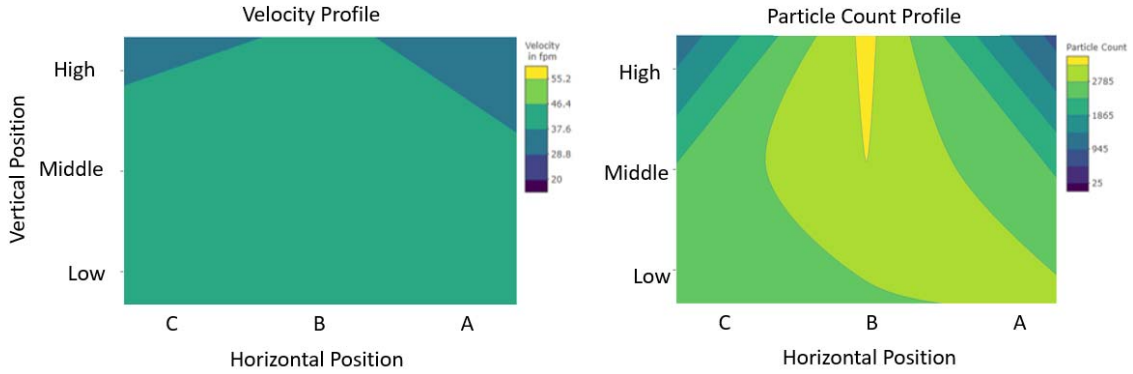

Figure I2. Velocity and Particle Count Profiles in Plane 8 at 16 Hz

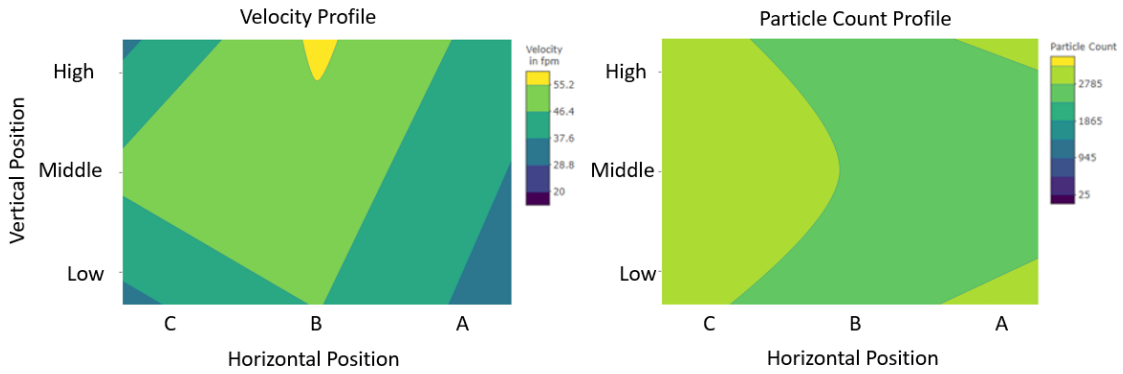

Figure I3. Velocity and Particle Count Profiles in Plane 10 at 16 Hz

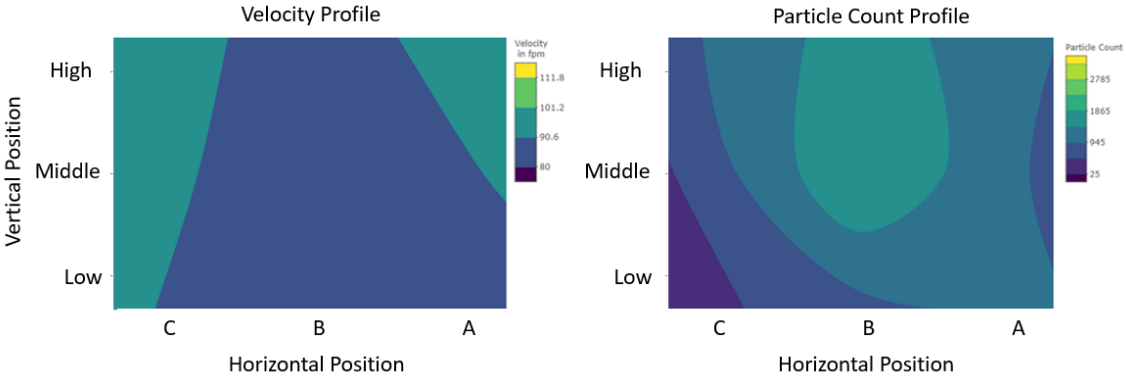

Figure I4. Velocity and Particle Count Profiles in Plane 5 at 30 Hz

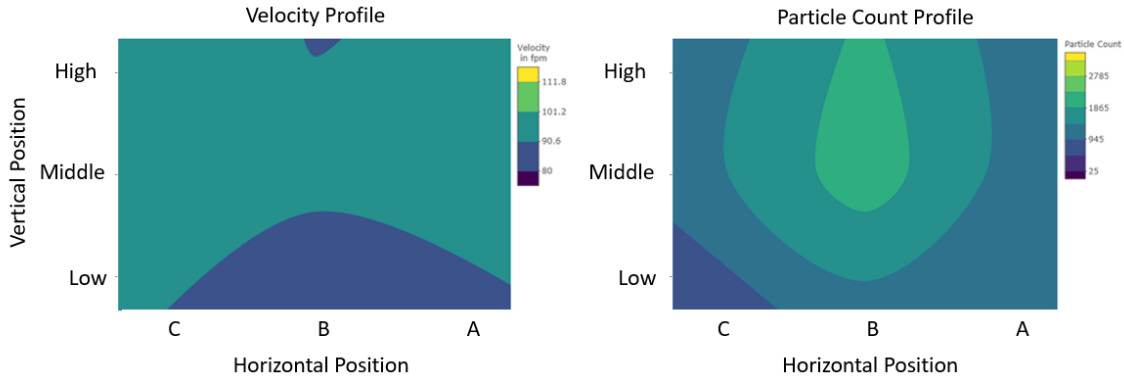

Figure I5. Velocity and Particle Count Profiles in Plane 7 at 30 Hz

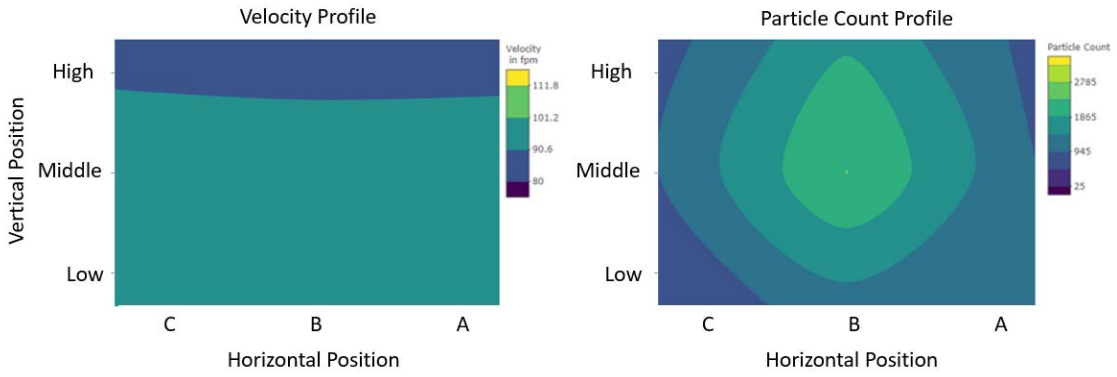

Figure I6. Velocity and Particle Count Profiles in Plane 8 at 30 Hz

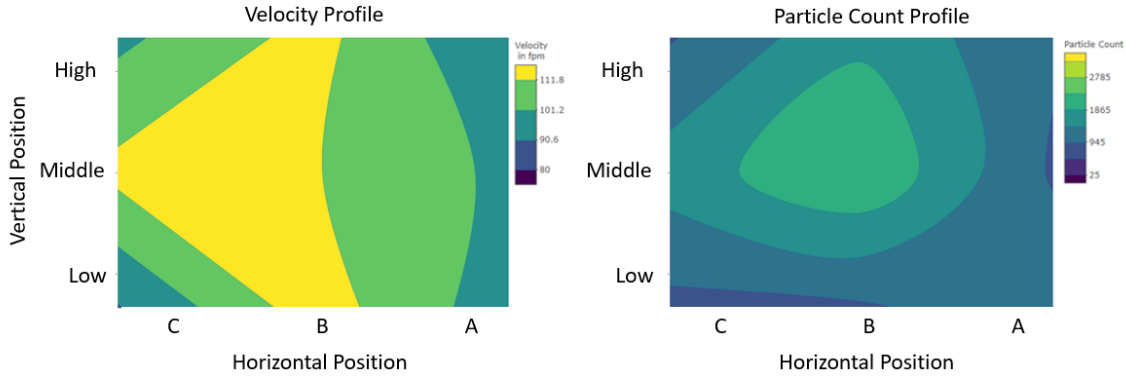

Figure I7. Velocity and Particle Count Profiles in Plane 10 at 30 Hz

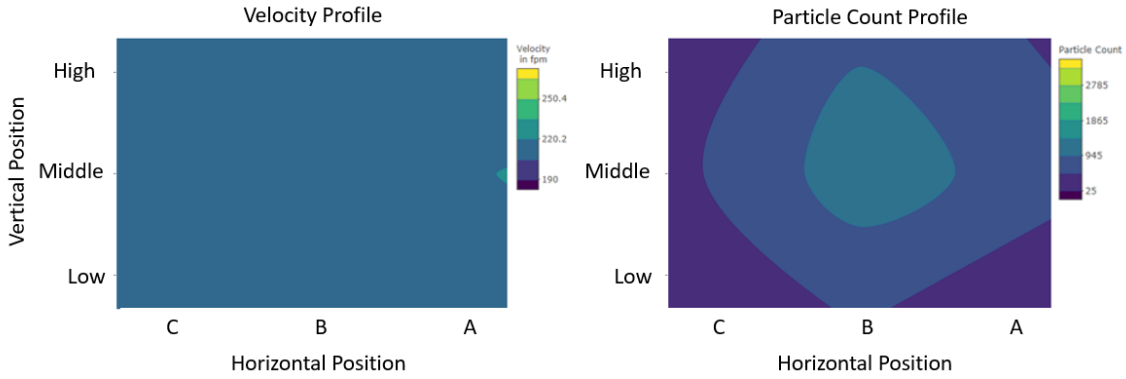

Figure I8. Velocity and Particle Count Profiles in Plane 5 at 60 Hz

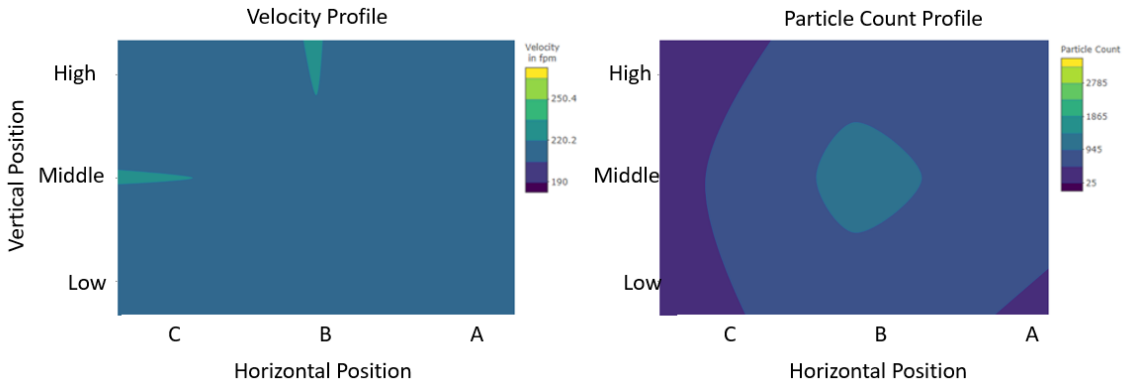

Figure I9. Velocity and Particle Count Profiles in Plane 7 at 60 Hz

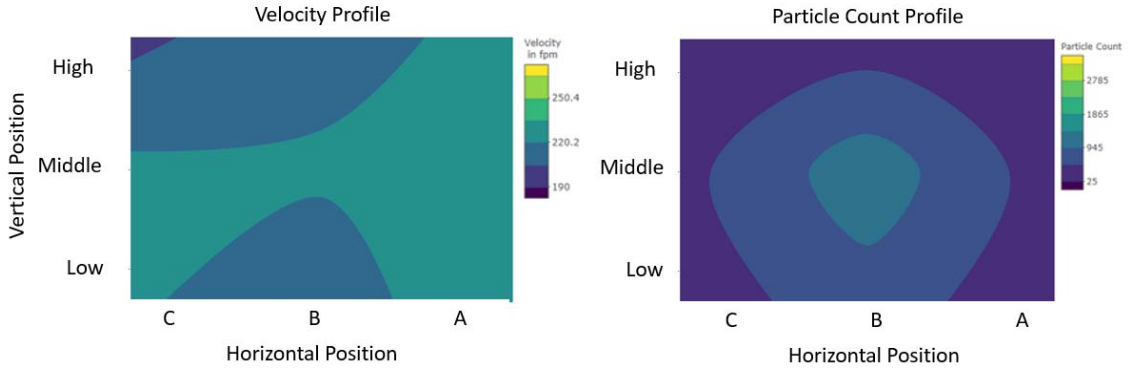

Figure I10. Velocity and Particle Count Profiles in Plane 8 at 60 Hz

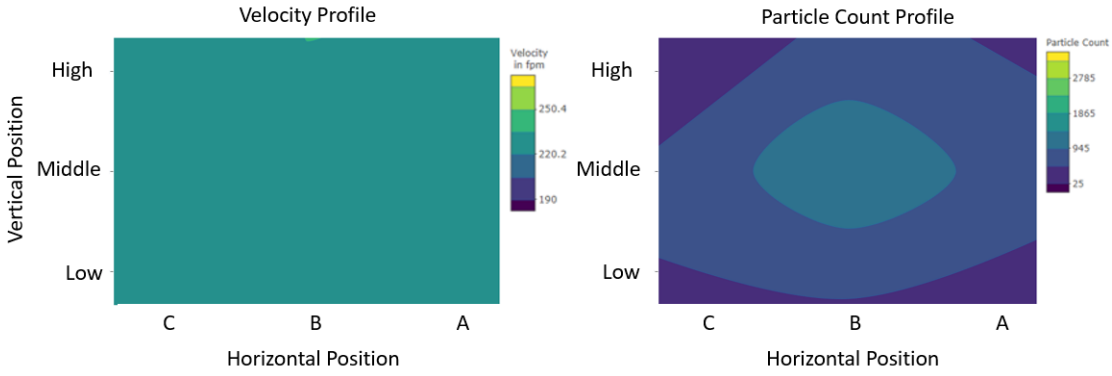

Figure I11. Velocity and Particle Count Profiles in Plane 10 at 60 Hz

Appendix J

Image Processing Parameter Definitions

Circularity: $4\pi \frac{Area}{Perimeter^2}$, with values between 0 to 1. The closer to 1, the closer to a true circle the particle is. Consider this also a measure of how irregular the particle is. As the perimeter increases, the circularity decreases even if the particle looks roughly like a circle, just with areas of concavity to increase the perimeter (Takashimizu, 2016).

Feret's Diameter: Also called the maximum calipers, this is the longest measurement along any axis for the particle (Figure 1).

Feret's Angle: The angle between the Feret's diameter and minimum Feret's diameter.

Minimum Feret's diameter: Also called the minimum caliper. This is the minimum distance along any axis in the particle (Figure J1).

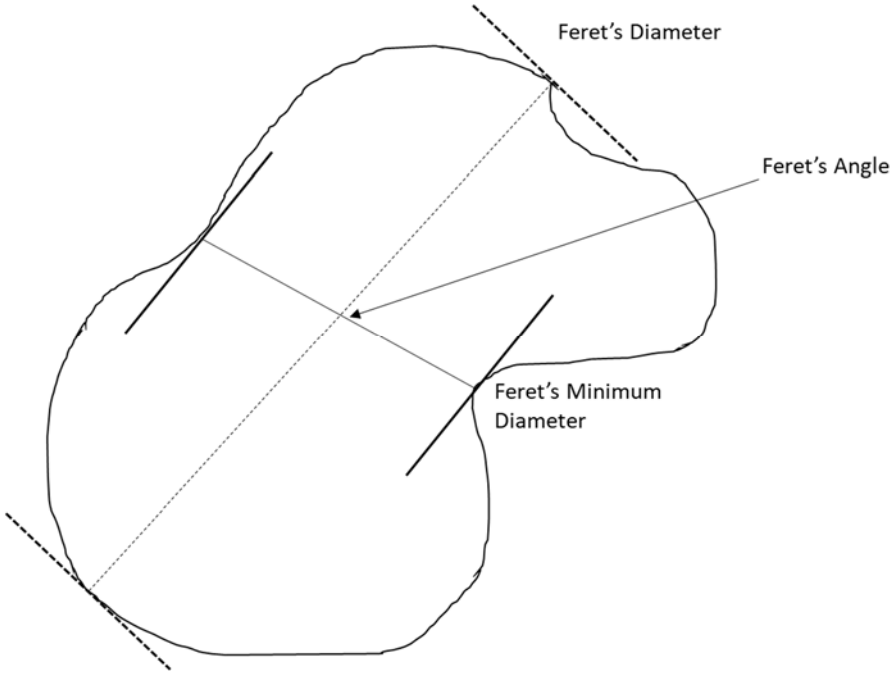

Figure J1. Determination of Minimum and Maximum Feret's Diameters

Aspect Ratio (AR): $\frac{Major\ Axis}{Minor\ Axis}$, based on a fitted ellipse for the outlined particle

Roundness: $\frac{1}{AR}$, a measure of how close the shape approaches a circle. The bigger the aspect ratio, the more the particle resembles an ellipse and the smaller the roundness measurement. The closer the aspect ratio approaches 1, the closer the roundness measurement approaches 1 (Takashimizu, 2016).

Solidity: $\frac{Area}{Convex\ Hull\ Area}$, based on the idea that if you have lots of concave places in the perimeter of the particle, the solidity will go down (Figure J2). If most of the particle is regularly shaped, the solidity approaches 1.

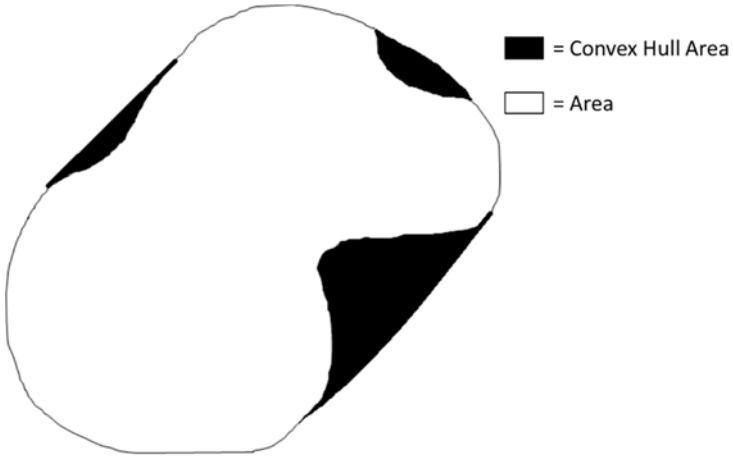

Figure J2. Example of Solidity

Bibliography

29 CFR §1910.1026 (2012).

ACGIH. Chromium and Inorganic Compounds in TLV Documentation. (2018).

Aizenberg, V., England, E., Grinshpun, S., Carlton, G., Willeke, K. Metal Exposure Among Abrasive Blasting Workers at Four U. S. Air Force Facilities. *Applied Occupational and Environmental Hygiene, 15*(10), pp 766-772. (2000).

ATSDR. Toxicological Profile for Chromium. Atlanta, GA: Agency for Toxic Substances and Disease Registry. (2012).

Avina, L., Codd, R., Killon, C. T., Lay, P. A. Chapter 2: Chromium in Biology: Toxicology and Nutritional Aspects in *Progress in Inorganic Chemistry, 51*, pp 145-250. Hoboken, NJ: John Wiley and Sons, Inc. (2003).

Baldwin, P. E. J., Maynard, A. D. A Survey of Wind Speeds in Indoor Workplaces. *Annals of Occupational Hygiene, 42* (1), pp 303-313. (1998).

Barceloux, D. G., Barceloux, D. Chromium. *Journal of Toxicology: Clinical Toxicology 37*(2), pp 173-194. (1999).

Bennett, J. S., Marlow, D. A., Nourian, F., Breay, J., Hammond, D. Hexavalent chromium and isocyanate exposures during military aircraft painting under crossflow ventilation. *Journal of Occupational and Environmental Hygiene, 13*(5), pp 356-371. (2016)

Bennett, J. S., Marlow, D. A., Nourian, F., Breay, J., Feng, A., Methner, M. Effect of ventilation velocity on hexavalent chromium and isocyanate exposures in aircraft paint spraying, *Journal of Occupational and Environmental Hygiene, 15*(3), pp167-181. (2018)

Bertini, I., Gray, H. B. Stiefel, E. I., Selverstone, J. Biological Inorganic Chemistry - Structure and Reactivity. University Science Books. (2007). Retrieved from https://app.knovel.com/hotlink/toc/id:kpBICSR00H/biological-inorganic/biological-inorganic

Blade, L.M., Yencken, M. Story, Wallace, M.E., Catalano, J. D., Khan, A., Topmiller, J. L., Shulman, S.A., Martinez, A., Crouch, K. G., Bennett, J. S. Hexavalent Chromium Exposures and Exposure-Control Technologies in American Enterprise: Results of a NIOSH Field Research Study. *Journal of Occupational and Environmental Hygiene, 4*(8), pp 596-618. (2007).

Christison, R. *A Treatise on Poisons in relation to Medical Jurisprudence, Physiology, and the Practice of Physic*, 4th Edition. London, England: Adam and Charles Black. (1845). Available from: https://collections.nlm.nih.gov/ocr/nlm:nlmuid-61910390R-bk.

DaCosta, J. C., Jones, J. F. Tanners' Ulcer. *Annals of Surgery, 63*(2), pp 155-166. (1916).

Department of Defense. United Facilities Criteria (UFC) Aircraft Corrosion Control and Paint Facilities. UFC 4-211-02. (2012).

DOEHRS. Business Object Common Services (BSC) search for NIOSH method 7605. (2018).

Carlton, G. N., Flynn, M. R. A Model to Estimate Worker Exposure to Spray Paint Mists. *Applied Occupational and Environmental Hygiene, 12*(5), pp 375-382. (1997a).

Carlton, G. N., Flynn, M. R. Influence of Spray Painting Parameters on Breathing Zone Particle Size Distributions. *Applied Occupational and Environmental Hygiene, 12*(11), pp 744-750. (1997c).

Carlton, G. N., England, E. C. Assessing Worker Exposures During Abrasive Blasting: Industrial Hygiene Field Guidance for Bioenvironmental Engineers. DTIC: IERA-RS-BR-TR-2000-0001. (2000).

Carlton, G. N. Hexavalent Chromium Exposures During Full-Aircraft Corrosion Control. *American Industrial Hygiene Association Journal, 64*(5), pp 668-672. (2003a).

Carlton, G. N. The Effectiveness of Handheld Ventilated Sanders in Reducing Inhalable Dust Concentrations. *Applied Occupational and Environmental Hygiene, 18* (1), pp 51-56. (2003b).

Carlton, G. N. The impact of a Change to Inhalable Occupational Exposure Limits: Strontium Chromate Exposure in the U. S. Air Force. *American Industrial Hygiene Association Journal, 64*(3), pp 306-311. (2003c).

England, E. Case Studies: Strontium Chromate Exposure Reduction During the Depainting and Priming of Fighter Aircraft. *Applied Occupational Environmental Hygiene, 13*(11), pp 747-751. (1998).

Ermolli, M., Menné, C., Pozzi, G., Serra, M. A., Clerici, L. A. Nickel, cobalt and chromium-induced cytotoxicity and intracellular accumulation in human hacat keratinocytes. *Toxicology, 159*, pp 23-31. (2001).

Gad, S. C. Acute and Chromic Systemic Chromium Toxicity. *The Science of the Total Environment, 86,* pp 149-157. (1989).

Gibb, H. J., Lees, P. S. J., Pinsky, P. F., Rooney, B. C. Lung Cancer Among Workers in Chromium Chemical Production. *American Journal of Industrial Medicine, 38*, pp 115-126 (2000a).

Gibb, H. J., Lees, P. S. J., Pinsky, P. F., Rooney, B. C. Clinical Findings of Irritation Among Chromium Chemical Production Workers. *American Journal of Industrial Medicine, 38*, pp 127-131 (2000b).

Gibb, H. J., Lees, P. S. J., Wang, J., O'Leary, K. G. Extended Followup of a Cohort of Chromium Production Workers. *American Journal of Industrial Medicine, 58*, pp 905-913 (2015).

Kiefer, M., Trout, D., Wallace, M. E. Avondale Shipyards Health Hazard Evaluation. Cincinnati, OH: NIOSH Publications Office. HETA 97-0260-2716. (1998).

Lucas, J. B., Kramkowski, R. S. HHE determination Report of Industrial Platers, Inc. Cincinnati, OH: NIOSH Publications Office. HHE-74-87-221. (1975).

Mattingly, D. Personal interview. (2019).

National Toxicology Program. Hexavalent Chromium. Retrieved 4 April 2019 from https://www.niehs.nih.gov/health/materials/hexavalent_chromium_508.pdf.

NIOSH. Criteria for a Recommended Standard Occupational Exposure to Hexavalent Chromium. Cincinnati, OH: Department of Health and Human Services. (2013).

Nethercott, J., Paustenbach, D., Adams, R., Fowler, J., Marks, J., Morton, C., Taylor, J., Horowitz, S., Finley, B. A study of chromium induced allergic contact dermatitis with 54 volunteers: implications for environmental risk assessment. *Occupational and Environmental Medicine, 51*, pp 371-380. (1994).

OSHA. Occupational Safety and Health Standards, 29 CFR §1910.1026—Chromium (VI) (2006).

Phalen, R. F. Airway Anatomy and Physiology. In J. H. Vincent (Ed.), *Particle Size-Selective Sampling for Particulate Air Contaminants* (pp. 29-49). Cincinnati, OH: ACGIH. (1999).

Singh, J., Pritchard, D. E., Carlisle, D. L., Mclean, J. A., Montaser, A., Orenstein, J. M., Patierno, S. R. Internalization of Carcinogenic Lead Chromate Particles by Cultured Normal Human Lung Epithelial Cells: Formation of Intracellular Lead-Inclusion Bodies and Induction of Apoptosis. *Toxicology and Applied Pharmacology, 161*, pp 240-248. (1999).

Suh, M., Wikoff, D., Lipworth, L., Goodman, M., Fitch, S., Mittal, L., Proctor, D. Hexavalent chromium and stomach cancer: a systematic review and meta-analysis. *Critical Reviews in Toxicology.* (2019).

United States Air Force (USAF). TO-1-1-8. Application and Removal of Organic Coatings, Aerospace and Non-Aerospace Equipment. (2008).

Vincent, J. B. Chromium: is it essential, pharmacologically relevant, or toxic? *Metal ions in Life Sciences, 13*, pp 171-198. (2013).

Williams, N. A survey of respiratory and dermatological disease in the chrome plating industry in the West Midlands, UK. *Journal of Occupational Medicine 46*(6), pp 432-434 (1996).

Zhou, Y., Cheng, Y.S. Evaluation of IOM Personal Sampler at Different Flow Rates. *J. Occup. Environ. Hyg. 7*(2), pp 88 – 93. (2009)

REPORT DOCUMENTATION PAGE

Form Approved
OMB No. 074-0188

1. REPORT DATE *(DD-MM-YYYY)*	2. REPORT TYPE	3. DATES COVERED *(From – To)*
22-03-2020	Master's Thesis	October 2018 – March 2020

TITLE AND SUBTITLE

Assessing Challenges Associated with Sampling Hexavalent Chromium Under New Consensus Guidelines

5a. CONTRACT NUMBER

5b. GRANT NUMBER

5c. PROGRAM ELEMENT NUMBER

6. AUTHOR(S)

Steele, Megan L., Contractor

5d. PROJECT NUMBER

5e. TASK NUMBER

5f. WORK UNIT NUMBER

7. PERFORMING ORGANIZATION NAMES(S) AND ADDRESS(S)
Air Force Institute of Technology
Graduate School of Systems Engineering (AFIT/ENV)
2950 Hobson Way, Building 640
WPAFB OH 45433-8865

8. PERFORMING ORGANIZATION REPORT NUMBER

AFIT-ENV-MS-20-M-242

9. SPONSORING/MONITORING AGENCY NAME(S) AND ADDRESS(ES)
US Air Force AFRL, 711th Human Performance Wing/RHMO
Attn: Dr. Dirk Yamamoto
2510 Fifth Street,
Wright Patterson AFB, OH 45433
(937) 426-6900 x407, dirk.yamamoto.2@us.af.mil

10. SPONSOR/MONITOR'S ACRONYM(S)
AFRL/RHMO

11. SPONSOR/MONITOR'S REPORT NUMBER(S)

12. DISTRIBUTION/AVAILABILITY STATEMENT
DISTRUBTION STATEMENT A. APPROVED FOR PUBLIC RELEASE; DISTRIBUTION UNLIMITED.

13. SUPPLEMENTARY NOTES
This material is declared a work of the U.S. Government and is not subject to copyright protection in the United States.

14. ABSTRACT

A consensus body recently suggested lowering the threshold limit value (TLV) for hexavalent chromium to 0.2 μg/m^3 and added a requirement to sample using an inhalable sampler. In order to generate enough mass to be above the limit of quantification, it is suggested practitioners increase the flow rate of the sampling pump. Since the sampler was designed to operate at 2 L/min to adhere to the inhalable convention, there is a possibility the higher flow rates will cause the sampler efficiency to deviate from the convention. An aerosol chamber was constructed and characterized to create well-defined test bed. The aerosol properties of abrasive blasting processes were characterized to determine if particle distribution and composition warranted the use of an inhalable sampler. Results from the aerosol characterization show that all particle sizes carried some chromium and the distribution included particles up to 100 μm. Institute of Medicine (IOM) inhalable samplers were paired, with one sample operating at 2 L/min and one sampler operating at 6 L/min. The pairs were exposed to particulate with an aerodynamic diameter of 70 μm in the aerosol chamber. Results show a 30% positive difference in the concentrations reported at 6 L/min compared to 2 L/min.

15. SUBJECT TERMS
Hexavalent chromium; air sampling; IOM; aerosol characterization

16. SECURITY CLASSIFICATION OF:			17. LIMITATION OF ABSTRACT	18. NUMBER OF PAGES	19a. NAME OF RESPONSIBLE PERSON
a. REPORT	b. ABSTRACT	c. THIS PAGE			Dr. Jeremy Slagley, AFIT/ENV
U	U	U	UU	123	19b. TELEPHONE NUMBER *(Include area code)* (937) 255-3636, ext 4632 (NOT DSN) (jeremy.slagley@afit.edu)

Standard Form 298 (Rev. 8-98)
Prescribed by ANSI Std. Z39-18